SPARSE FREQUENCY LASER RADAR SIGNAL MODELING AND DOPPLER PROCESSING

Thesis

Submitted to

The School of Engineering of the

UNIVERSITY OF DAYTON

In Partial Fulfillment of the Requirements for

The Degree of

Master of Science in Electro-Optics

Eric Stanton Bailey

UNIVERSITY OF DAYTON

DAYTON, OHIO

May 2010

SPARSE FREQUENCY LASER RADAR SIGNAL MODELING AND DOPPLER PROCESSING

APPROVED BY:

Peter E. Powers, Ph. D.
Advisory Committee Chairman
Professor Physics & Electro-Optics

Matthew P. Dierking, Ph. D.
Committee Member
Technical Advisor
AFRL/RYJM, WPAFB, OH

Joseph W. Haus, Ph. D.
Committee Member
Professor & Director
Electro-Optics

Malcolm W. Daniels, Ph. D.
Associate Dean
School of Engineering

Tony E. Saliba, Ph. D.
Dean
School of Engineering

ABSTRACT

SPARSE FREQUENCY LASER RADAR SIGNAL MODELING AND DOPPLER PROCESSING

Bailey, Eric Stanton
University of Dayton, 2010

Advisor: Peter E. Powers, Ph.D.

Sparse frequency, linearly frequency modulated laser radar (ladar) signals achieve improved range resolution comparable to a larger signal bandwidth. From basic radar/ladar principles it is known that the bandwidth of a signal is inversely proportional to range resolution. Hence, the effective bandwidth of a ladar signal using sparse frequency techniques is larger than the bandwidth of each modulated laser frequency. Previous experiments have validated range resolution and peak to sidelobe ratio derived from models utilizing two segmented bandwidths. This thesis discusses the modeling with three segmented bandwidths. The model is verified against an experimental setup using three frequency offset lasers.

The two segmented bandwidth, sparse frequency ladar signal is reexamined to include Doppler effects. The new modeling utilizes a coherent on receive setup allowing for phase information to be processed from the signal. The extracted phase information can be used to determine characteristics about a target, namely its speed and direction with respect to the receiver. This modeling was experimentally verified for cases where the target was next to the receiver, at a distance (simulated through a fiber delay line), and for multiple targets. As a final check of the modeling, the velocity determined from the phase information was compared against the velocity readout of a stage with a built in optical encoder.

To my parents, Jay and Nancy – your support of every step I have taken throughout my life has encouraged me to do what I love and be proud of it. Thank you for pushing me to be the best that I can.

To my brother, Calvin – your enthusiasm towards life and your obsession with conquering mountain after mountain, both metaphorically and literally, has been an inspiration to me. Thank you, and never stop pushing your limits.

To Jill – your support of me has been unwavering whether it was a stressful day or the long distance of our relationship. Thank you; I will never forget it.

ACKNOWLEDGEMENTS

I would like to thank everyone involved in making this thesis possible. First and foremost, my advisor Peter Powers, thank you for the direction and assistance over the past couple years. I would also like to thank Joseph Haus for the opportunity to work at LOCI and funding to complete not only my research but my masters degree. I would especially like to thank Matthew Dierking of Air Force Research Labs for mentoring me in the principles of laser radar signals and for being available (even on the weekends) when I needed guidance on my research. I would also like to express appreciation to Nicholas Miller, Bradley Duncan, Paul McManamon, Ed Watson, and everyone else at LOCI for their insight and support.

This research was supported in part by the U.S. Air Force through contract number FA8650-06-2-1081 and the University of Dayton Ladar and Optical Communications Institute (LOCI). The views expressed in this article are those of the authors and do not reflect on the official policy of the Air Force, Department of Defense or the U.S. Government.

TABLE OF CONTENTS

LIST OF FIGURES

CHAPTER 1 -
INTRODUCTION

A. Background

The relationship between techniques in the radar communities and those used in the ladar communities can be quite similar if not identical. It is worth acknowledging that much of the research in ladar can be correlated to previous work done in the radar community, albeit at much different frequencies. The goal of this section is to provide a brief history for the development of frequency modulated laser radar and laser rangefinder signals including the relevance to recent publications.

In 1943, D. O. North presented his work “Analysis of factors which determine signal-to-noise discrimination in radar” [1]. His paper laid the mathematical foundation for what an ideal receiver should be. The process called *matched filtering* is still in wide use today and prevalent throughout this thesis. The name *matched filter* comes from work done by Van Vleck and Middleton, who first coined the term [2]. Synonymously, *matched filter* is sometimes called a *North Filter* after D. O. North. The next major realization in radar signals came about one decade later in 1953 when P. M. Woodward published a paper entitled “Probability and Information Theory, with Applications to Radar” where he detailed how range resolution was not a function of the transmitted pulse width but actually a function of the signal’s bandwidth [3]. The work inspected how range resolution requirements could be met by coding the transmitted signal with wideband modulation. Over the next two decades work was done on radar signals, and the reader is referred to the publications on radar signals by Cook 1958 and 1959, Fowle 1963, and Bernfeld 1965 [4, 5, 6, 7].

Around the mid 1970's, works involving CO_2 lasers as rangefinders and some applications to laser radar were starting to emerge. One of the earliest papers published was by A. J. Hughes in 1972 where he used a CO_2 laser to perform range measurements at the 10 µm wavelength [8]. Other papers involving CO_2 laser started emerging soon after, including work by Hulme using heterodyne detection and chirped pulse compression, Forrester on laser rangefinders, and Collins, who used a CO_2 laser in conjunction with an acousto-optic modulator to do heterodyne detection [9, 10, 11]. By the mid 1980's a new subfield had developed based around CO_2 lasers for use in determining atmospheric conditions (atmospheric lidar). Since atmospheric lidar is a topic of its own and does not have much bearing on this thesis, the reader is referred to two recent works on lidar signals. Adany presents results on chirped lidar that utilizes homodyne detection, and Tsuji offers a paper which treats resolution in coherent reflectometry [12,13].

The last part of this section covers the placement of this work among other related works. It focuses on recent work in the ladar signals field. The work that is most closely related was done by Robert Chimenti on sparse frequency linearly frequency modulated laser radar signals. His papers on theory and experimental verification laid the foundation for the derivative work presented here. His works and mine provide a mechanism for increasing the bandwidth of ladar signals by modulating multiple laser lines, which is commonly referred to simply as 'lines', simultaneously. The increased bandwidth provides for an increase in the range resolution of the signal [14,15].

One of the more novel techniques for increasing bandwidth of a signal was pioneered by Kevin Holman of MIT's Lincoln Laboratory. His technique employs a 5 GHz modulator to create two signals spaced by 10 GHz, upon which they are multiplexed, on/off modulated, and demultiplexed to create a signal that is one frequency for half the signal period and another frequency for the other half, where the frequency difference is 10 GHz. The signal is then modulated with 10 GHz twice over the signal period. This creates one large 20 GHz linear chirp. His work allows for sub millimeter range resolution but adds greatly in hardware complexity [16,17].

Another technique that has been utilized in recent years is the use of pseudo-random code or white noise waveforms. In particular, a group from Spectrum Labs associated with the Montana State University has developed a technique to store, compare, and read out the waveform at a slower rate to reduce detection and post processing requirements. The process works by taking a transmit laser and encoding it via a PN code generator/electro-optic modulator. The signal is then split where one is used as the reference and the other is transmitted to the target. They are both run through a cryogenically cooled, nonlinear material, where the information is stored. The information is read out with a second laser that is linearly frequency modulated. Since the speed at which the signal is read out is proportional to the slope of the linearly modulated signal, detector requirements are reduced. The major advantage of this work is the optical correlation done in the nonlinear material. However, the major drawback is the nonlinear material needing to be cooled to 4 degrees Kelvin [18,19].

Furher research on periodic pseudo noise waveforms has been done by Matt Dierking of Air Force Research Laboratory. His work uses a PN code generator and an I/Q detection setup with matched filtering to determine the range resolution and sidelobe structure of a specific code set. The code is then altered and the new code is accepted if the sidelobe structure is reduced in the area around the target. The process is iterated multiple times to drastically reduce the sidelobe structure around a target. However, this suppression of the sidelobes around the target increases the sidelobes that are not around the target. This technique would be advantageous if looking at a narrow range is desired [20].

A large body of other work has been published on ladar signals. To finish this background section, the following papers are cited here but not discussed in detail: Zheng paper on continuous wave optical frequency modulation interference [21]; Duartes' paper on vessel detection using continuous wave linearly frequency modulated radar signals [22]; and range resolution limits of time-of-flight laser radar are presented in a conference paper by Khoury [23]. Lastly, three conference papers are worthy of mention to the reader from the Lockheed Martin Coherent Technologies group about range precision in both coherent ladar and direct detection systems, and micro-Doppler lidar signals [24,25,26].

B. Thesis Overview

The research presented in this thesis investigates the use of sparse frequency linearly frequency modulated (SF-LFM) ladar signals for use in range-Doppler ladar systems. Chapter 2 explains fundamental concepts in ladar/radar signal processing. It describes the basic concepts one needs to understand in order to comprehend the research, including information on matched filter processing, coherent signals and processing, ambiguity functions, and both linear and nonlinear frequency modulation. Chapter 3 is a review of SF-LFM signals. It includes discussion on how the signals are generated and detected as well as how the signals are mathematically defined. The last part of the chapter focuses on the metrics (range resolution and peak to sidelobe ratio) used to characterize the signal.

Chapter 4 is the start of continued research and begins with a mathematical form of SF-LFM signals defined by Chimenti et al. to create what is called a three chirp SF-LFM signal [15]. The chapter addresses the modeling of the signal, the experimental setup used to determine the validity of the model, the signal processing utilized, and finally the results of the actual experimental verification.

Chapters 5 and 6 introduce Doppler effects into the SF-LFM signals. They cover a new modeling that utilizes matched filter processing, where the phase of the signal can be recovered and used to determine both the speed of a target as well as the radial direction. The experimental setup and its requirements are discussed and experimental verifications are presented on targets at no range and targets at range. Chapter 6 specifically cover the case where there are multiple targets, a close and a distant target, and shows both the experimental setup and the results of that experiment.

Chapter 7 takes a brief look at how nonlinear frequency modulation can be used to increase range resolution and peak to sidelobe ratio of ladar signals. More specifically it looks at nonlinearities in the acousto-optic modulator and how they can be exploited to improve both the range resolution and the peak to sidelobe ratio simultaneously.

CHAPTER 2 -
LADAR SIGNAL PROCESSING

This chapter covers some terminology and basic concepts involved in the processing of ladar signals, the most important of which is matched filter processing.

In order to recognize how Doppler signal processing is utilized, two essential relationships are required governing the time delay and phase impacs associated with the targets geometry and motion. First, the target range R is written as of an object with the time delay (τ) of the received signal,

$$R = \frac{1}{2} c\tau, \tag{2.1}$$

where c is the speed of light and τ is the propagation delay of the received signal. The factor of one half is due to the round trip travel, where the total distance traversed by the signal is twice the actual range of the object. The second relationship, is the Doppler shift due to relative target motion and is written as,

$$\upsilon \approx -\frac{2\dot{R}}{\lambda}, \tag{2.2}$$

where $\dot{R}$ is the target velocity and λ is the carrier wavelength. A more detailed analysis of Equations 2.1 and 2.2 can be found in *Radar Signals* by Levonon and Mozeson's [27].

A. Matched Filter Processing

Matched filter processing was developed from optimizing the signal to noise ratio (SNR) of an incoming signal. Most radar signals books, including Levonon's *Radar Signals* or Cook and Bernfeld's *Radar Signals: An Introduction to Theory and Application* [27, 28], show that in order to maximize the signal-tonoise ratio (SNR), the impulse response of the system should be given by,

$$h(t) = Ks^{*}(t_0 - t), \tag{2.3}$$

where $h(t)$ is the impulse response, K is a scaling constant, $\mathrm{s}(t)$ is the signal, and t_0 is a time delay/reference point. To determine the output of a linear system, the input signal is convolved with the impulse response, a derivation that can be found in most signals and systems books [29, 30, 31]

$$s_o(t) = (s * h)(t) = \int_{-\infty}^{\infty} s(\tau)h^{*}(\tau - t)d\tau. \tag{2.4}$$

Equation 2.4 shows the signal output as a function of the input signal and the impulse response. If the assumption is made that there is no time delay for the input signal (i.e. $t_0 = 0$), the output signal can be reduced to the autocorrelation of the signal,

$$s_o(t) = K\int_{-\infty}^{\infty} s(\tau)s^{*}(\tau - t)d\tau \tag{2.5}$$

where once again, K is a scaling constant, $s(\tau)$is the signal, τ is a dummy variable of integration, and s^{*} is the conjugate of s. Later this assumption is dropped in order to account for targets at range.

The simplest example of a matched filter process is a single frequency signal, where the signal is defined by,

$$s(t) = \frac{1}{\sqrt{T}}Rect\left(\frac{t}{T}\right). \tag{2.6}$$

where T is the period of the signal and $Rect\left(\frac{t}{T}\right)$ is the rectangle function which is 1 form $-\frac{T}{2} \leq t \leq \frac{T}{2}$ and zero elsewhere.

The results of using Equation 2.6 in Equation 2.5 and assuming $K = 1$, see [27, 28] for a detailed derivation.

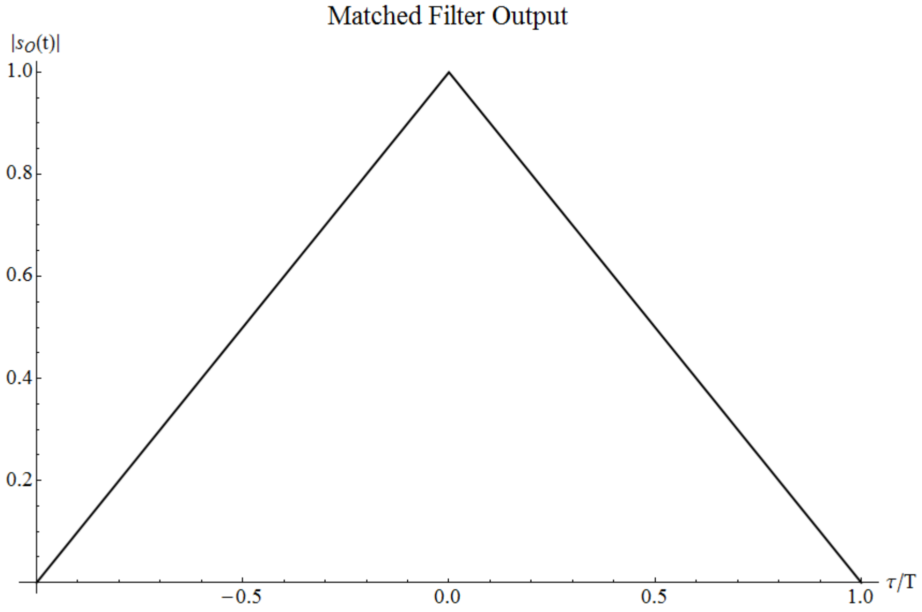

Figure 2.1: Matched filter output of a single tone radar signal.

The results of using Equation 2.6 in Equation 2.5 and assuming $K = 1$ is shown in Figure 2.1, see [27, 28] for a detailed derivation. Range resolution is defined as the full width half max (FWHM) of the primary lobe of the matched filter output. Figure 2.1 shows a FWHM of T corresponding to a range resolution of $cT/2$. Remember there is direct mapping between the time delay, τ, and range, R, given in Equation 2.1 and from this, range resolution can be deduced.

For a more detailed analysis of the previous equations and general information about matched filter processing, the reader may refer to *Radar Signals*, *Radar Signals: An Introduction to Theory and Application*, and D. O. North's work on radar signals [1, 27, 28].

B. Coherent Processing

To explain coherent processing, a train of unmodulated pulses is used as an example. It is important note that the Doppler resolution of a radar or ladar signal is directly proportional to the duration of the signal. The Doppler shift is small for most target motions for the shot duration of most common radar waveforms. However, a train of pulses can be beneficially used in increasing the Doppler resolution.

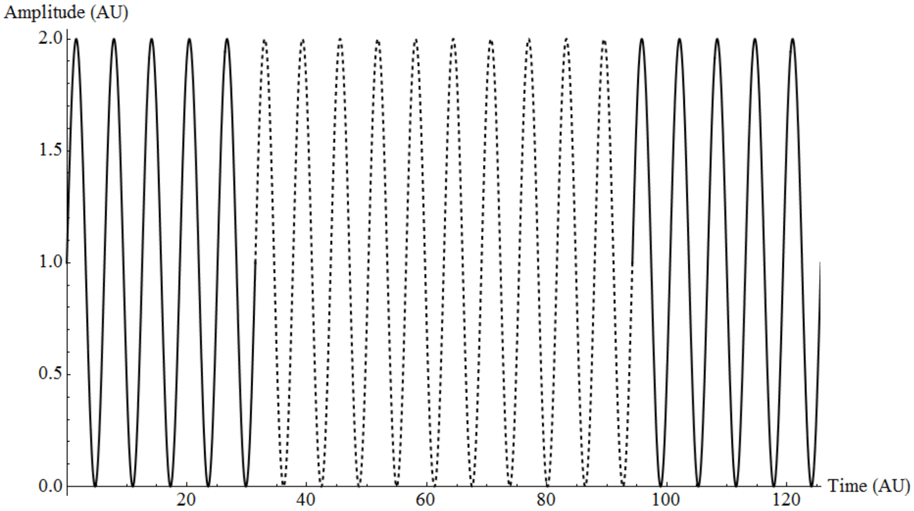

Figure 2.2: On(solid)/off(dashed) gating of a radar signal showing two coherent pulses.

In order to utilize the Doppler information between each of the pulses it is necessary for each of the pulses to be coherent with each other. Figure 2.2 shows an example of two pulses that are coherent. When the pulses are coherent with each other and the initial phase of each pulse is known to the receiver, a Doppler-induced phase change can be detected.

For many radar and especially ladar systems it is difficult to be coherent over large durations of time. Because of this, a technique call *coherent on receive* was developed [27]. In a system utilizing coherent on receive, the phase of the transmitted pulse is recorded as a reference for the return signal, but it is important to note that the phase is only known for the previous pulse. Later, additional stipulations are added to the definition of coherent on receive to account for differences between radar versus ladar detection and processing.

C. Ambiguity Function

The ambiguity function, or uncertainty function as it is sometimes called, establishes the effectiveness of a matched filter waveform, and is typically used for determining the velocity and range of a single pulse or of multiple targets. Throughout this thesis, the ambiguity function is defined by, and was originally developed by P.M. Woodward in 1953 [3].

$$|\chi(\tau,\nu)| = \left|\int_{-\infty}^{\infty} u(t)u^*(t+\tau)e^{i2\pi\nu t}\,dt\right| \tag{2.7}$$

Equation 2.7 shows the ambiguity function defined by Woodward, where τ describes an input signal's time delay, ν is the Doppler shifted frequency of the input signal, and $u(t)$ is the complex representation of the signal.

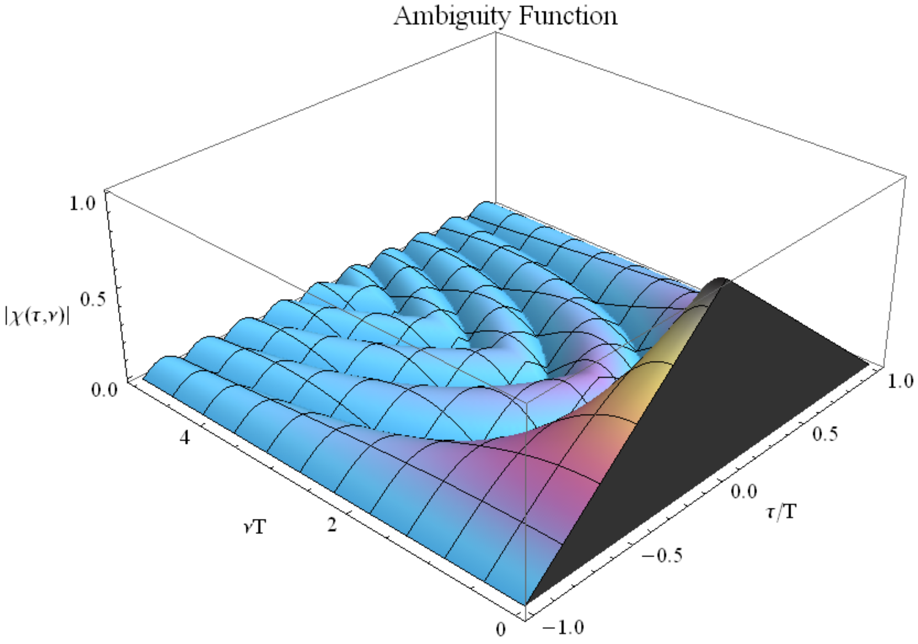

Figure 2.3: Ambiguity function of a single tone radar signal.

We proceed with the single frequency example in Section A and using Equation 2.6, an example ambiguity function was plotted in Figure 2.3 showing the first two quadrants. It is easy to see that the zero Doppler cut in Figure 2.3 is the same as the matched filter output in Figure 2.1. By removing the Doppler portion of Equation 2.7, the function reduces to the autocorrelation of the complex envelope as seen,

$$|\chi(\tau,\nu)| = \left|\int_{-\infty}^{\infty} u(t)u^*(t+\tau)dt\right|. \tag{2.8}$$

D. Linear Frequency Modulation

As mentioned previously, matched filter radar and ladar signals have a range resolution proportional to their bandwidth. With the exception of using shorter transform limited pulses, which lower the signal to noise ratio for constant peak power waveforms, a common way to add bandwidth is by modulating the frequency of the signal.

Of the various forms of modulation techniques, the most common and first to be conceived, is linear frequency modulation (LFM) [28]. The main idea behind LFM is to sweep the frequency of the pulse linearly over its duration. The complex envelope of an LFM radar pulse is given by,

$$u(t) = \frac{1}{\sqrt{T}} rect\left(\frac{t}{T}\right) e^{i\left(2\pi f t + \frac{1}{2}\beta t^2\right)}, \tag{2.9}$$

where T is the pulse duration, f is the carrier frequency, and β is the chirp coefficient defined by,

$$\beta = \frac{2\pi B}{T}, \tag{2.10}$$

where B is the modulation bandwidth and T is the pulse duration.

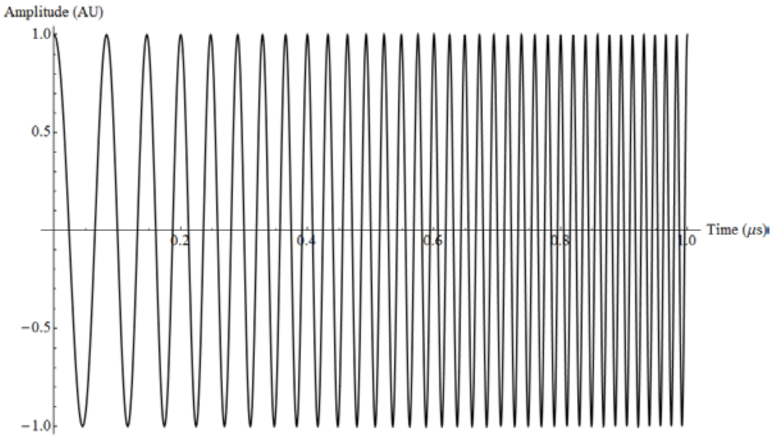

Figure 2.4: LFM signal with a time bandwidth product = 50.

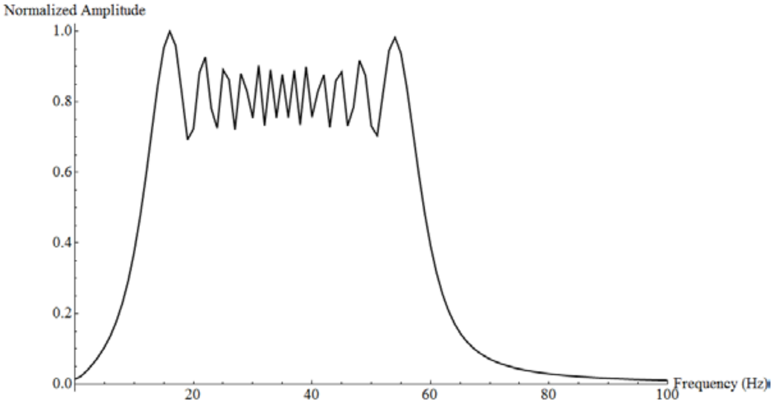

Figure 2.5: LFM spectrum with a time bandwidth product = 50.

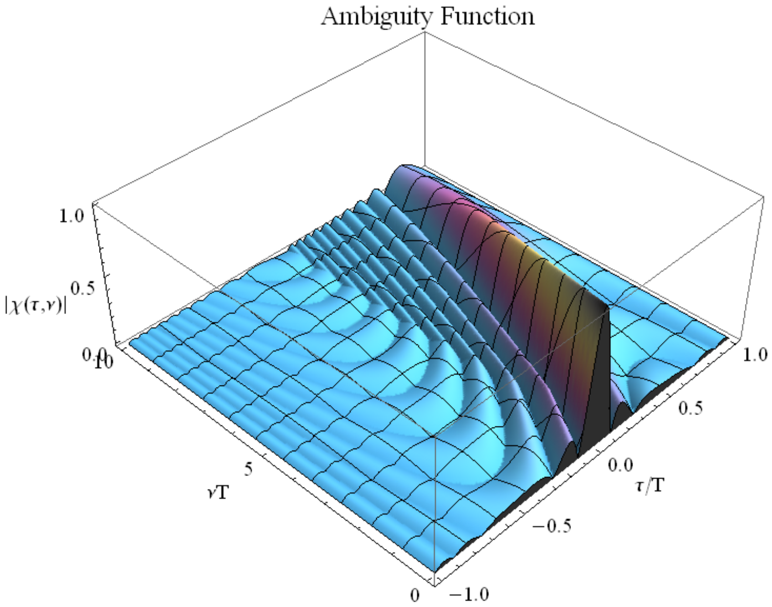

Figure 2.6: Ambiguity function of an LFM radar signal using a time bandwidth product = 10.

Figure 2.4 and Figure 2.5 show an LFM chirp and its frequency spectrum respectively, where both are utilizing a time bandwidth product of 50. By using Equation

2.8 in 2.7, the ambiguity function of an LFM pulse can be shown. Figure 2.6 shows an example of an LFM ambiguity function with a time bandwidth product of 10.

E. Nonlinear Frequency Modulation

One of the more significant hurdles with LFM pulse compression is its nature to have relatively high sidelobes in the autocorrelation. Nonlinear frequency modulation (NLFM) can simply be defined as a modulation where the instantaneous frequency is not linear in time, unlike an LFM pulse. The idea behind NLFM is to spend more time at the frequencies that need to be enhanced and less at those that do not.

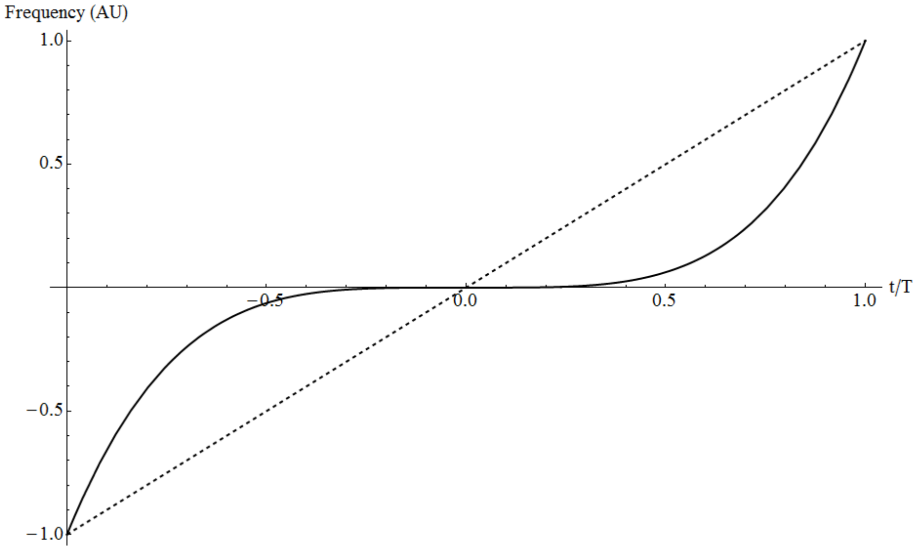

Figure 2.7: Instantaneous frequency of a nonlinear signal (Solid) and linear signal (Dashed).

Figure 2.7 shows an example of the instantaneous frequency of a nonlinear signal and linear signal.

As an aside, it is known that the inverse Fourier transform of the power spectrum is an autocorrelation. So by applying an amplitude weighted window to the signal, one can reduce the sidelobes of the autocorrelation. A multitude of windowing functions already exist, including Rectangular, Hamming, Hann, Cosine, Bartlett, etc., to perform various alterations on sidelobes [32].

CHAPTER 3 -
SPARSE FREQUENCY LADAR SIGNALS

The basic concept of sparse frequency, linear frequency modulated signals can be developed from a similar one in radar and ladar called synthetic aperture radar (SAR) or synthetic aperture ladar (SAL). The idea behind these two concepts is that by moving antennas in radar or apertures in ladar, then one is able to resolve a target with higher resolution without the need for a continuous antenna/aperture. In both SAR and SAL, the idea is to physically move antennas/apertures to allow access to higher spatial frequency content [33,34]. In sparse frequency ladar, the same concept is applied in the time domain instead of the spatial domain. By taking and modulating the signal so that smaller modulated portions are spaced in frequency, the effective bandwidth of the signal can be increased. Remember, the range resolution of a signal is proportional to the bandwidth of that signal. However, just as in SAR and SAL, there is a drawback to using a non-continuous aperture, namely a decrease in range resolution, which leads to a tradeoff in the peak to side lobe ratio of the signal.

Since the theory for this has been well developed by Chimenti et al, the reader is referred to works on theory and experimental results [35,36,37]. The following is a brief review of SF-LFM signals, including generation and detection of ladar signals, development of theory including the modeling of the complex envelope, and finally the metrics used to determine the value of the signal.

A. Generation & Detection

When generating LFM signals, there are two common ways of applying the modulation to the signal, intracavity and extracavity. In intracavity modulation, the cavity length of the laser is modulated in such a way that the output of the laser is linearly swept in frequency. In extracavity modulation, an additional device such as an acousto-optic modulator (AOM) is used to linearly modulate the signal. This work focuses on the use of an AOM as an extracavity device for linearly modulating the ladar signal.

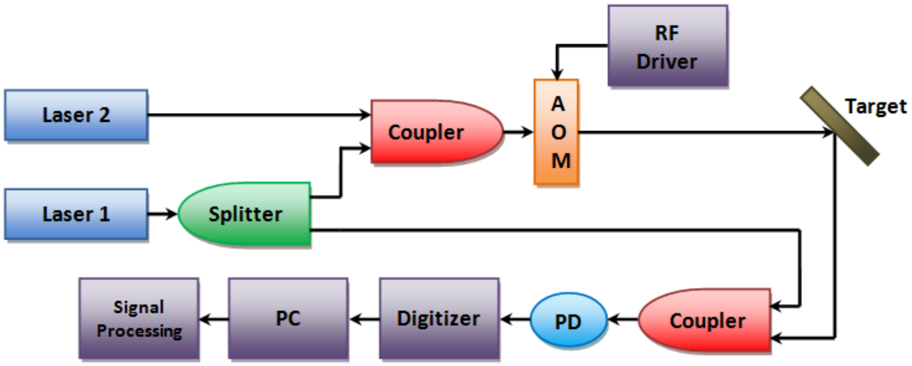

Figure 3.1: Two chirp SF-LFM ladar signal generation, detection, and processing.

To generate a two chirp sparse frequency signal, two frequency offset locked lasers are coupled into a single fiber. The signal is then linearly modulated by an AOM to generate what is called the sparse frequency linearly frequency modulated (SF-LFM) ladar signal. The idea behind combining the signals before the AOM is twofold: first, it requires only a single modulator to generate the signal and second, it ensures that the noise added by the modulator is correlated for both chirps. Upon return from the target, the signal is mixed with an un-modulated local oscillator that was originally split off from one of the sources. The heterodyned signal, which is mixed on a high speed photodiode, is digitized and autocorrelated. Figure 3.1 shows schematically how an SF-LFM signal is generated.

B. Complex Envelope

Using what is defined as an SF-LFM signal, it is easy to develop a model of the complex envelope given what is already known about LFM signals [27]. The electric field of a single LFM chirp that is generated via an AOM can be defined by

$$E(t)|_0^T = \tilde{A}e^{i\left(2\pi(f+f_0)t+\frac{1}{2}\beta t^2\right)} + c.c, \tag{3.1}$$

where f is the carrier frequency of the signal, f_0 is the frequency offset of the AOM, $\tilde{A}$ is the complex amplitude of the field, and β represents the chirp coefficient which is defined as a function of the AOM modulator bandwidth (B) and the signal period (T) as,

$$\beta = \frac{2\pi B}{T}. \tag{3.2}$$

The superposition of an electric field is linear, and is therefore additive, so in order to create a two chirp SF-LFM signal the electric field is given as

$$E(t)|_0^T = \tilde{A}_1 e^{i\left(2\pi(f+f_0)t+\frac{1}{2}\beta t^2\right)} + \tilde{A}_2 e^{i\left(2\pi(f+f_0+df)t+\frac{1}{2}\beta t^2\right)} + c.c, \tag{3.3}$$

where df is the difference frequency between the two offset laser sources.

When the SF-LFM field is added to the local oscillator field and mixed on a photodiode, the current produced by that photodiode is proportional to the modulus squared of the total field given by

$$s(t)|_0^T = \left|\tilde{A}_1 e^{i\left(2\pi(f+f_0)t+\frac{1}{2}\beta t^2\right)} + \tilde{A}_2 e^{i\left(2\pi(f+f_0+df)t+\frac{1}{2}\beta t^2\right)} + \tilde{A}_{LO} e^{i2\pi ft}\right|^2, \tag{3.4}$$

where $\tilde{A}_{LO} e^{i2\pi ft}$ is the complex field of the local oscillator. Assuming the complex amplitudes of the signal are approximately equal ($\tilde{A}_1 \approx \tilde{A}_2 = \tilde{A}$) and they are significantly lower than the amplitude of the local oscillator, then Equation 3.4 can be approximated by,

$$s(t)|_0^T = I_{LO} + \left[\tilde{A}\tilde{A}_{LO}^* e^{i\left(2\pi f_0 t+\frac{1}{2}\beta t^2\right)} + \tilde{A}\tilde{A}_{LO}^* e^{i\left(2\pi(f_0+df)t+\frac{1}{2}\beta t^2\right)} + c.c.\right] \tag{3.5}$$

where I_{LO} is equal to the modulus squared of the local oscillator's complex amplitude.

$$u(t)|_0^T = \tilde{A}\tilde{A}_{LO}^* \left[e^{i\left(2\pi f_0 t+\frac{1}{2}\beta t^2\right)} + e^{i\left(2\pi (f_0+df)t+\frac{1}{2}\beta t^2\right)}\right] \tag{3.6}$$

The last step is to extract the complex envelope of the signal defined in Equation 3.5. This is done in practice through I/Q detection or in the case of a single photodiode, the Hilbert transform of the recorded signal. Equation 3.6 shows the complex envelope of a two chirp SF-LFM signal, which is representative of what occurs in Figure 3.1.

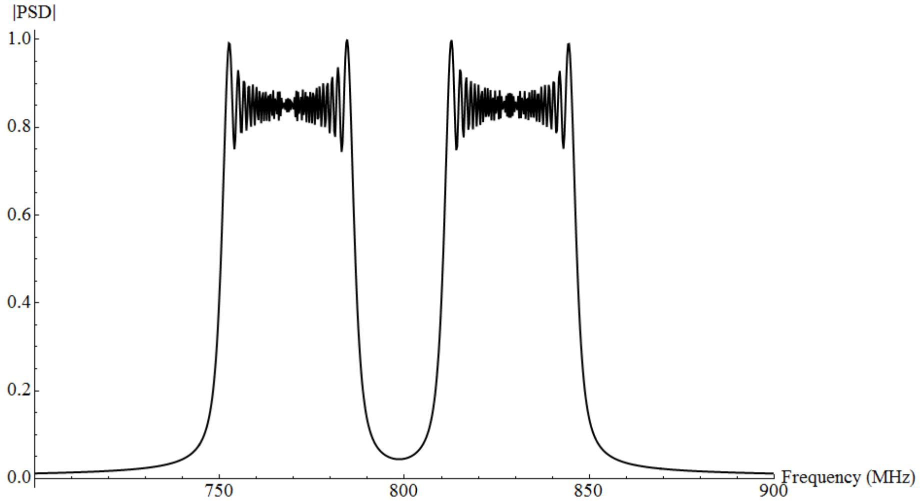

Figure 3.2: SF-LFM spectrum with $f_0 = 750\ MHz$, B $= 37\ MHz$, df $= 60\ MHz$, and T$= 4\ \mu s$.

Similar to Figure 2.5, Figure 3.2 shows the spectrum of an SF-LFM ladar signal. From Figure 3.2 it is easy to see and understand how a two chirp SF-LFM signal results in two segmented bandwidths, which in turn results in an increase in effective bandwidth.

C. Modeling

Much work has been done by Chimenti et al. in the development of modeling SF-LFM signals and the verification of the two chirp SF-LFM ladar signal [14, 15, 35, 36, 37]. In his work, Chimenti chose to utilize the ambiguity function as a modeling tool for SF-LFM signals. During that process he used the analytic expressions to understand the underlying physics while using the numerical models to quickly obtain plots of the ambiguity. Figure 3.3 and Figure 3.4 shows a typical zero Doppler cut of the ambiguity function and a zoomed in version of the central peak respectively.

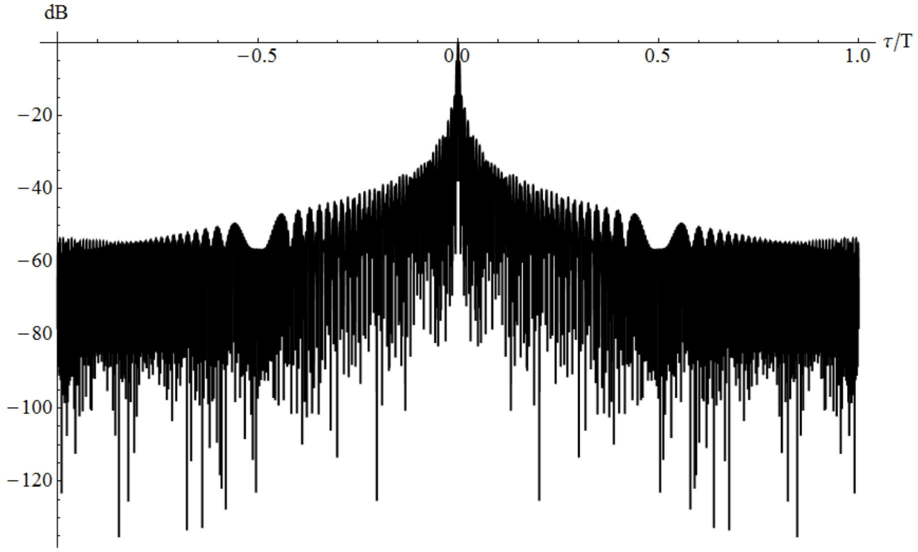

Figure 3.3: Zero Doppler ambiguity function of an SF-LFM signal with $f_0 = 750\ MHz$, B = $37\ MHz$, df = $37\ MHz$, and T= 4 μs.

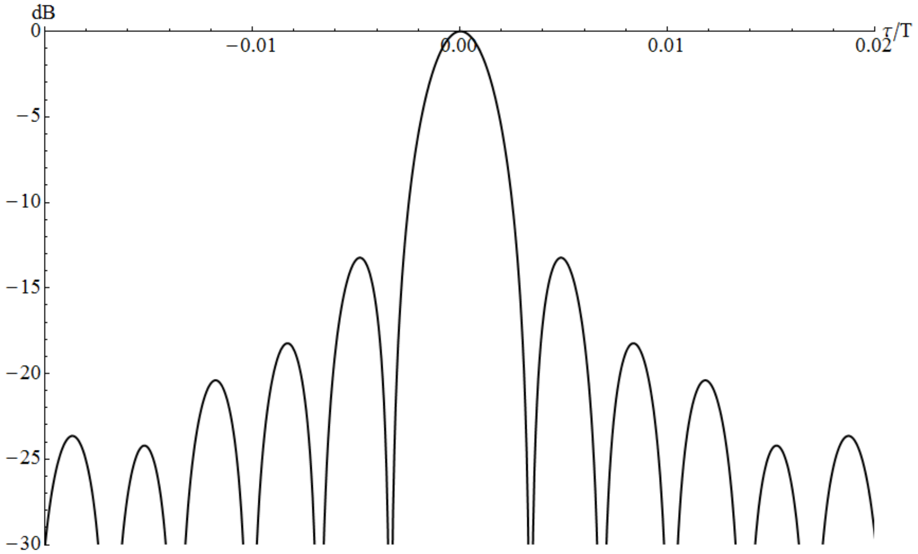

Figure 3.4: Central peak of a zero Doppler ambiguity function of an SF-LFM signal with $f_0 = 750\ MHz$, B = $37\ MHz$, df = $37\ MHz$, and T= 4 μs.

Two of the most important figures of merit in determining the worth of a ladar signal are its range resolution (δR) and peak to sidelobe ratio (PSLR). From numerical modeling of SF-LFM signals, range resolution can be calculated via the following relationship,

$$\delta R = \frac{\delta\tau * c}{2} \tag{3.7}$$

where $\delta\tau$ is the time delay ambiguity given by the FWHM of the central lobe and c is the speed of light. The other metric, PSLR, is calculated by taking the ratio of the maximum sidelobe to the center lobe, or in dB the subtraction of the center lobe from the maximum sidelobe, given as,

$$PSLR = |Max\ Sidelobe_{dB}| - |Central\ Peak_{dB}|. \tag{3.8}$$

Figure 3.5 and Figure 3.6 shows a typical range resolution and PSLR curve for an SF-LFM signal in terms of the difference frequency.

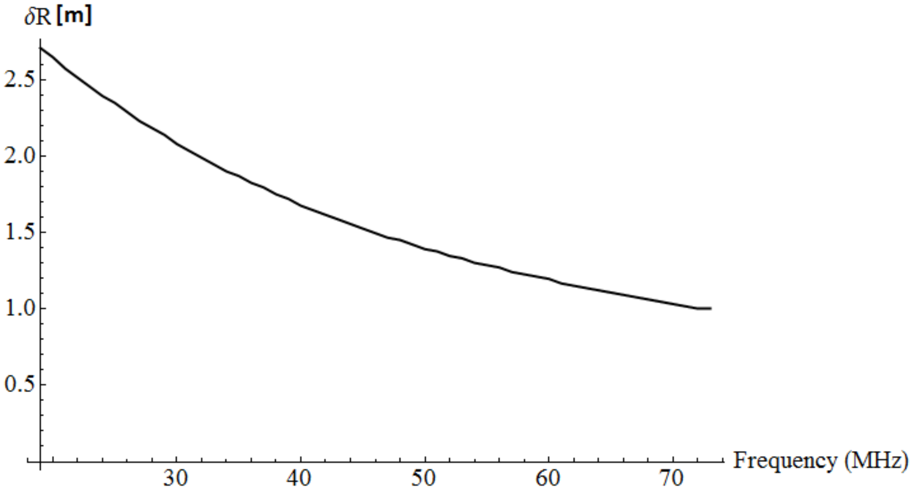

Figure 3.5: Range resolution of an SF-LFM signal as a function of difference frequency df, with $f_0 = 750\ MHz$, B = $37\ MHz$, and T= $4\ \mu s$.

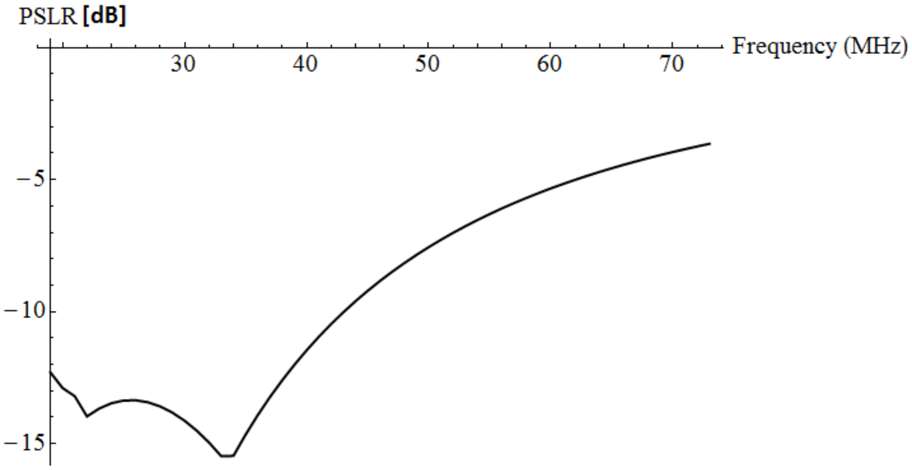

Figure 3.6: PSLR of an SF-LFM signal as a function of difference frequency df, with $f_0 = 750\ MHz$, B $= 37\ MHz$, and T= $4\ \mu s$.

The range resolution of a common system would generally be around the millimeter mark, even less for some applications, and by comparing this to Figure 3.5, the setup would fall short. This is easily redeemable by using a modulator with a higher bandwidth. PSLR of a single chirped waveform is always -13 dB and a good point of comparison. From Figure 3.6, the PSLR is below the -13 dB point when the signals are slightly overlapped to slightly separate, showing a small improvement in the region. However, outside of this region the PSLR tends to move away from the -13 dB point towards 0 dB as the difference frequency is increased.

CHAPTER 4 -
VERIFICATION OF THREE CHIRP SPARSE FREQUENCY LFM MODEL

The modeling originally performed by Chimenti et al. has shown that the extra bandwidth which results from the segmented signal increases the range resolution when compared to an LFM ladar signal [15]. An previously performed experiment verified the modeling of a two chirp SF-LFM ladar signal[14]. In this section of the thesis, the focus is on further verifying an altered version of the aforementioned model.

A. Multiple Chirp Sparse Frequency LFM Model

In the above-mentioned work, models were created to suit higher order SF-LFM ladar signals, up to six chirps. The modeling pointed out that for each superimposed chirp, two sidelobes symmetric about the central peak, of great enough value to be considered false targets, would appear if the segmented bandwidths overlapped [14]. Since the idea behind segmented bandwidth is to increase the range resolution, and significant sidelobes only occur when the segmented bands are overlapped, then the region of interest has been narrowed to where the bandwidths are no longer overlapping. The complex envelope is given by,

$$u(t)\big|_0^T = \tilde{A}\tilde{A}_{LO}^{*} \sum_{n=1}^{N} e^{i\left(2\pi(f_0+(n-1)\,df)t+\frac{1}{2}\beta t^2\right)} \tag{4.1}$$

where N represents the number of chirps and the remaining nomenclature is the same as previously defined. This model of the complex envelope was developed in such a way that the difference frequency between each chirp is a constant. In order to fully verify whether or not the model is valid for higher orders, Equation 4.1 needs to be altered only slightly to,

$$u(t)|_0^T = \tilde{A}\tilde{A}_{LO}^* \sum_{n=0}^{N} e^{i\left(2\pi(f_0 + df_n)t + \frac{1}{2}\beta t^2\right)}. \tag{4.2}$$

The changing of df to df_n allows the difference frequencies between lines to vary between each other. Also the removal of the $(n-1)$ term makes it easier to see that each line's difference frequency is with respect to what would be considered the local oscillator or equivalently, the first chirp has no additional offset frequency, $df_0 = 0$.

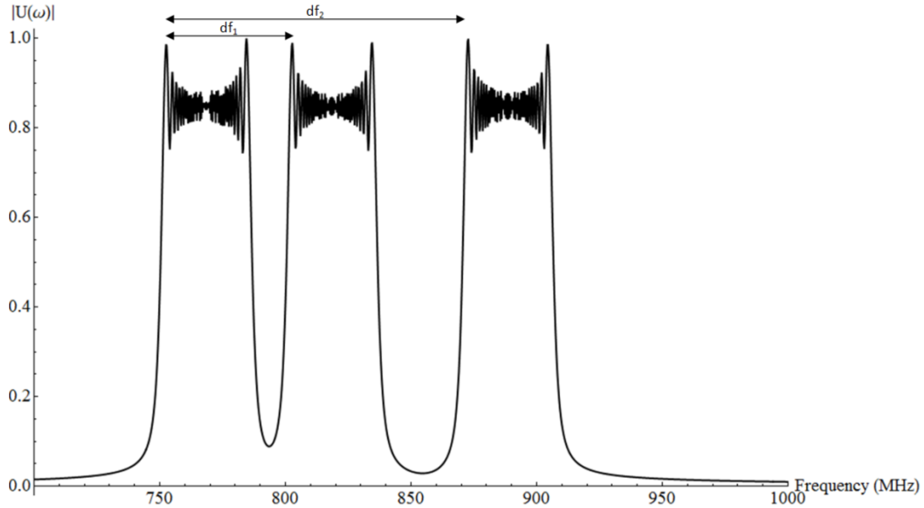

Figure 4.1: Frequency spectrum of a three chirp SF-LFM signal with $f_0 = 750\ MHz$, B $= 37\ MHz$, T= 4 μs, df$_1 = 50\ Mhz$, and df$_2 = 120\ Mhz$.

Figure 4.1 shows an example of a three chirp SF-LFM signal with two difference frequencies.

Just as in Figure 3.5 and Figure 3.6 where a model of the range resolution and PSLR was created for a two chirp SF-LFM signal, a model was created for a three chirp SF-LFM signal. This time the model was plotted in three dimensions where the x and y axes were each of the difference frequencies with respect to the local oscillator and their verticals were range resolution and PSLR respectively.

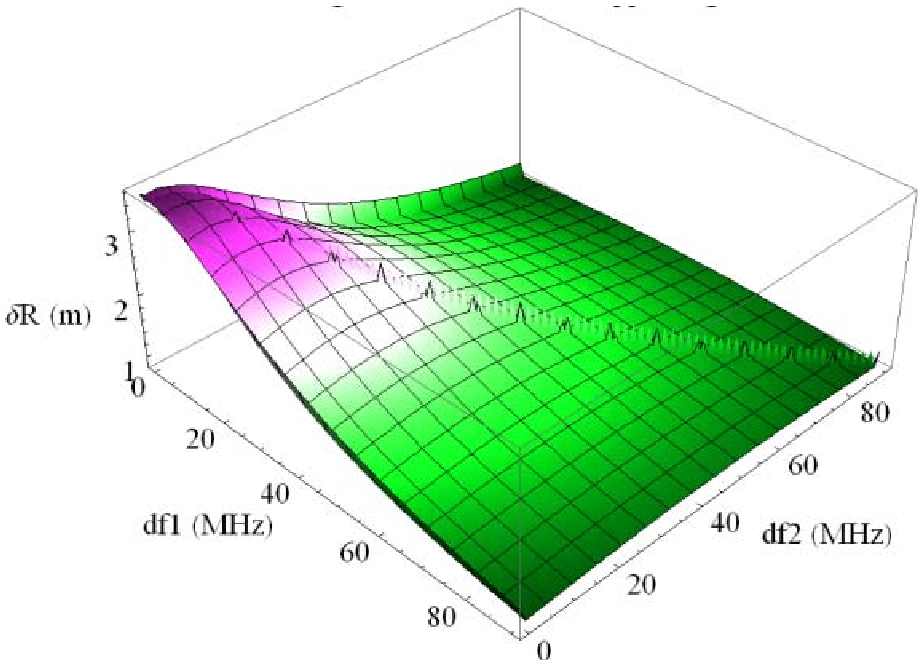

Figure 4.2: Range Resolution of a three chirp SF-LFM signal.

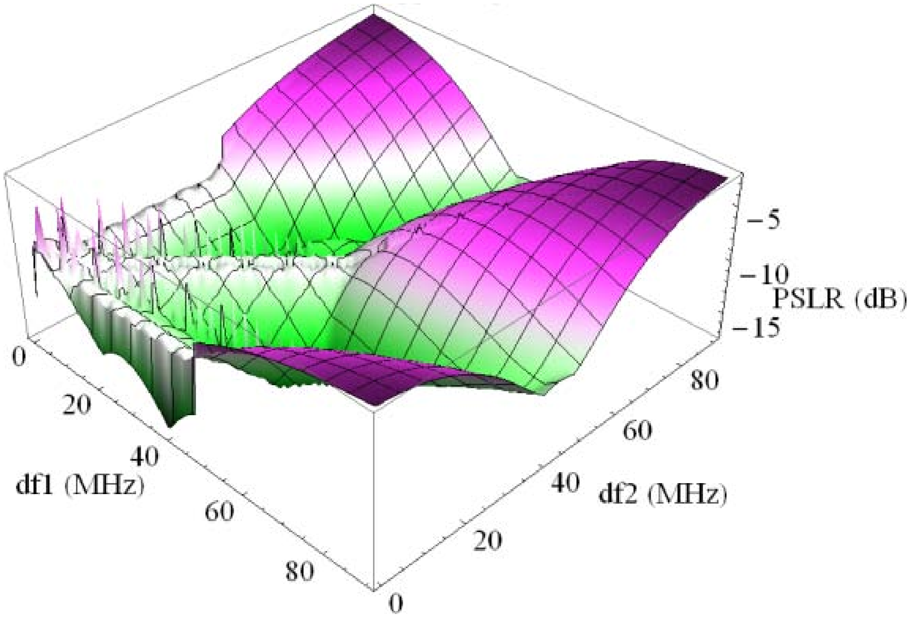

Figure 4.3: PSLR of a three chirp SF-LFM signal.

Figure 4.2 shows the range resolution of a three chirp SF-LFM signal as a function of its two difference frequencies. One should note that as each difference frequency is increased, the range resolution of the signal is also increased. Also, it can be seen that when any chirp completely overlaps with another, a ridge of decreased range resolution is seen, i.e. when $df_0 = df_1 = 0$ or, $df_0 = df_2 = 0$ or $df_1 = df_2$. This is due to the fact that range resolution is proportional to the amount of bandwidth in a signal. Note, the central ridge is continuous, however Figure 4.2 shows a periodic structure on this ridge which come about from the construction of the graphic and is not real. The PSLR model of a three chirp SF-LFM signal can be seen in Figure 4.3. From it, similarities can be deduced between the two chirp and three chirp models. An unstable area, where the PSLR changes rapidly, exists when either chirp is overlapped with the df_0 chirp, or when $df_1 = df_2$. Additionally, one can see a similar double dip followed by an asymptotically increasing PSLR.

B. Experimental Setup

As previously demonstrated with the two chirp experiments, the entire experiment was performed in polarization maintaining (PM) fiber optics [37]. PM fiber optics maintains the polarization state in fiber allowing for efficient heterodyne mixing. In order to perform a three chirp experiment, three laser sources were required. Two laser sources came via a custom designed highly stable diode laser system which utilized micro-Kelvin ovens and current controllers to set the specific frequency of each of the lines. The third source was an Agilent telecom laser. Of the sources, the custom designed one had the ability to continuously tune over a given frequency range. In addition, the stability of that frequency is sub kilohertz over the recording time and sometimes even less. The Agilent was tunable in frequency in discrete steps. Its stability in frequency was not as well behaved as the custom source, but over the short recording intervals was more than sufficient.

To linearly modulate the signal, an acousto-optic modulator was employed. The device, designed by Brimrose, provided for a linear frequency shift from 730 MHz at .0 V to 850 MHz at 5V [38].

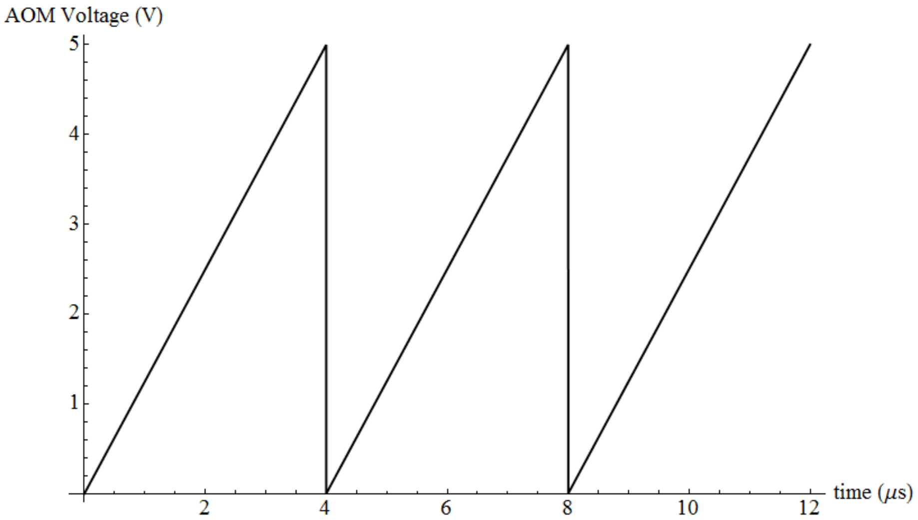

Figure 4.4: Waveform applied to the acousto-optic modulator.

Due to the high frequency content of the signals, potentially GHz and up, high speed detectors needed to be utilized. Fiber coupled photodetectors (no. SIR5-FC) from ThorLabs were utilized. The detectors, which have a bandwidth of around 6.5 GHz, could readily detect the approximately 1 GHz worth of signal bandwidth created by a three chirp SF-LFM signal [39].

In order to interpret information about the signal, an Acqiris DC252 high speed digitizer recorded the signal, which allowed for digital processing, or post processing, to be performed. The Acqiris is a two channel digitizer that has a maximum sampling rate of 4 GS/s when recording on both channels [40].

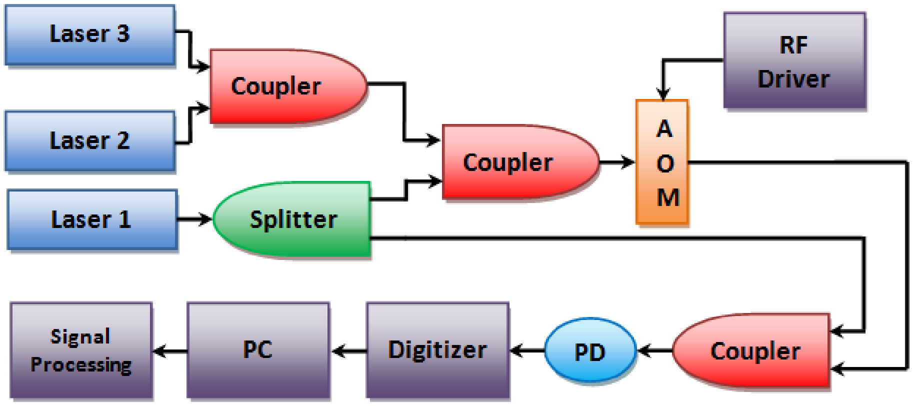

Figure 4.5: Experimental setup for a three chirp SF-LFM ladar signal's generation, detection and processing.

Figure 4.4 shows the experimental setup. All of the devices in the experiment are fiber-coupled, so no free-space optics were involved. For a three chirp setup, laser 1 (single output of the custom system) is split to serve two functions. One, it is used as the local oscillator for the heterodyned signal and second, it is used as the first of three lines to create the sparse frequency signal. The outputs of lasers 2 and 3 (one of the outputs of the custom system and the other the Agilent) were coupled together to create two more lines in the sparse frequency signal. All laser lines were then combined together to create a three line sparse frequency signal. The three line sparse frequency signal was then sent through an AOM, where the lines where shifted by approximately 750 MHz and linearly modulated for a total bandwidth of 37 MHz (per chirp) to create a three chirp SF-LFM signal. The SF-LFM signal was combined with the local oscillator and mixed on a photodiode. The signal was then digitized by the Acqiris and sent to a computer for processing. Note, only one photodiode is required to process a signal since the matched filter, just like the ambiguity function, reduces to the autocorrelation of the original function (ie the three chrip function), when there is not Doppler or time delay.

C. Digital Signal Processing

The amplitude of the three chirp SF-LFM signal is recorded by the digitizer and sent to the computer.

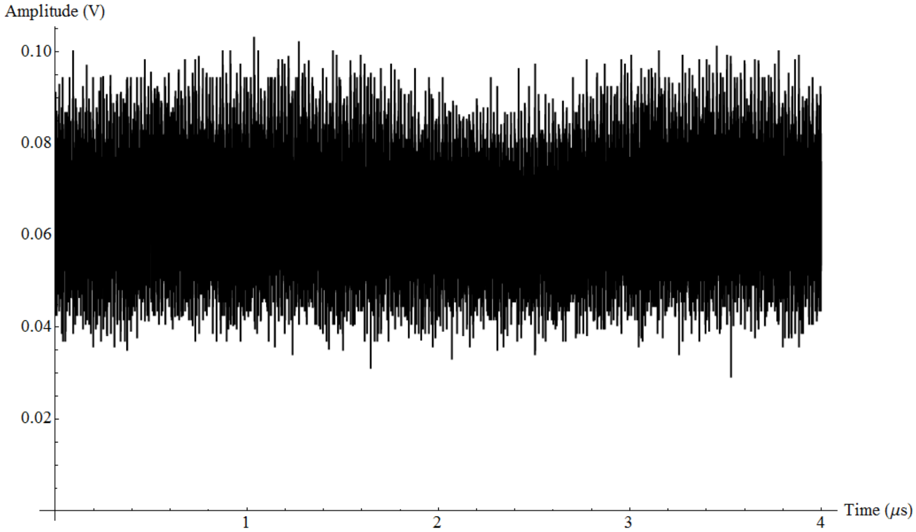

Figure 4.6: Three chirp SF-LFM signal recorded by the Acqiris.

Figure 4.5 shows the raw, unprocessed amplitude of a 4 μs signal. When the signal in Figure 4.5 is processed with a matched filter (autocorrelated), the output signal has significant additive noise.

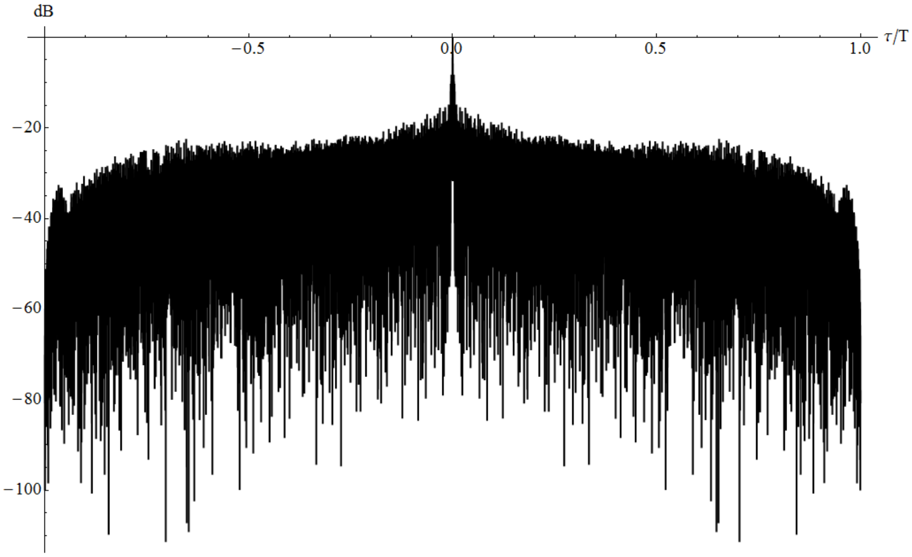

Figure 4.7: Autocorrelation of a three chirp SF-LFM signal.

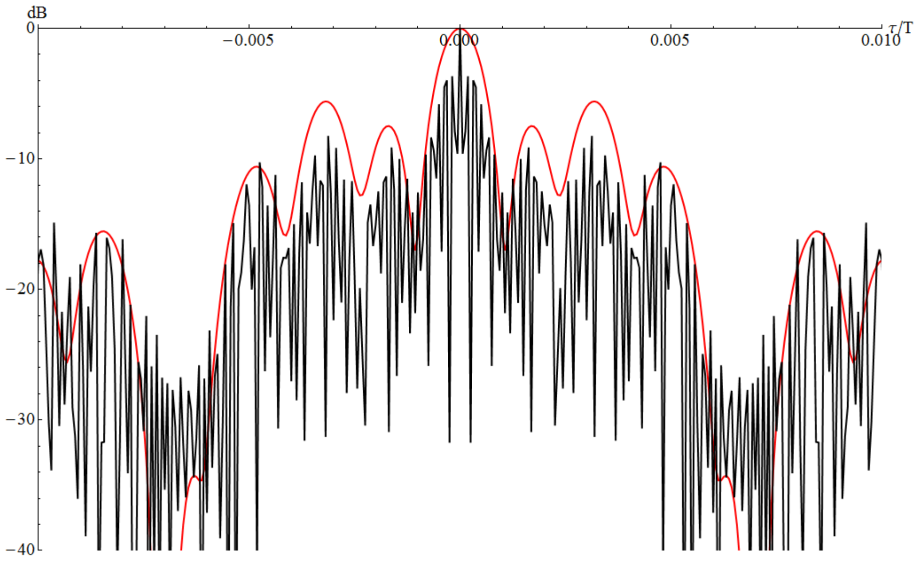

Figure 4.8: Central peak of a three chirp SF-LFM signal (Black) with the theoretical overlay (red)

Figure 4.6 and Figure 4.7 show a full matched filter output (MFO) and the same MFO zoomed in on the central peak. Figure 4.7 also shows the theoretical autocorrelation curve for that specific SF-LFM signal. From Figure 4.7 it is simple to see that noise from the raw signal is a limiting factor in performing matched filter processing. However, the noisy signal does roughly follow the theory envelope.

One thing that is important to remember is that in the theory an I/Q detection setup was assumed. In order to compensate for a lack of an I/Q setup, a Hilbert transform of the signal is required. A Hilbert Transform was performed on the signal given in Figure 4.5 and then autocorrelated.

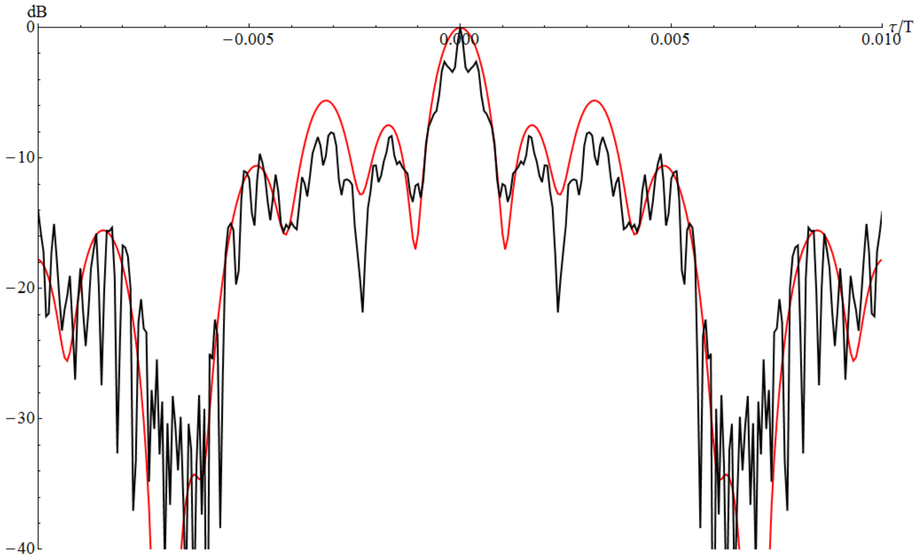

Figure 4.9: Central peak of a matched filter output for a three chirp SF-LFM signal that has been discrete Hilbert transformed (Black) and theory (Red).

Figure 4.8 shows the same peak with overlaid theory where the SF-LFM signal has been processed with a discrete Hilbert transform (DHT). By comparing Figure 4.7 and Figure 4.8, a vast improvement can be seen in the MFO with respect to the noise.

However, even though the noise has been reduced by a significant amount, it can be reduced further. By looking at the frequency spectrum of the signal, more insight can be gained into where the additive noise is originating from.

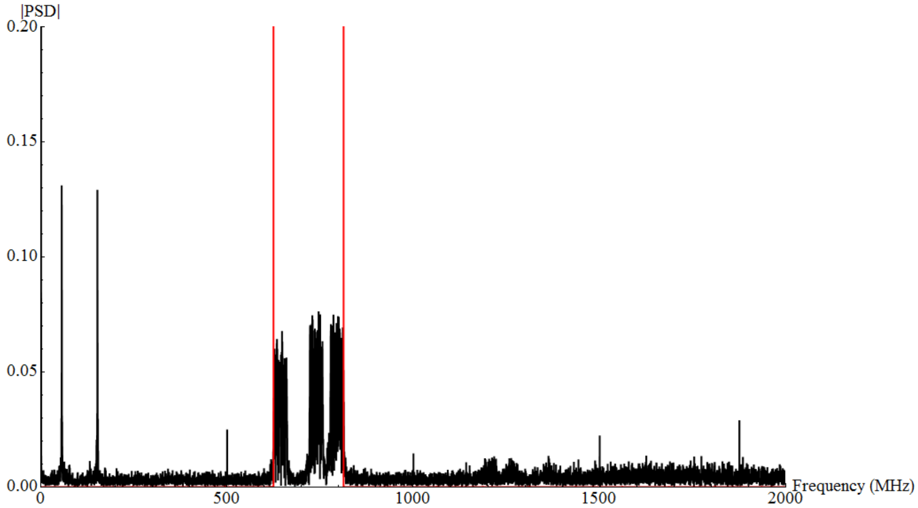

Figure 4.10: Frequency spectrum of a three chirp SF-LFM signal from figure 4.5 with $f_0 = 600\ MHz$, B = $37\ MHz$, T= 4 μs, df$_1 = 92\ Mhz$, and df$_2 = 150\ Mhz$ (Black) and window created to further reduce noise (Red).

Figure 4.9 shows the positive frequency spectrum of the unprocessed signal. From the spectrum shown in Figure 4.9, sources of additive noise can be seen. Some of the more prominent noise devices are the two difference frequencies (two peaks on the left side of the plot) which come about from the heterodyning process. Also, aliasing about the 1000 MHz causes additional noise to be added to the MFO. In order to eliminate as much noise as possible, a windowing function was created about the region of interest.

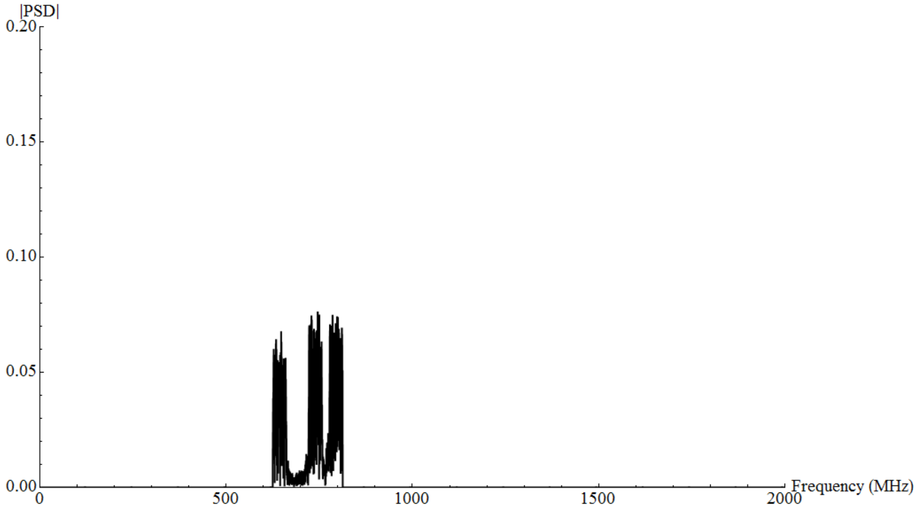

Figure 4.11: Frequency spectrum of a three chirp SF-LFM signal from Figure 4.5 with $f_0 = 600\ MHz$, B $= 37\ MHz$, T= 4 μs, df$_1$ $= 92\ Mhz$, and df$_2$ $= 150\ Mhz$

The red lines in Figure 4.9 show the window range and Figure 4.10 shows the spectrum of the signal post-windowing.

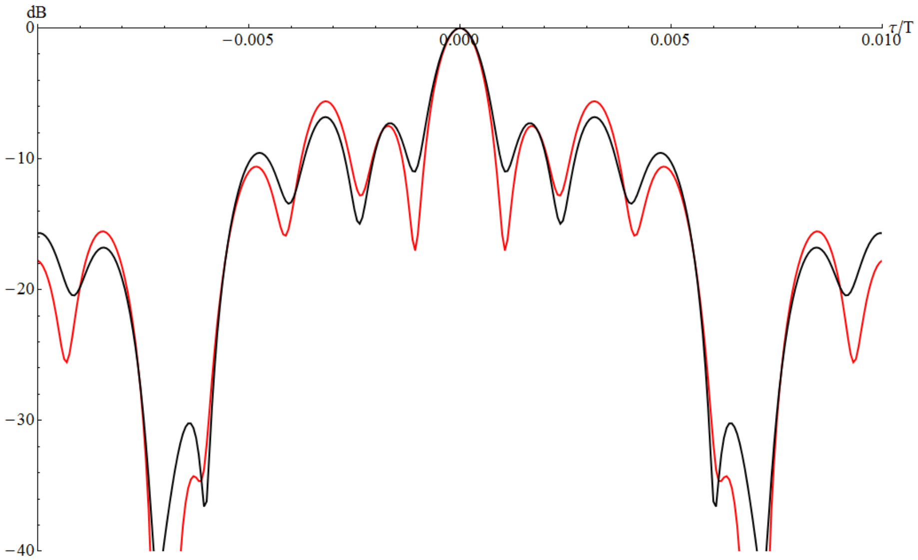

Figure 4.12: Central peak of a matched filter output for a three chirp SF-LFM signal that has been digitally filtered with a window function (Black) and theory (Red).

By applying this digital filter to the signal, a low noise MFO can be obtained. Figure 4.11 shows the central peak of the MFO after the digital filter was applied to the signal. Due to the vast improvement of the MFO quality, this type of windowing filter is utilized from this point on unless explicitly specified. Based on this type of processing, a large set of three chirp SF-LFM signals with different difference frequencies were recorded in order to determine their range resolution and PSLR.

D. Verification of Range and PSLR Model

To accurately compare the modeling to the system, a matchup of the number of data points used needs to be taken into account. The figures shown in 4.2 and 4.3 assume that the digitizer would be able to produce 100,000 data points in the 4 µs period. In the actual setup the following parameters are used. A two chirp ($N = 2$) SF-LFM signal is given by Equation 4.2, where the pulse duration is $T = 4\ \mu s$, the modulator bandwidth is $B = 37\ MHz$, and $f_0 = 750\ MHz$. The Acqiris digitizer runs at 4 GS/s in two channel mode, or 16,000 data points in the 4 µs period [40].

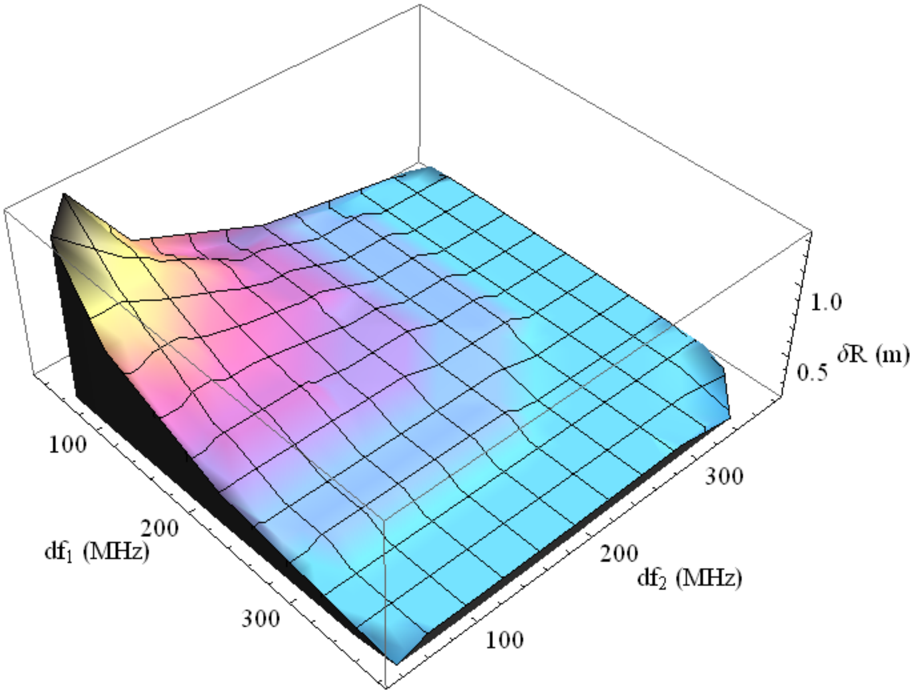

Figure 4.13: Range resolution model for the actual system setup, plotted for only the points measured.

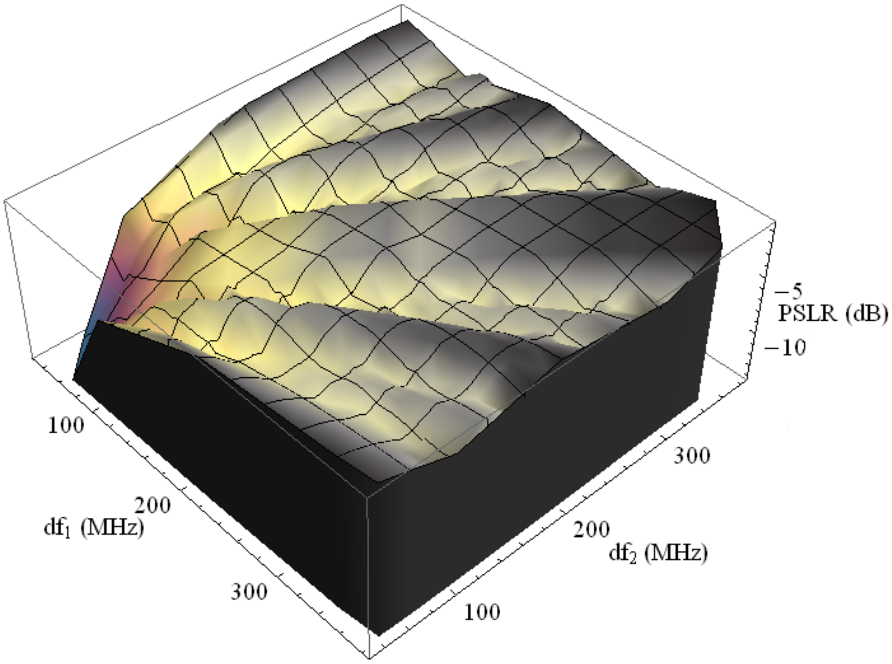

Figure 4.14: PSLR model for the actual system setup, plotted for only the points measured.

Figure 4.12 and Figure 4.13 show the model updated to the specific parameters of the system.

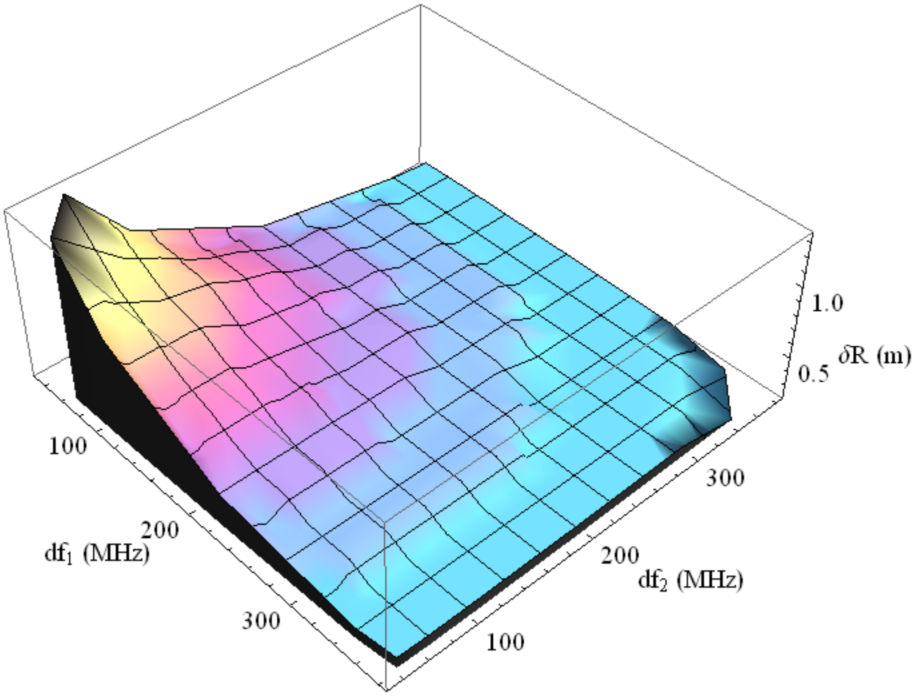

Figure 4.15: Measured range resolution for a system with parameters $f_0 = 775\ MHz$, B $= 37\ MHz$, T= $4\ \mu s$.

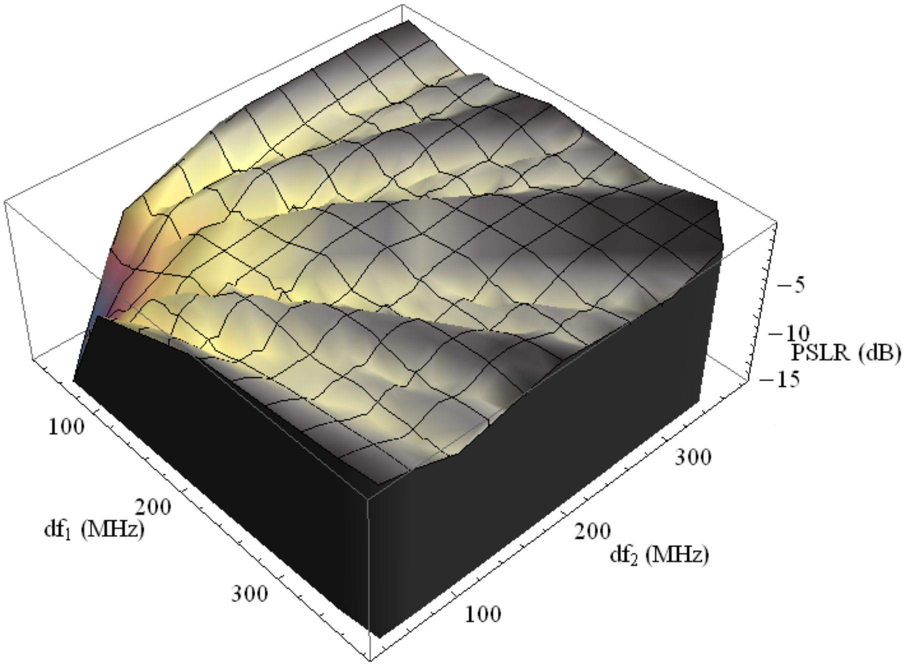

Figure 4.16: Measured PSLR for a system with parameters $f_0 = 775\ MHz$, B $= 37\ MHz$, T= $4\ \mu s$.

The measured data found in Figure 4.14 and Figure 4.15 for the range resolution and PSLR shows the general trends of their respective modeling found in Figure 4.12 and Figure 4.13 matching very well.

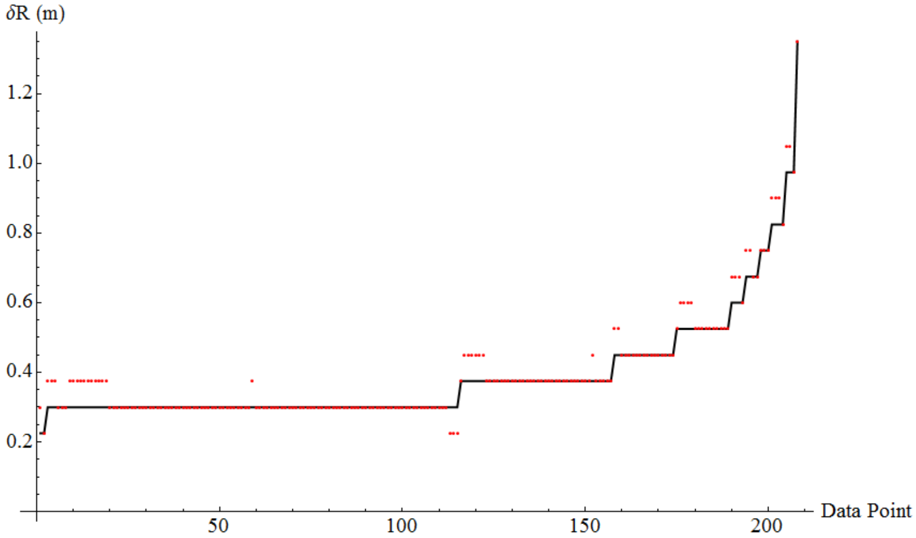

Figure 4.17: Range resolution comparison of each individually measured data point (Red) to its corresponding theory (Black).

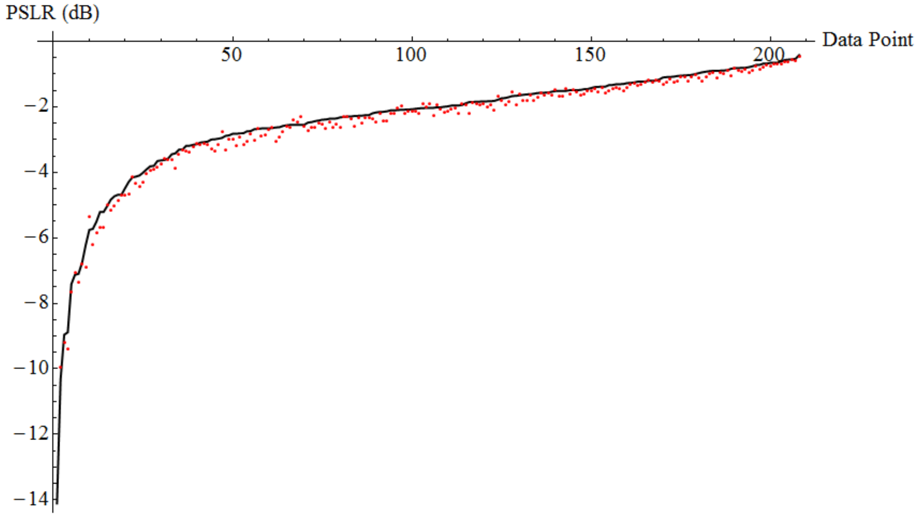

Figure 4.18: PSLR comparison of each individually measured data point (Red) to its corresponding theory (Black).

However, in order to make a more accurate comparison, a plot of each data point was sorted by its range resolution theory and PSLR theory respectively and yielded more insight into how well the model performed. Figure 4.16 shows the range resolution theory and its corresponding measured value. From the figure it can be seen that the model accurately represents the range resolution of the signal. Note that the discrete steps are from the digitization of the signal, where higher sample frequency would mean smaller steps. Figure 4.17, shows PSLR theory and its measured value, also showing that the model accurately represents the PSLR of the signal.

CHAPTER 5 -
DOPPLER SIMULATIONS AND MEASUREMENTS

One of the most important characteristics of Doppler ladar or radar is its ability to detect the speed at which a target is moving. This ability comes from a well known phenomenon called the *Doppler Effect*, or *Doppler shift*. The effect was credited to a physicist, Christian Doppler, who in 1842 proposed that the frequency of a wave for a moving observer was relative to the source of the wave [41]. The most common example of the Doppler Effect is a siren passing by a stationary person. When the siren is approaching, the person hears a higher frequency. When the siren has passed and is receeding from the stationary person, a lower frequency is heard.

This chapter covers how the Doppler Effect is introduced into SF-LFM ladar signal, its detection, and processing. An experimental setup is described along with requirements for system components. Finally, experimental results are compared with the model and with an alternate velocity measurement, which uses a translation stage with a built in optical encoder.

A. Two Chirp Sparse Frequency LFM Doppler Modeling

In this heterodyne ladar setup, a matched filter analysis is required in order to characterize the effects of the Doppler shift. Additionally, for reasons which are explained later, the setup is required to be a coherent on receive system, i.e. the recorded matched filter kernel needs to be coherent with the return signal.

Matched filter processing is a means of optimizing the signal to noise ratio. The impulse response of a matched filter is always be given by Equation 2.3, repeated here,

$$h(t) = Ks^*(t_0 - t) \tag{5.1}$$

where the scaling constant K can be set equal to 1, since in practice a normalization is commonly performed on the matched filter output (MFO). The reference point t_0 can be set equal to zero assuming an appropriate offset range. These two assumptions applied to Equation 5.1 then become,

$$h(t) = s^*(-t). \tag{5.2}$$

The standard two chirp SF-LFM signal is defined as

$$s(t) = \frac{1}{\sqrt{2T}} Rect\left[\frac{t}{T}\right]\left[\tilde{A}_1 e^{i\left(2\pi f_0 t + \frac{1}{2}\beta t^2\right)} + \tilde{A}_2 e^{i\left(2\pi (f_0 + df)t + \frac{1}{2}\beta t^2\right)}\right], \tag{5.2}$$

where the nomenclature remains consistent with the previous signal equations. The matched filter of the system is then given by

$$h(t) = \frac{1}{\sqrt{2T}} Rect\left[\frac{-t}{T}\right]\left[\tilde{A}_1^* e^{i\left(2\pi f_0 t - \frac{1}{2}\beta t^2\right)} + \tilde{A}_2^* e^{i\left(2\pi (f_0 + df)t - \frac{1}{2}\beta t^2\right)}\right]. \tag{5.3}$$

As previously stated, the output of a linear system is given by the convolution of the input with the impulse response function. The definition of convolution is given as,

$$(f * g)(t) \overset{\text{def}}{=} \int_{-\infty}^{\infty} f(\tau)g(t-\tau)d\tau = \int_{-\infty}^{\infty} f(t-\tau)g(\tau)d\tau. \tag{5.4}$$

The input of the system is the time delayed Doppler shifted version of Equation 5.2 and is given as

$$s_R(t) = \frac{1}{\sqrt{2T}} Rect\left[\frac{t-t_1}{T}\right]\left[\begin{matrix} \tilde{A}_3 e^{i\left(2\pi f_0 (t-t_1) + \frac{1}{2}\beta (t-t_1)^2\right)} + \\ \tilde{A}_4 e^{i\left(2\pi (f_0 + df)(t-t_1) + \frac{1}{2}\beta (t-t_1)^2\right)} \end{matrix}\right] e^{i2\pi\nu(t-t_1)}, \tag{5.5}$$

where t_1 is the time delay of the signal and ν is the Doppler frequency shift, which can be defined in terms of the target velocity as given as

$$\nu = \frac{2*V}{\lambda}, \tag{5.6}$$

where $\tilde{A}_3 \; and \; \tilde{A}_4$ are complex amplitudes that were $\tilde{A}_1 \; and \; \tilde{A}_2$ respectively, but have changed because the signal has traveled over a given time. In general, the relative amplitudes of $\tilde{A}_1 \; and \; \tilde{A}_2$ will be greater than that of $\tilde{A}_3 \; and \; \tilde{A}_4$ because there will be attenuation in the interrogating signal. Equation 5.6 shows the relationship between the Doppler frequency shift and the velocity of the target, where V is the velocity of the target and λ is the carrier wavelength.

$$(s_R * h)(t) = \int_{-\infty}^{\infty} \begin{matrix} \frac{1}{\sqrt{2T}} Rect\left[\frac{t-\tau-t_1}{T}\right] \begin{bmatrix} \tilde{A}_3 e^{i\left(2\pi f_0 (t-\tau-t_1)+\frac{1}{2}\beta(t-\tau-t_1)^2\right)} + \\ \tilde{A}_4 e^{i\left(2\pi (f_0+df)(t-\tau-t_1)+\frac{1}{2}\beta(t-\tau-t_1)^2\right)} \end{bmatrix} e^{i2\pi\nu(t-\tau-t_1)} * \\ \frac{1}{\sqrt{2T}} Rect\left[\frac{-\tau}{T}\right] \left[\tilde{A}_1^* e^{i\left(2\pi f_0 \tau - \frac{1}{2}\beta\tau^2\right)} + \tilde{A}_2^* e^{i\left(2\pi (f_0+df)\tau - \frac{1}{2}\beta\tau^2\right)}\right] d\tau \end{matrix} \tag{5.7}$$

The convolution of Equations 5.3 and 5.5, or the matched filter output, is given by Equation 5.7 and is simplified combining terms and using the substitutions,

$$\eta = t - t_1 \tag{5.8}$$

and

$$\tilde{\gamma} = e^{i\left(2\pi f_0 \eta + \frac{1}{2}\beta\eta^2 + 2\pi\nu\eta\right)}, \tag{5.9}$$

which yields a simplified MFO

$$(s_R * h)(t) = \frac{\tilde{\gamma}}{2T} \int_{-T/2}^{T/2} Rect\left[\frac{-\tau+\eta}{T}\right] \begin{bmatrix} \tilde{A}_1^* \tilde{A}_3 e^{-i\beta\eta\tau} + \\ \tilde{A}_2^* \tilde{A}_3 e^{i(2\pi df - \beta\eta)\tau} + \\ \tilde{A}_1^* \tilde{A}_4 e^{i2\pi df\eta} \, e^{i(-2\pi df - \beta\eta)\tau} + \\ \tilde{A}_2^* \tilde{A}_4 e^{i2\pi df\eta} \, e^{-i\beta\eta\tau} \end{bmatrix} e^{-i2\pi\nu\tau} \, d\tau. \tag{5.10}$$

Further simplification of Equation 5.10 can be made by realizing that a relationship exists between $\tilde{A}_1 \; and \; \tilde{A}_3$ and $\tilde{A}_2 \; and \; \tilde{A}_4$ respectively. This relationship comes from the fact that each laser beam is overlapped in space, and therefore the change in optical path length between $\tilde{A}_1 \; and \; \tilde{A}_3$ and $\tilde{A}_2 \; and \; \tilde{A}_4$ is the same and can be given as,

$$\tilde{A}_3 = \tilde{B}\tilde{A}_1 \tag{5.11}$$

and

$$\tilde{A}_4 = \tilde{B}\tilde{A}_2 \tag{5.12}$$

where $\tilde{B}$ is a phase chang. Additionally, an assumption that the complex magnitudes are unity and have a phase angle ϕ and a phase difference $\Delta\phi$ and each can be seen respectively:

$$|\tilde{A}_1| = |\tilde{A}_2| = 1, \tag{5.13}$$

$$\angle\tilde{A}_1 = \phi_1 \; and \; \angle\tilde{A}_2 = \phi_2, \tag{5.14}$$

$$\Delta\phi = \phi_1 - \phi_2. \tag{5.15}$$

By applying the additional simplifications, Equation 5.10 is further reduced to,

$$(s_R * h)(t) = \frac{\tilde{B}\tilde{\gamma}}{2T}\int_{-T/2}^{T/2} Rect\left[\frac{-\tau+\eta}{T}\right]\begin{bmatrix} \left(1 + e^{i2\pi df\eta}\right)e^{-i\beta\eta\tau} + \\ e^{i\Delta\phi}e^{i(2\pi df - \beta\eta)\tau} + \\ e^{-i\Delta\phi}e^{i2\pi df\eta}e^{i(-2\pi df - \beta\eta)\tau} \end{bmatrix} e^{-i2\pi\nu\tau}\, d\tau. \tag{5.16}$$

Performing the integral in Equation 5.16 yields the final matched filter output of the system to be,

$$(s_R * h)(t) = \begin{bmatrix} \tilde{B}e^{i(2\pi f_0 + \pi df + \pi\nu)\eta}\left(1 - \frac{|\eta|}{T}\right) * \\ \begin{Bmatrix} \cos[\pi df\eta]\,\mathrm{sinc}\left[\left(\frac{1}{2}\beta\eta + \pi\nu\right)(T - |\eta|)\right] + \\ \frac{e^{i\Delta\phi}}{2}\mathrm{sinc}\left[\left(\pi df - \frac{1}{2}\beta\eta - \pi\nu\right)(T - |\eta|)\right] + \\ \frac{e^{-i\Delta\phi}}{2}\mathrm{sinc}\left[\left(\pi df + \frac{1}{2}\beta\eta + \pi\nu\right)(T - |\eta|)\right] \end{Bmatrix} \end{bmatrix};\; |t - t_1| \le T \tag{5.17}$$

A complete derivation of Equation 5.17 can be found in Appendix A.

By looking at the phase term at the beginning of Equation 5.17, it can be seen that by holding the frequency offset of the laser, the difference frequencies between the lasers, and the velocity of the target constant, that portion of the phase is constant for every pulse. By looking at the phase between two consecutive pulses, i.e. where $\eta_1 = t - t_1$ and $\eta_2 = t - t_1 - T$, or alternatively as

$$\Delta\varphi = \varphi_1 - \varphi_2 \tag{5.18}$$

where φ_1 is the phase term resulting from η_1 and φ_2 is the phase term resulting from η_2.

A relation between φ_1 and φ_2 can be given through the velocity of the target as,

$$\varphi_2 = \varphi_1 + \frac{4\pi v \Delta t}{\lambda_{Carrier}}, \tag{5.19}$$

where Δt is the time difference between the two pulses and v is the target velocity. The phase change can be calculated in terms of the target velocity by using Equation 5.19 in Equation 5.18 and is given by,

$$\Delta\varphi = -\frac{4\pi v \Delta t}{\lambda_{Carrier}}. \tag{5.20}$$

Likewise, from phase change, and slightly generalized, the velocity of the target can be calculated as

$$V = \frac{\Delta\theta}{2\pi}\frac{\lambda_{Carrier}}{2t_{total}}, \tag{5.21}$$

where $\Delta\theta$ is the phase change between the first and last pulse and t_{total} is the time difference between the first and last pulse.

By utilizing matched filtering setup, a time delayed Doppler shifted signal can be used to determine the velocity of a target at range. The next section describes the experimental matched filter setup, as dictated by the derivation and requirements on the sources.

B. Experimental Setup and Requirements

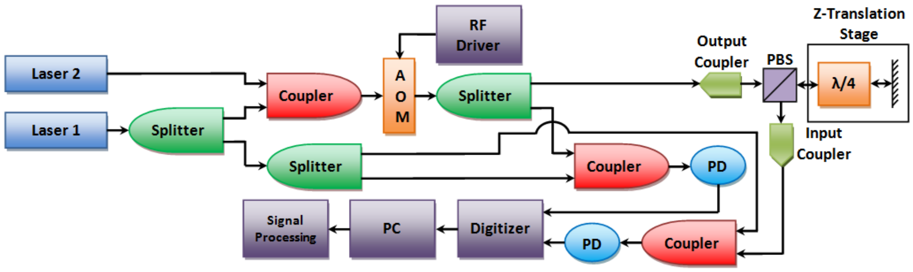

Figure 5.1: Matched filter setup for detecting the Doppler shift of a target with respect to a stationary reference.

Figure 5.1 shows a schematic of the experimental setup. Similar to the experimental three chirp verification, the experiment was performed with polarization maintaining fiber in order to maximize the effects of the heterodyning process. Like the modeling, the signal created was a two chirp SF-LFM signal and therefore requires the use of two laser sources. The first source, which was used as laser two in Figure 5.1, is one of the lines from the custom laser system described in the previous chapter. The other source was an NP Photonics (NPP) *The Rock* single frequency narrow linewidth fiber laser [42]. The reason for the change in laser one, or equivalently the local oscillator, is explained later in section C.

Just as before, the linear modulation of the signal was performed by an AOM which provided a linear frequency shift from 730 MHz as .5 V to 850 MHz at 10V. The same ThorLabs SIR5-FC 6.5 GHz bandwidth photodetectors were utilized in combination with the Acqiris DC252 high speed digitizer, which allowed for a sampling rate of 4 GS/s while recording on both channels.

For a two chirp setup, laser 1 (NPP) is split to serve two functions. One, it is used as the local oscillator for the heterodyned signals and second, it is used as the first of two lines to create the sparse frequency signal. The output of laser 2 (from the custom system) was coupled together with laser 1 to create a two line ladar signal. The two line sparse frequency signal was then directed through an AOM, where the lines were shifted by approximately 750 MHz and linearly modulated for a total bandwidth of 37 MHz (per chirp) to create a two chirp SF-LFM signal. The SF-LFM signal was split into two separate signals, one to be used as the matched filter kernel (reference) and the other to be used to interrogate the target. The matched filter kernel was mixed with the local oscillator on a photodiode where the signal was digitized and recorded. The target signal was collimated to free space via an output coupler. The signal passed through a simple transmit/receive switch, reflected off a mirror, and returned through the transmit/receive switch, after which the signal was collimated back into the fiber mixed with the local oscillator and digitized.

The transmit/receive switch can be characterized by simple Jones matrices. Each of the components in the T/R switch has a corresponding matrix. The matrices of the polarization beam splitters (vertical and horizontal), quarter wave plates, and the target (mirror) are [43,44]:

$$PBS_V = \begin{bmatrix} 0 & 0 \\ 0 & 1 \end{bmatrix} \tag{5.22}$$

$$PBS_H = \begin{bmatrix} 1 & 0 \\ 0 & 0 \end{bmatrix} \tag{5.23}$$

$$QWP = \begin{bmatrix} e^{i\pi/4} & 0 \\ 0 & ie^{i\pi/4} \end{bmatrix} \tag{5.24}$$

$$\text{TGT}= \begin{bmatrix} 1 & 0 \\ 0 & -1 \end{bmatrix}. \tag{5.25}$$

In the transmit/receive switch the quarter wave plate is rotated by 45° with respect to vertical and requires the use of a rotation matrix, where the general form of the rotation matrix is given by

$$R(\theta) = \begin{bmatrix} \cos(\theta) & -\sin(\theta) \\ \sin(\theta) & \cos(\theta) \end{bmatrix}, \tag{5.26}$$

where θ is the angle of rotation. To find the matrix for the rotated quarter wave plate, the rotation matrix is applied with the following relationship,

$$QWP^{'} = R(\theta)QWP\, R(\theta)^{-1}. \tag{5.27}$$

Derivations of the matrices and the rotation matrix can be found in most geometric optics books [43, 44]. The final result of the system is given by,

$$Out = PBS_H . QWP_2 . TGT . QWP_1 . PBS_V . \begin{bmatrix} 0 \\ 1 \end{bmatrix} \tag{5.28}$$

or,

$$\begin{bmatrix} 1 \\ 0 \end{bmatrix} = \left\{ \begin{matrix} \begin{bmatrix} 1 & 0 \\ 0 & 0 \end{bmatrix} \left(\begin{bmatrix} \cos(\theta) & -\sin(\theta) \\ \sin(\theta) & \cos(\theta) \end{bmatrix} \begin{bmatrix} e^{\frac{i\pi}{4}} & 0 \\ 0 & ie^{-\frac{i\pi}{4}} \end{bmatrix} \begin{bmatrix} \cos(\theta) & \sin(\theta) \\ -\sin(\theta) & \cos(\theta) \end{bmatrix} \right) * \\ \begin{bmatrix} 1 & 0 \\ 0 & -1 \end{bmatrix} \left(\begin{bmatrix} \cos(\theta) & -\sin(\theta) \\ \sin(\theta) & \cos(\theta) \end{bmatrix} \begin{bmatrix} e^{\frac{i\pi}{4}} & 0 \\ 0 & ie^{\frac{i\pi}{4}} \end{bmatrix} \begin{bmatrix} \cos(\theta) & \sin(\theta) \\ -\sin(\theta) & \cos(\theta) \end{bmatrix} \right) * \\ \begin{bmatrix} 0 & 0 \\ 0 & 1 \end{bmatrix} \begin{bmatrix} 0 \\ 1 \end{bmatrix} \end{matrix} \right\}. \tag{5.29}$$

Equation 5.29 shows the polarization was rotated by 90° with respect to the input polarization, and exits the PBS with vertical polarization.

C. Verification of Doppler Modeling

To verify that the Doppler processing was correct, multiple cases were constructed to test the validity of the model. The first case was a close target, i.e. zero delay, which is stationary for one iteration and moving for the other. The close target case is depicted in Figure 5.1. The other case considered was a target “at range”, approximately a 1 μs round trip delay, and once again for a stationary and moving target. For each case, 1 ms worth of data, or 250 pulses, was collected and analyzed. The pulses had a 100% duty cycle, where each was a linear ramped as previously described. Note, the down-chirp has little effect on the matched filter process and is subsequently ignored. Each pulse was processed in the same fashion as described in Chapter 4, Section C. Each pulse had its target signal correlated with its matched filter kernel to create a matched filter output.

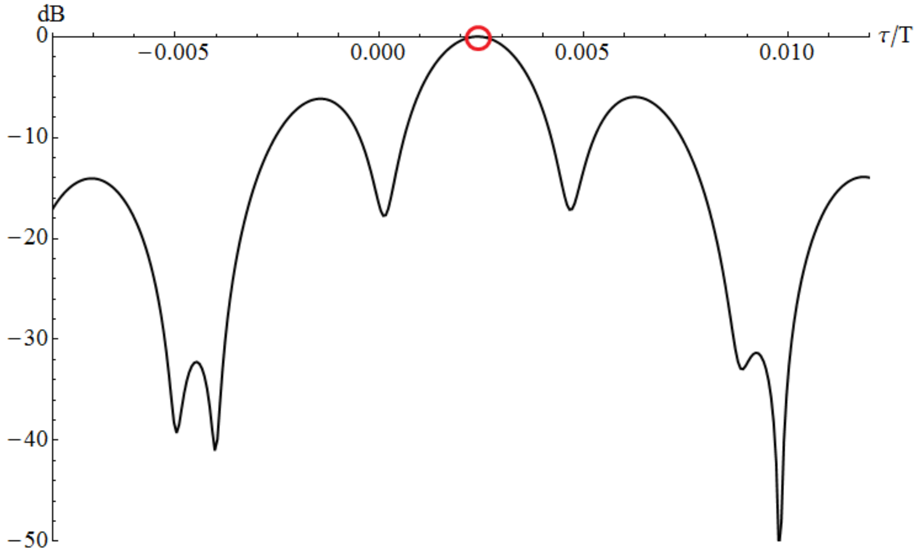

Figure 5.2: Central peak of the matched filter output for a coherent on receive setup (Black) and the location where phase and amplitude information is extracted (Red).

Figure 5.2 shows the MFO of a single pulse, where the target is not moving. It is important to note that the peak is shifted from the center slightly due to an unequal path length between the matched filter signal and the target signal. The red circle at the correlation peak in Figure 5.2 shows the data point where the phase information is extracted.

The phase and amplitude information is extracted from each subsequent pulse and plotted in Figure 5.3. As the theory predicts, if the velocity of the target is zero, the phase change is constant. Figure 5.3 is a prime example of how the phase remains stationary in the lower left only very slightly drifting about in amplitude and phase, which can be accounted for by either amplitude changes in the laser and/or mechanical drift in the free space components.

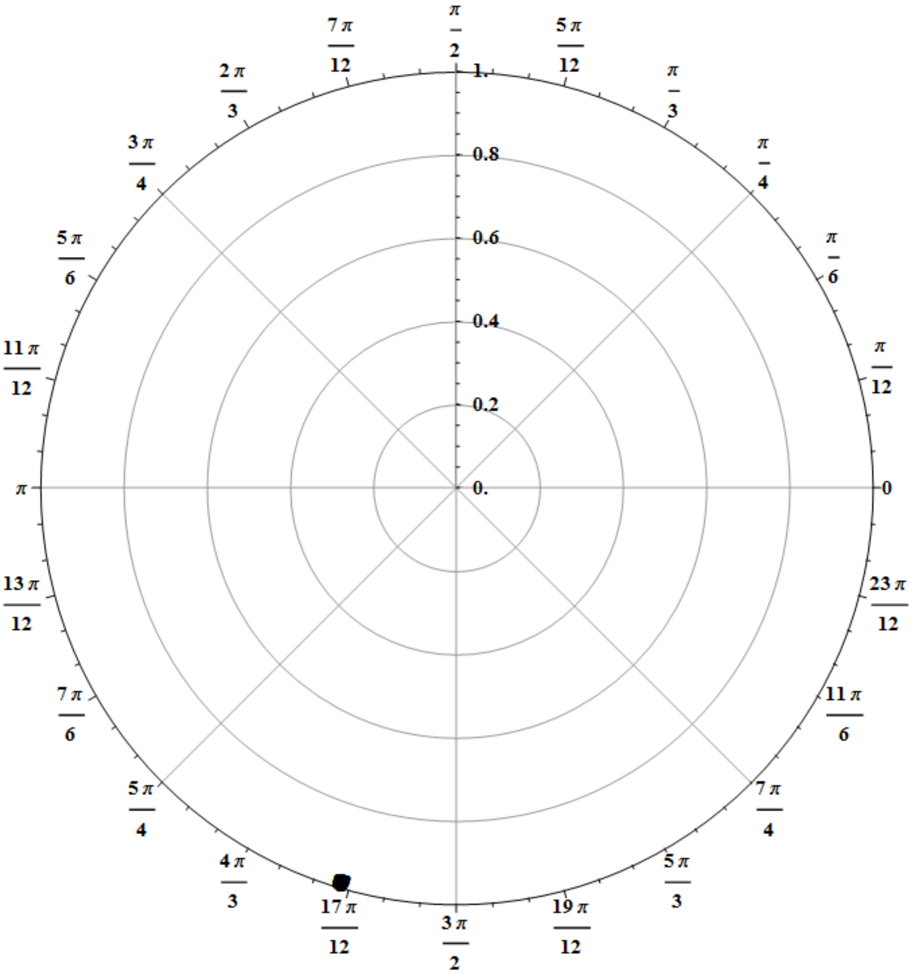

Figure 5.3: Normalized amplitude and phase information obtained from a close stationary target being interrogated by a two chirp SF-LFM signal.

The steps were repeated for a close moving target. Figure 5.4 shows how the phase evolves over all of the pulses. The phase rotation occurs because the velocity induced phase change between consecutive realizations, and since the velocity is approximately constant over the entire signal duration, the change between each pulse is approximately the same.

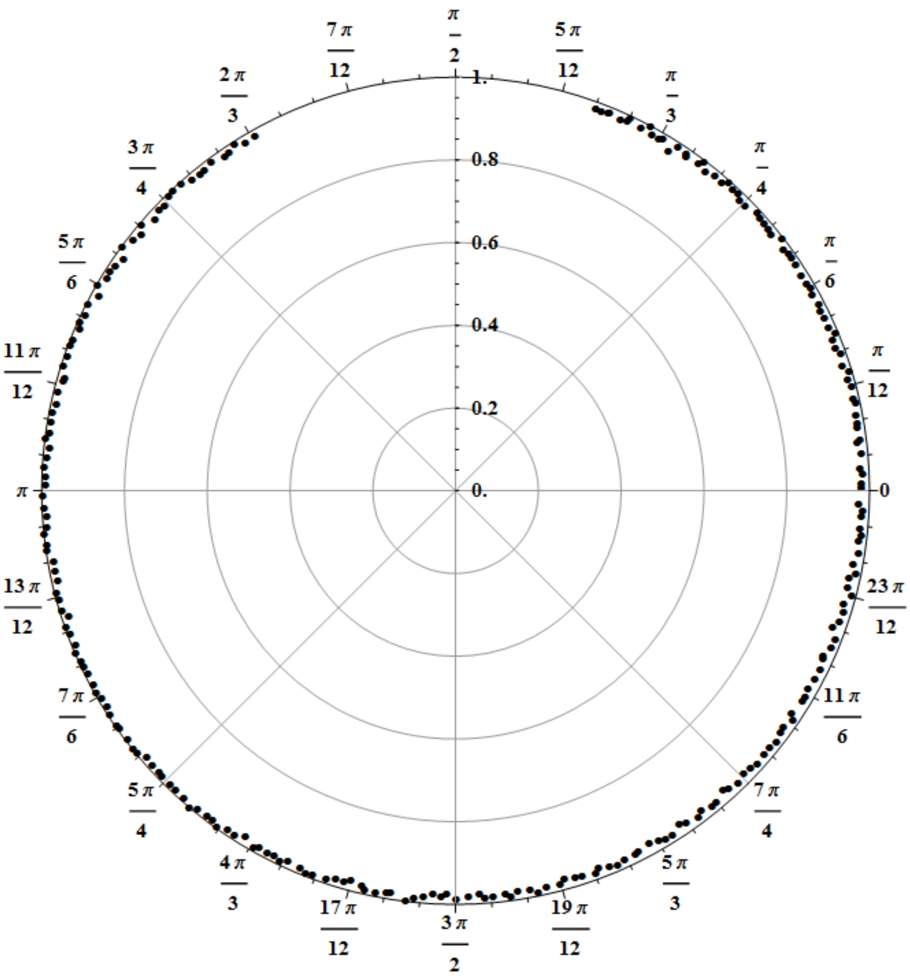

Figure 5.4: Normalized amplitude and phase information obtained from a close moving target being interrogated by a two chirp SF-LFM signal.

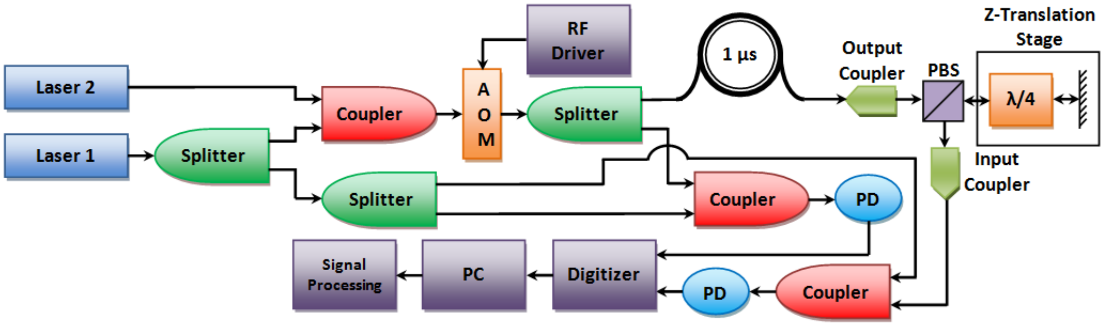

Figure 5.5: Matched filter setup for detecting the Doppler shift of a target at a distance with respect to a stationary reference.

The second case schematically depicted in Figure 5.5 shows an added 1 μs delay line to simulate the target being at a distance. Figure 5.6 shows the zoomed in central peak with the added 1 μs delay or .25 normalized delay built into the setup.

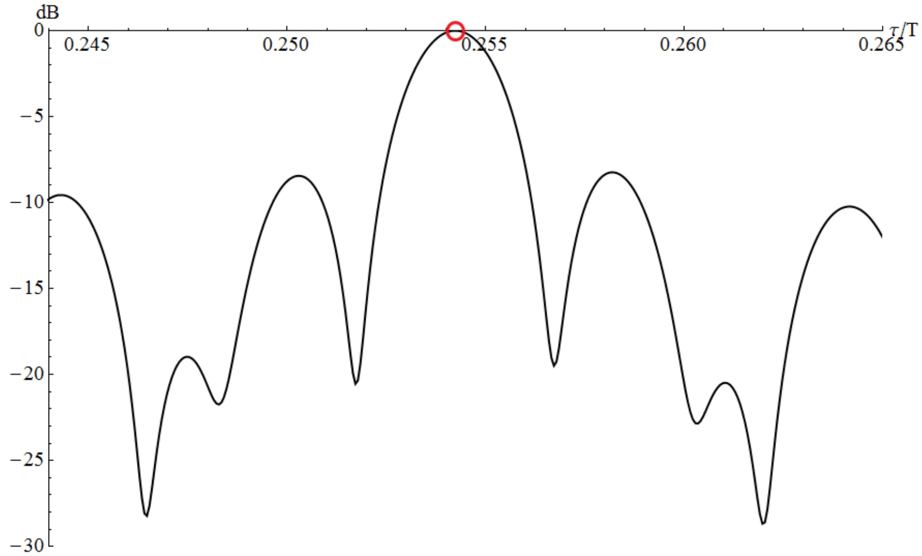

Figure 5.6: Central peak of the matched filter output for a coherent on receive setup (Black) and the location where phase and amplitude information is extracted (Red).

It is important to note that when distance is added to the target, the stability of the sources starts to come into play. As stated in the experimental setup, the local oscillator line was replaced by a narrow line width laser source. Linewidth is important because there is a direct relationship between the linewidth of a source and its coherence length. The coherence length is an important factor for the reason that when a signal is created, a reference or matched filter is also created by recording the signal on a photodiode. This reference has a certain phase attributed to it. The local oscillator does not have a built in delay line, which means that if the coherence jumps while the signal is still in the delay line, the phase attributed to it is no longer referenced to the matched filter. This means that the phase between each pulse is completely random. In order to make sure the matched filter and the target are coherent with each other, the local oscillator needs to have a coherence length longer than that of the delay line or propagation path. To recap these points, the phase must be measure to a fraction of a cycle; laser phase noise corrupts the signal and limits the lower bounds on the measurement; linewidth/coherence time must be chosen so phase variance is small within the observation time.

To demonstrate this concept, Figure 5.7 shows the phase where the local oscillator was the first output of the custom laser system by Innovative Photonic Solutions instead of the NPP system. The delay line in the system is approximately 300 m. The coherence length of the custom system is approximately 100 m, which means that the coherence length is about three times less than the minimum distance required to perform phase retrieval of the signal.

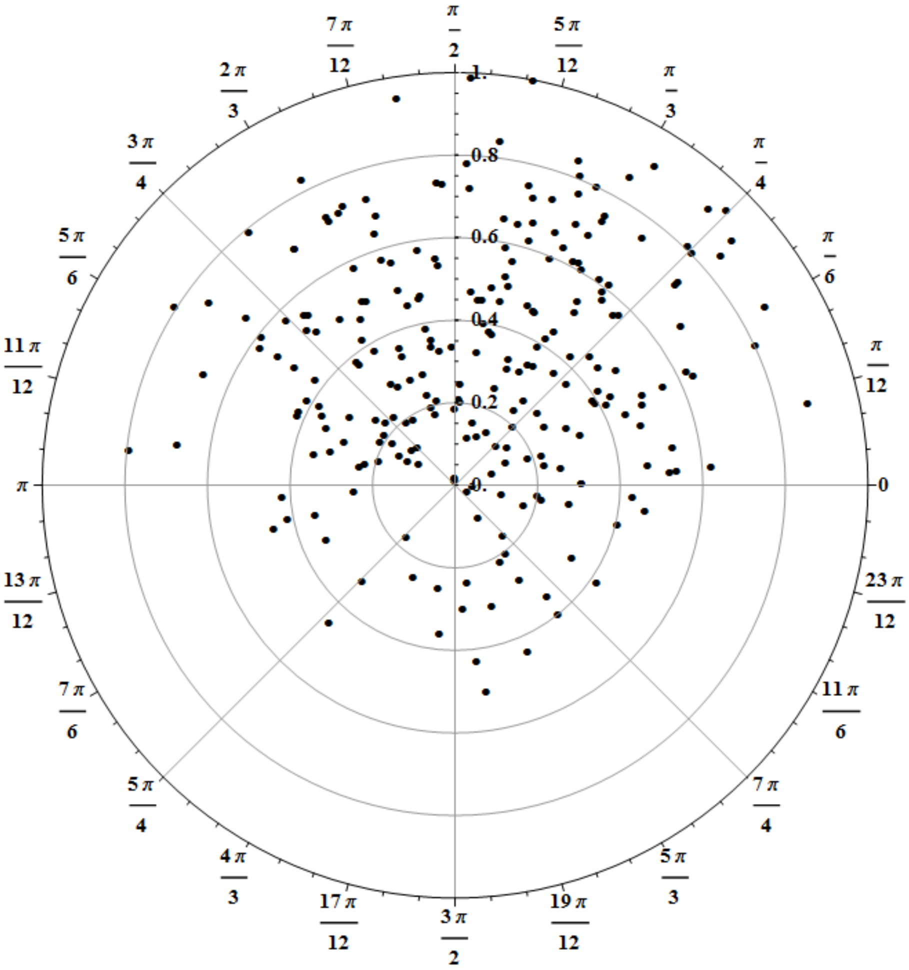

Figure 5.7: Normalized amplitude and phase information obtained from a distant stationary target where the local oscillator has a coherence length less than that of the round trip distance.

The NPP laser has a coherence length of approximately 95 km, which is more than sufficient to retrieve the phase information.

Each case, stationary and moving, was processed the same as in the close target cases.

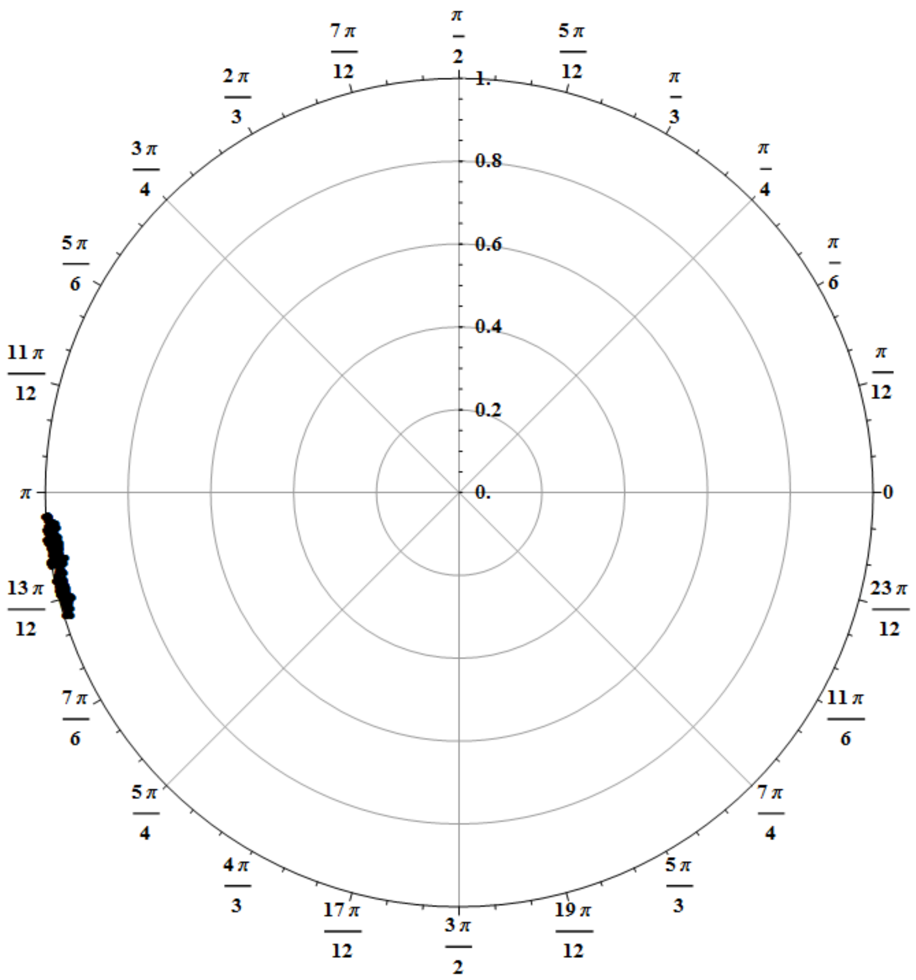

Figure 5.8: Normalized amplitude and phase information obtained from a distant stationary target being interrogated by a two chirp SF-LFM signal.

Figure 5.8 shows the stationary case of a distant target. The additional broadening comes from the fiber delay line. The delay lines expansion and contraction over time changes the phase term slightly between each realization. However, it is more than sufficient to broaden the phase when compared to the close target. Figure 5.9 shows the moving case, which is similar to that of Figure 5.4. Although the phase noise due to the fiber still broadens the resulting signal.

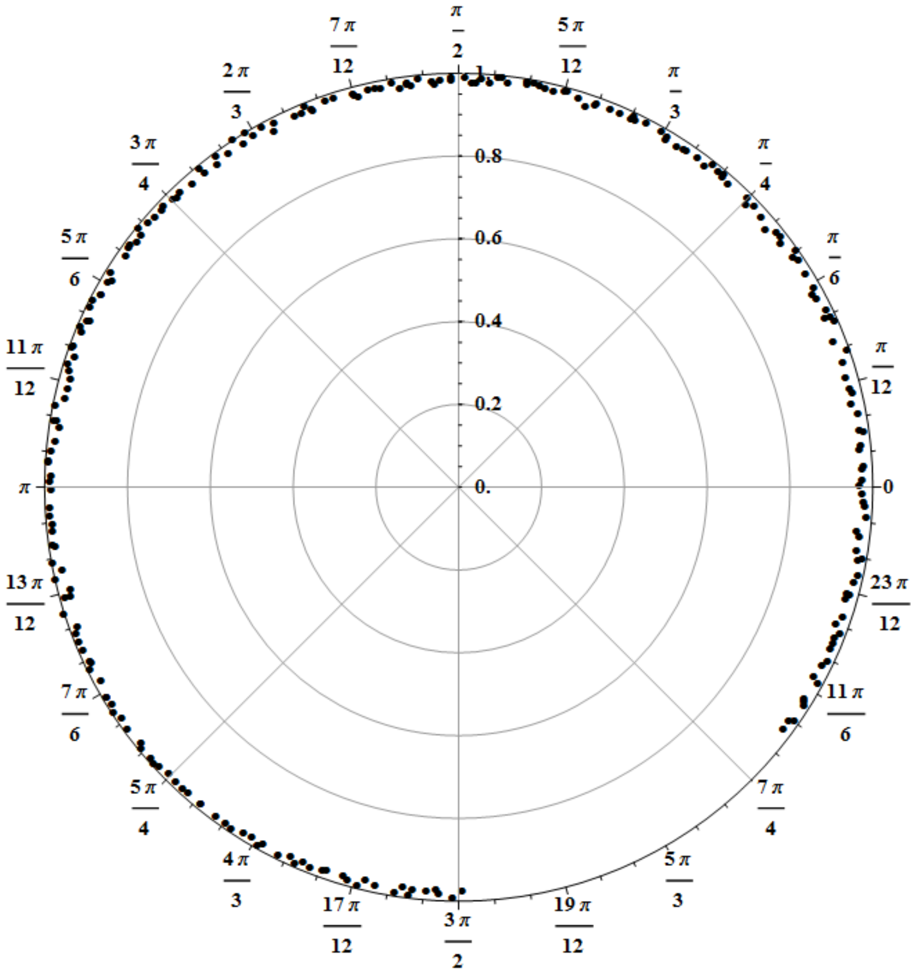

Figure 5.9: Normalized amplitude and phase information obtained from a distant moving target being interrogated by a two chirp SF-LFM signal.

D. Target Directionality

The target directionality can be deduced from the direction of rotation of the phase rotation. The determination of the target's direction is extracted from Equations 5.4 and 5.5. In Equation 5.4, repeated here,

$$(f * g)(t) \stackrel{\text{def}}{=} \int_{-\infty}^{\infty} f(\tau)g(t-\tau)d\tau = \int_{-\infty}^{\infty} f(t-\tau)g(\tau)d\tau, \tag{5.30}$$

choosing whether the matched filter kernel is $f(\tau)$ or $g(t-\tau)$ changes the rotation direction of the phase. Additionally, the sign of the Doppler exponential term in Equation 5.5, defined here with a plus minus sign,

$$e^{\pm i2\pi\nu(t-t_1)}, \tag{5.31}$$

affects the direction of rotation. Once this is determined and fixed, only the exponential term changes in sign, because the velocity term changes sign depending on if the target is traveling towards or away from the receiver, and as a direct result, a change the direction of rotation in phase. Given the previous setups described with the negative exponential and the matched filter kernel being the recorded reference, it can be seen through Figure 5.10 and Figure 5.11 that targets approaching the receiver cause the phase to rotate in a clockwise direction and targets moving away from the receiver are counter-clockwise. Note that the axes were placed to coincide with the first phase recovered.

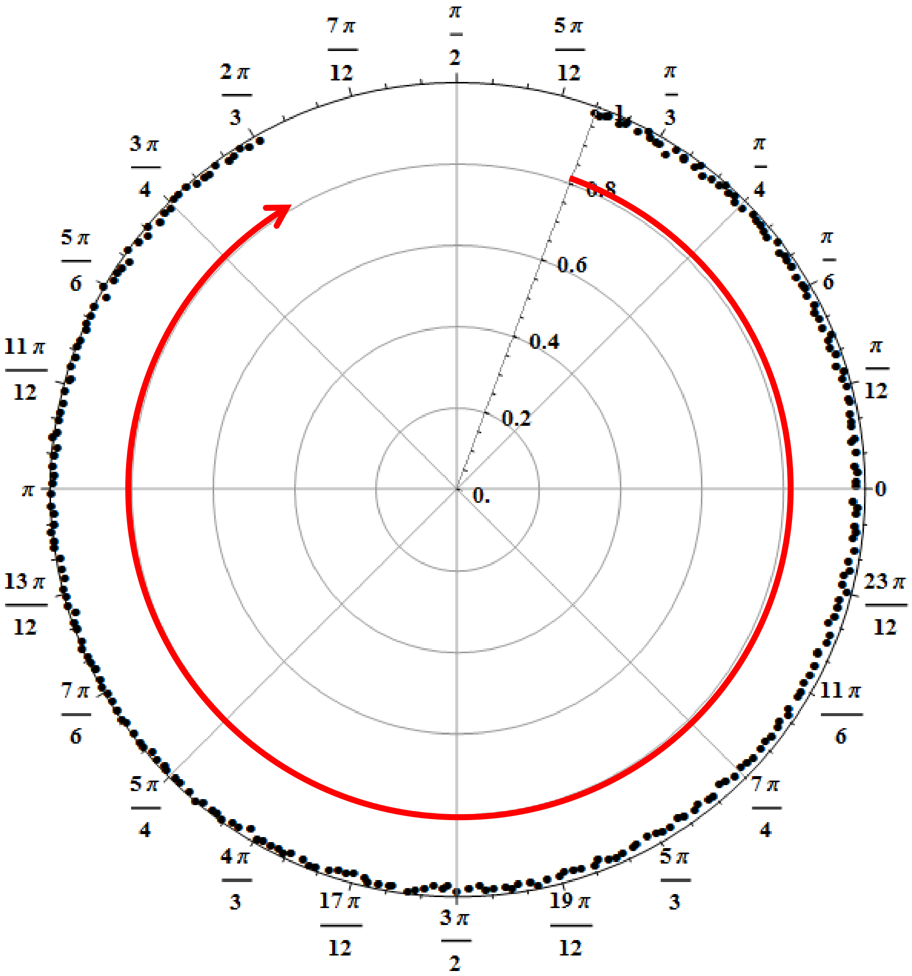

Figure 5.10: Phase recovered from a forward moving target (Clockwise rotation).

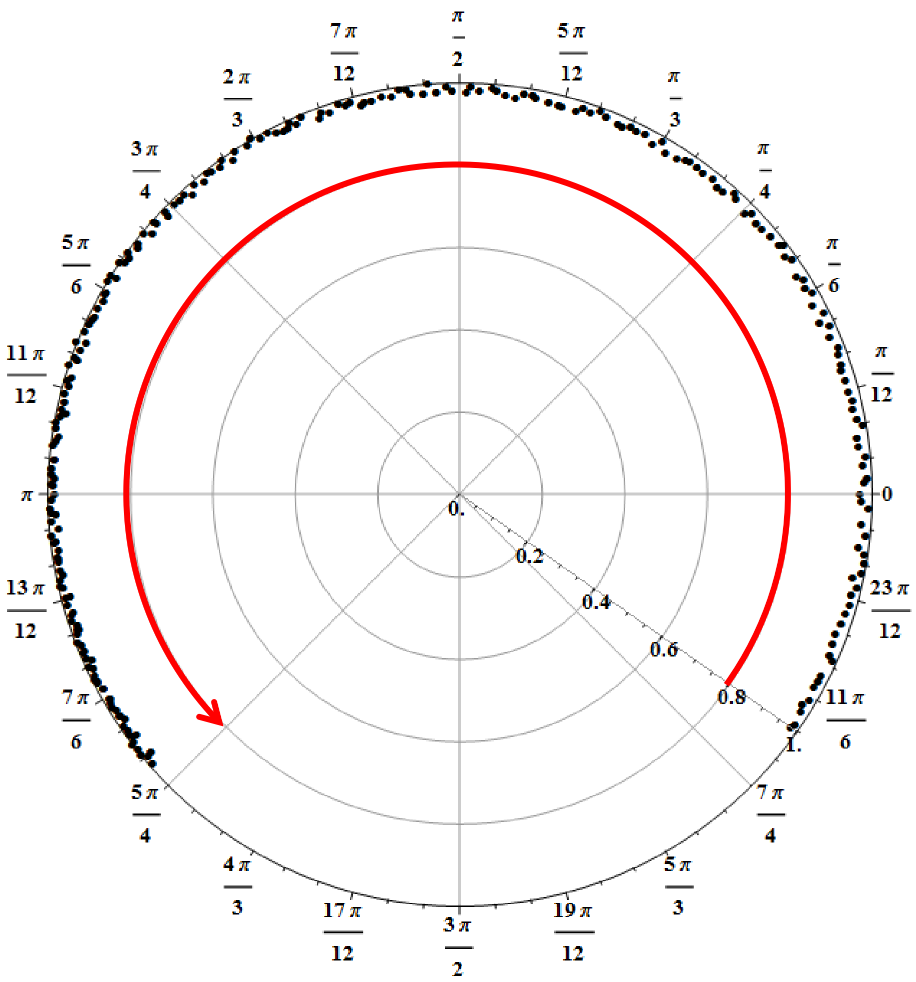

Figure 5.11: Phase recovered from a backwards moving target (Counter-Clockwise rotation).

E. Velocity Comparison

The second part of the modeling described in Section 1 dealt with the ability to determine the velocity of a target from the extracted phase information. To verify the modeling of the velocity, a secondary means of measuring velocity was needed. A computer controlled stage, physic instrumente M-413, with an optical encoder built was used. The stage velocity was set by the computer and was controlled by its own circuitry. The velocity was calculated via the phase by use of Equation 5.22, where the change in phase $\Delta\theta$ is the phase change between the first and the last pulse and t_{total} is the relative time change between the first and the last pulse. Using the first and last pulse to measure speed instead of measuring the speed between each consecutive pulse allows for improved resolution and uncertainty. Figure 5.12 shows the comparison between the velocity set by the stage and the velocity calculated via the phase, which are in excellent agreement and therefore validate the model. The uncertainty in the velocity that comes from the stage is much greater than that of the uncertainty in the phase measurement. This comes mostly from the technique utilized in making the measurement. The stage employs an optical encoder which only has discrete steps, versus an interferometric process in the Doppler phase recovery measurement. In order to more accurately compare, a different technique/device could be utilized, such as a Michelson interferometer.

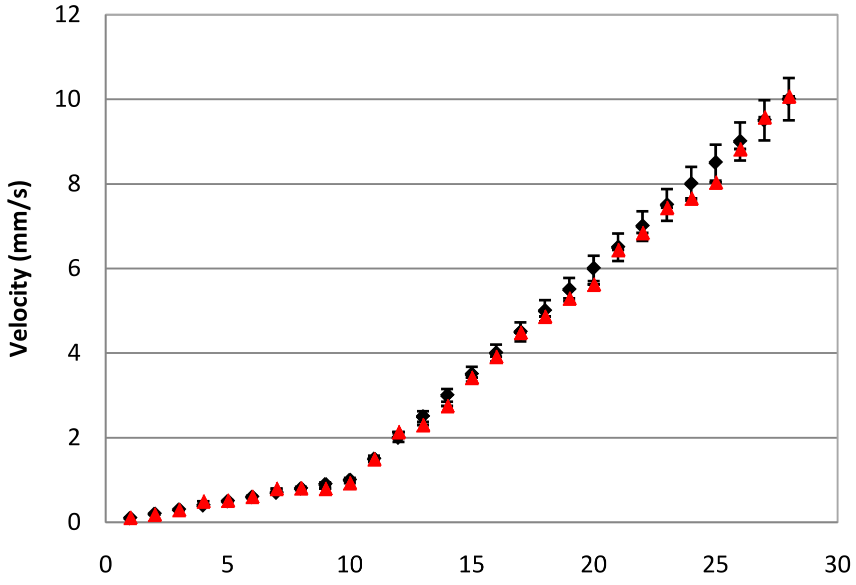

Figure 5.12: Comparison of the stage velocity (Black) to the velocity measured by the SF-LFM signal (Red).

CHAPTER 6 -
MULTIPLE TARGET SIMULATION

A. Experimental Setup and Requirements

In general, standard ladar or radar systems will illuminate multiple targets. The ability of a system to resolve each target's characteristics individually is of great interest. The multiple target Doppler processing is the same as single target Doppler processing with the exception that two correlation peaks have to be processed. The experiment was performed with polarization maintaining fiber to maximize the heterodyning effects. The signal was a two chirp SF-LFM signal, i.e. two sources. Figure 6.1 schematically depicts a multiple target setup being interrogated by a two chirp SF-LFM signal.

The first source (Laser 1) was an NP Photonics (NPP) *The Rock* single frequency narrow linewidth fiber laser. The second (Laser 2) was from the custom system described in Chapter 4. Just as before, the linear modulation of the signal was performed by an AOM which provided a linear frequency shift from 730 MHz as .5 V to 850 MHz at 10V. The same ThorLabs SIR5-FC 6.5 GHz bandwidth photodetectors were utilized in combination with the Acqiris DC252 high speed digitizer, which allowed for a sampling rate of 4 GS/s while recording on both channels.

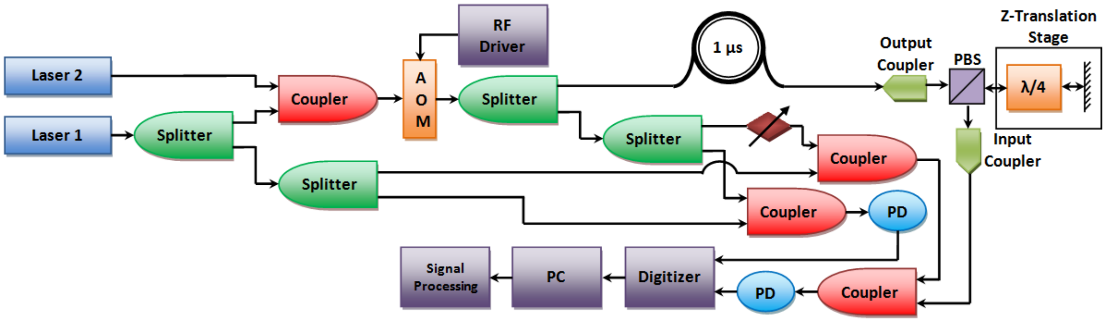

Figure 6.1: Matched filter setup for detecting the phase rotation of multiple targets with respect to a stationary reference.

As shown in Figure 6.1, laser 1 is split. One line is used to create the local oscillator and the other is combined with laser 2 and linearly modulated to create a two chirp SF-LFM signal. The sparse frequency signal is split after the AOM. The first line is split into two more lines. One is mixed with the local oscillator on a photodiode to create the matched filter kernel; the other line runs through a variable attenuator to become the close target (no delay) and gets combined with the local oscillator. The second line runs through a 1 µs fiber delay line and the transmit/receive switch described in the previous chapter before being combined with the local oscillator and close target signal. The multiple target signal is then mixed on the photodiode.

B. Multiple Target Doppler Processing

To verify that multiple targets can be Doppler processed, the setup depicted in Figure 6.1 was utilized. From this setup two cases can be constructed. The first case consists of a stationary distant target and a stationary close target. The second case consists of a moving distant target and a stationary close target. Due to the way the setup was designed, the close target is always stationary. To test a moving close target, the transmit/receive switch with moving target would need to be moved from the distant target to the close target or an additional transmit/receive switch with moving target would need to be added.

As done previously, the data was processed as described in Chapter 4, Section 3. Each case took 1 ms worth of data, or 250 pulses, which were collected and analyzed. Each pulse had its multiple target signal correlated with its respective matched filter kernel to produce an MFO. Figure 6.2 shows the MFO of a single pulse where both targets are stationary. The figure shows two correlation peaks representing the close and distant targets respectfully. The data points at the correlation peaks are where the phase and amplitude information is extracted for each target.

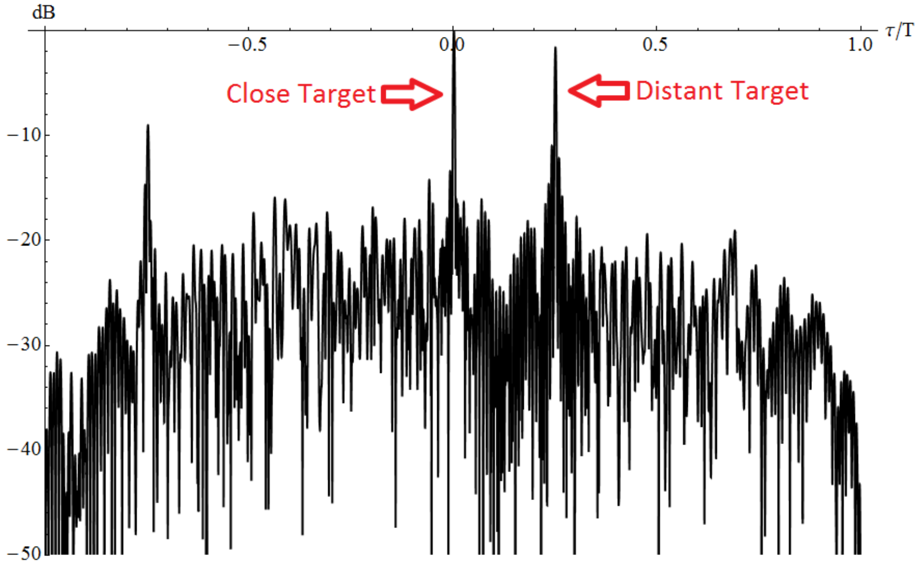

Figure 6.2: Full matched filter output for a coherent on receive setup for multiple stationary targets.

The phase and amplitude information of two stationary targets is extracted from each subsequent pulse and plotted in Figure 6.3. Just like in the single target verification, the multiple targets behave in the same way. Both targets have no phase change, which would indicate that neither target has an associated velocity. There is broadening in phase on the distant target from the fiber delay line’s change in optical path length, an alteration of the phase, over the recorded duration. There is also additional broadening on both the close and the distant targets in both amplitude and in phase. This is due to correlations of the close target and distant target overlapping. Overall, these overlapped correlations have little effect on the phase rotation until most of the primary lobe of each target is overlapping.

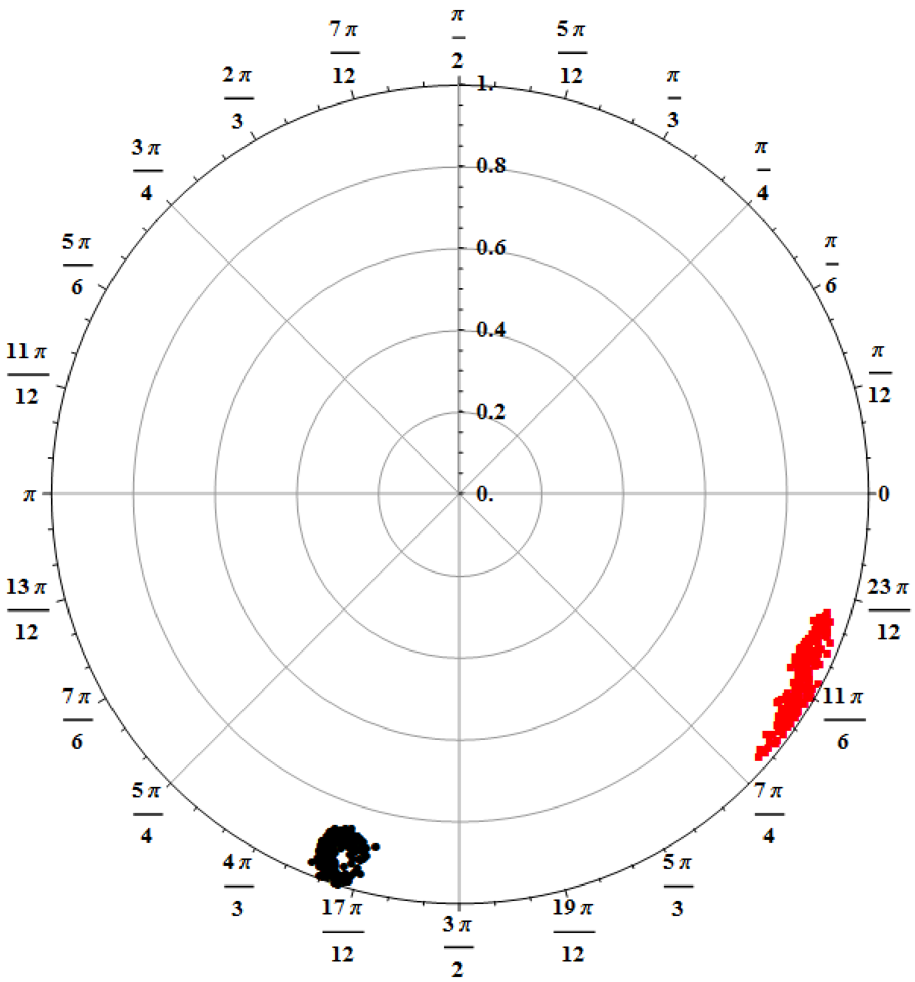

Figure 6.3: Normalized amplitude and phase information obtained from multiple stationary targets being interrogated by a two chirp SF-LFM signal. Stationary close (Black) and stationary distant (Red).

The moving target case was performed in the same manner. The phase and amplitude information was extracted from the two correlation peaks and plotted in Figure 6.4. The figure shows that the close target has no phase change and therefore no velocity associated with it. Also, it shows that the second targets phase is rotating when the target is moving, and one can calculate its velocity via Equation 5.22. The two targets have similar broadening in both phase and amplitude as shown in the stationary case. Again, the additional broadening is a result of the correlations overlapping.

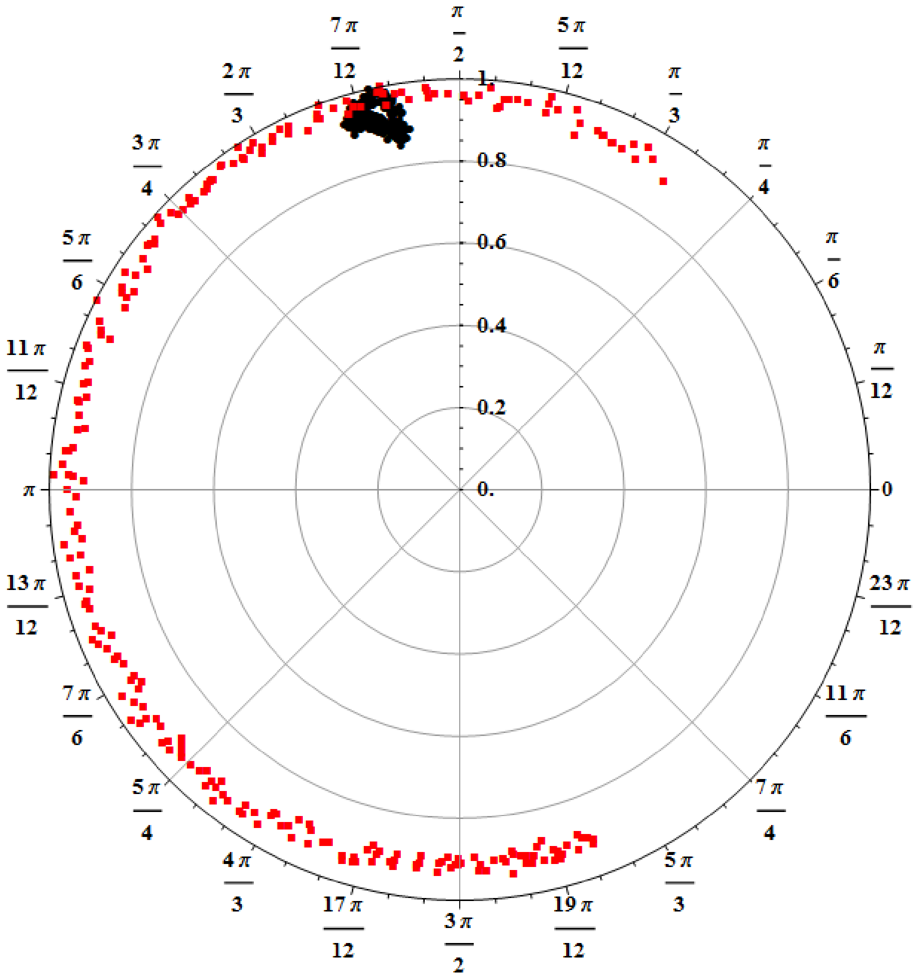

Figure 6.4: Normalized amplitude and phase information obtained from multiple targets, being interrogated by a two chirp SF-LFM signal. Stationary close (Black) and moving distant (Red).

CHAPTER 7 -
EFFECTS OF NONLINEAR FREQUENCY MODULATION

A. Nonlinear Frequency Modulation Background

In Chapter 2, the definition of nonlinear frequency modulation was kept generic and defined as an instantaneous frequency that is a function of time. One type of nonlinear modulation technique is implemented by shaping the pulse amplitude temporally to a common weighted window such as Hann or Hamming windows [32]. Figure 7.1 shows the autocorrelation of an unweighted LFM pulse. Figure 7.2 shows a Hamming weighted LFM pulse. The effects are a major reduction in the sidelobes, from approximately -13 dB to about -50 dB. However, there is a cost in the range resolution of the signal, as can be seen from the broadening of the correlation peak.

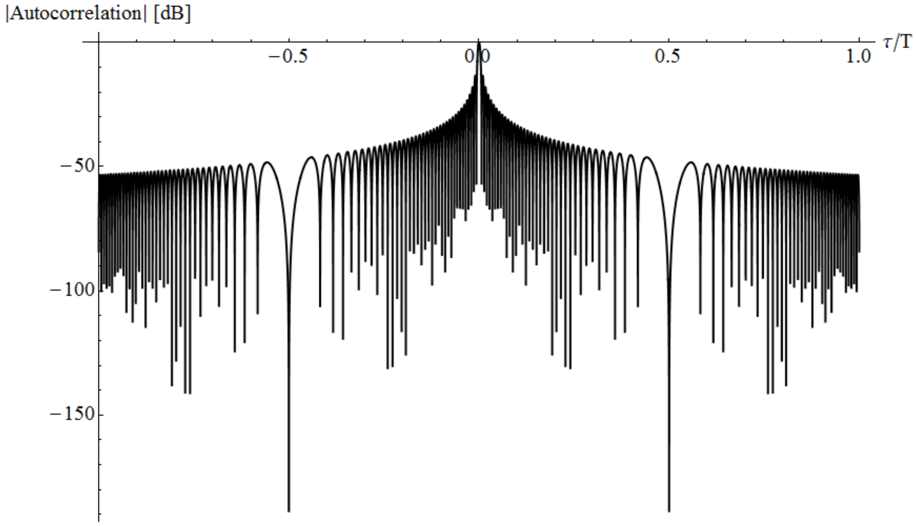

Figure 7.1: Autocorrelation of an unweighted LFM pulse.

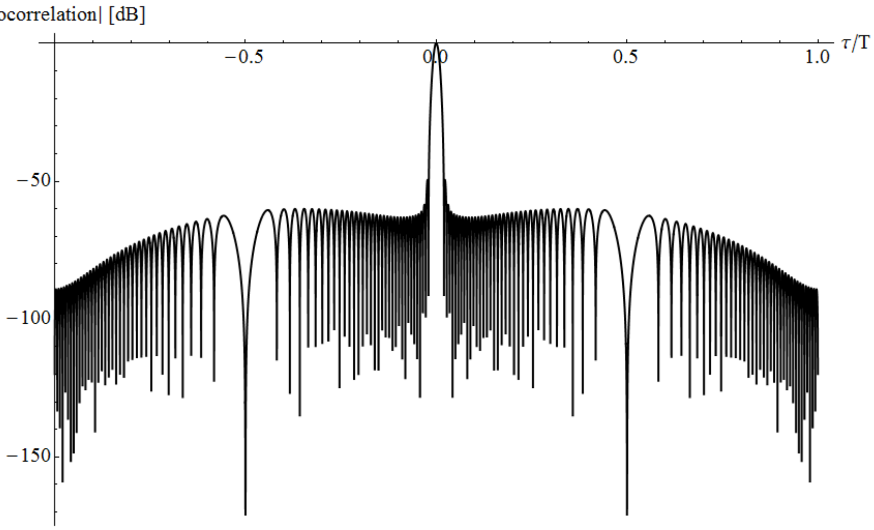

Figure 7.2: Autocorrelation of a Hamming weighted LFM pulse.

Implementation of this technique would require the use of a secondary extracavity amplitude modulator to be synced with the generation of the pulse in time. Although this can be done, it would be difficult to get the timing correct.

The other approach is to change the instantaneous frequency directly in time. Figure 7.2 shows a nonlinear frequency profile in time. The phase of the function is given by,

$$\phi(t) = 2\pi \int_0^t f(x)dx, \tag{7.1}$$

where $f(x)$ is the frequency as a function of x (dummy variable). Phase is then used in the complex envelope function given by,

$$u(t) = g(t)e^{i\phi(t)}, \tag{7.2}$$

where $g(t) = 1$ is the amplitude function. The autocorrelation of the complex envelope given by the frequency in Figure 7.2 is shown in Figure 7.3.

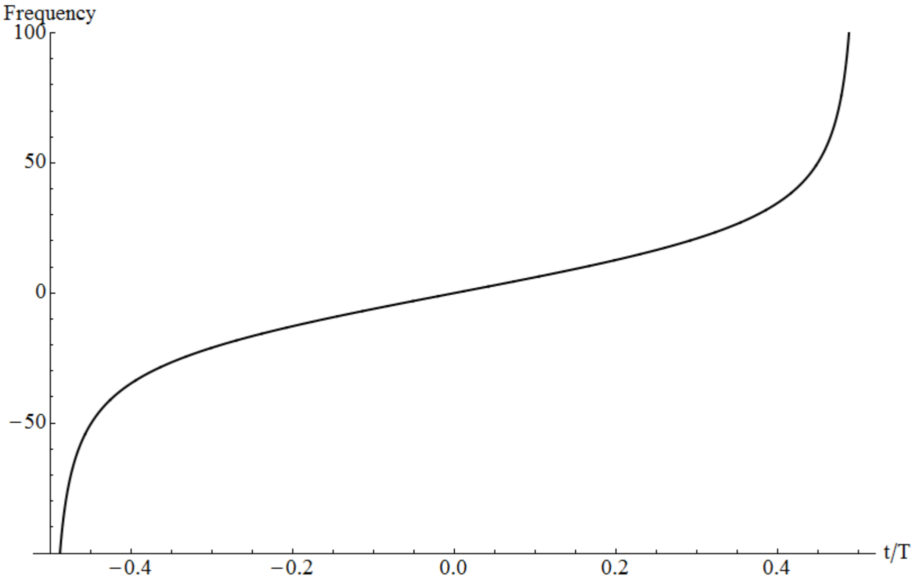

Figure 7.3: Frequency versus time of a nonlinear ladar signal.

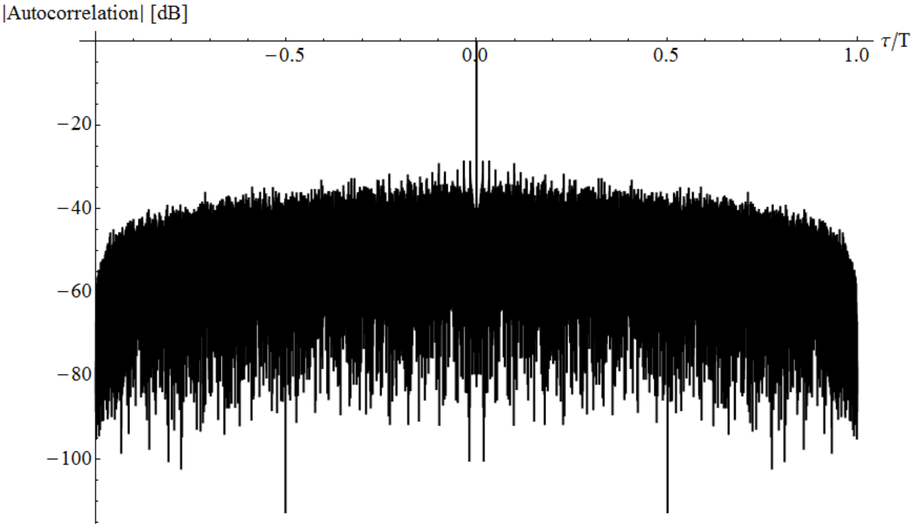

Figure 7.4: Autocorrelation of a nonlinear frequency modulation.

From Figure 7.4 it is easy to see an immense improvement in the peak to sidelobe ratio.

B. Nonlinearities of an Acousto-Optic Modulator

The nonlinear modulation characterized here is not defined by a frequency or an amplitude function, but rather be a qualitative look at how nonlinearities in certain regimes of the AOM can be exploited to increase range resolution and peak to sidelobe ratios of the transmitted waveform. The AOM itself provides linear modulation over a 4 μs pulse duration. If that time duration is increased, the signal goes from linear to nonlinear and the range resolution and PSLR can be characterized. Figure 7.5 shows the schematic setup for determining range resolution and PSLR for nonlinear signals.

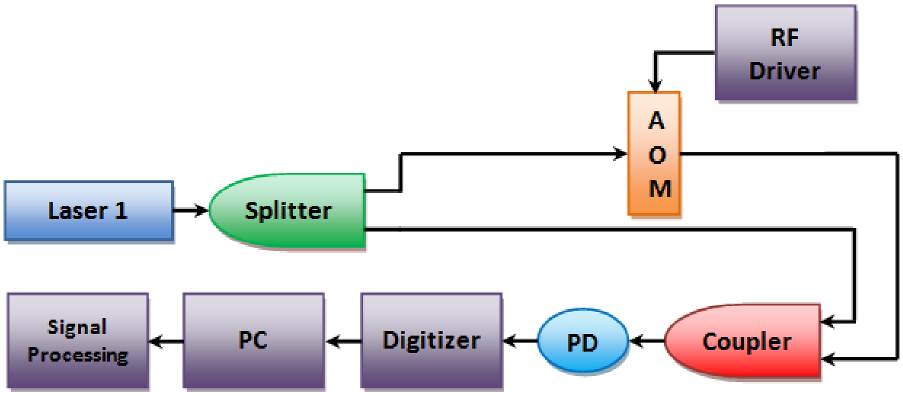

Figure 7.5: Single chirp NLFM ladar signal generation, detection, and processing.

Just as in the previous experiments, polarization maintaining fiber was used. Since this is a single chirp waveform, only one source was needed, which was the NP Photonics (NPP) *The Rock* single frequency narrow linewidth fiber laser. The modulation of the signal was performed by an AOM. The detectors were ThorLabs SIR5-FC 6.5 GHz bandwidth photodetectors. The signal was digitized by an Acqiris DC252 high speed digitizer, which allowed for a sampling rate of 4 GS/s while recording on both channels. The laser was split into two parts, one to be the local oscillator and the other to be modulated by the AOM. The modulated signal and the local oscillator were combined and mixed on a photodiode. The signal was digitized and processed the same way described in Chapter 4, Section C. It was then autocorrelated to attain the range resolution and PSLR for the given signal period. Figure 7.6 shows the spectrum of a nonlinear pulse.

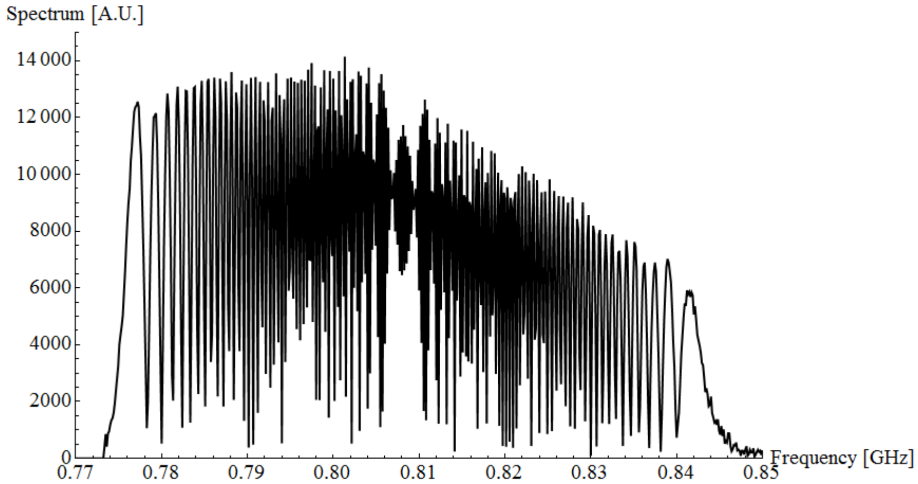

Figure 7.6: Spectrum of a nonlinear pulse resulting from the AOM's nonlinearities.

Figure 7.7 shows an example of the autocorrelation of a pulse which has a range resolution of 2.3 m and a PSLR of -20.4 dB, a significant improvement over the set PSLR of -13 dB for a single LFM pulse.

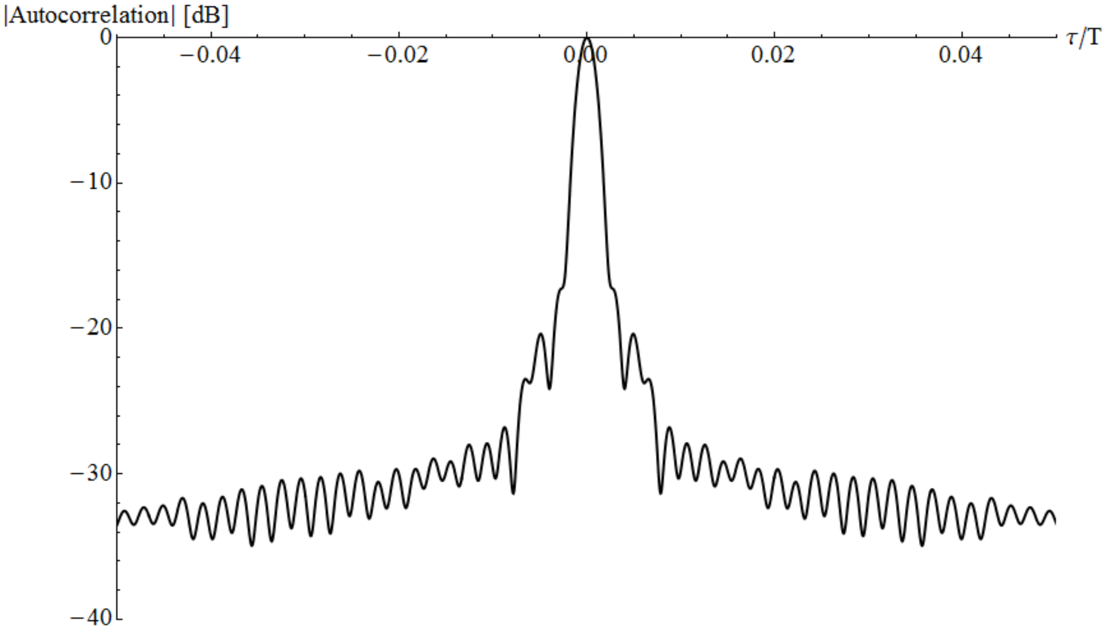

Figure 7.7: Correlation peak of a nonlinear frequency modulated ladar signal.

By plotting these two metrics as a function of signal period, an optimized or rather preferred nonlinear signal can be established. Signals were recorded for pulse durations of 4 μs to 10 μs in .5 μs steps. From each pulse, the range resolution and PSLR was calculated. Figure 7.8 and Figure 7.9 show the range resolution and PSLR respectively.

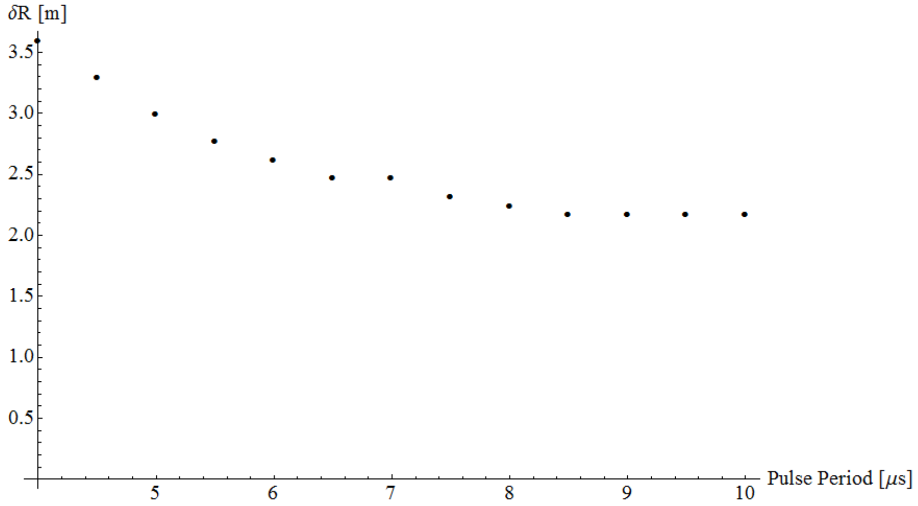

Figure 7.8: Range resolution as a function of pulse period.

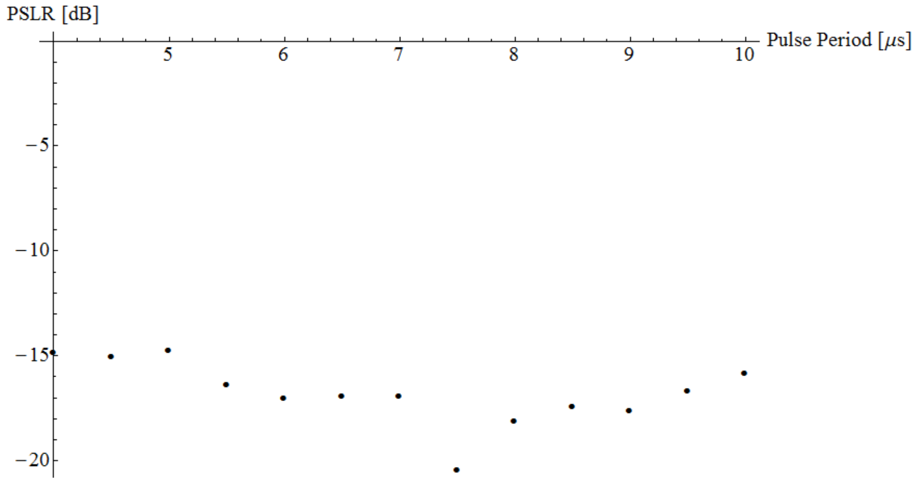

Figure 7.9: Peak to sidelobe ratio as a function of pulse period.

Figure 7.8 shows that as the signal period is increased, the range resolution drops because the modulator is able to apply more bandwidth to the signal. Recall that range resolution is proportional to bandwidth, so the more bandwidth you have, the better your range resolution. The PSLR in Figure 7.9 shows that by increasing the signal period to 7.5 μs results in the signal having its lowest PSLR. From this, the most logical pulse duration to work at is 7.5 μs because it results in the best PSLR and is already very close to the minimum range resolution. In other words, the gain made in PSLR at 7.5 μs outweighs the only .15 m gain in range resolution if one were to pick the PSLR at 10 μs.

CHAPTER 8 -
CONCLUSIONS

Sparse frequency ladar signals have been shown previously to increase the effective bandwidth and consequently, the range resolution of a ladar signal. This work expanded on the two chirp modeling and experimental verification performed by Chimenti et al. [14, 36, 37]. The modeling was expanded to three chirps and experimentally tested. The results showed good agreement with the predicted theory. These results show a continuation of the ability of sparse frequency linearly frequency modulated ladar signals to increase the bandwidth of a LFM ladar signal by using a single low bandwidth modulator. The cost of segmented bandwidth is the increase in PSLR caused by the separating of the segments in frequency. One needs to weigh the cost of increased range resolution against the increase in PSLR.

New on Doppler processing for segmented bandwidth linearly frequency modulated ladar signals was explored. Models were created utilizing matched filter processing to accurately predict the effects of the Doppler frequency shift. From the modeling, the speed at which the target was moving was predicted and experimentally verified. The directionality of the target was also extracted from the sign of the phase difference.

Doppler processing was then applied to targets at a distance. The results showed that at range, the targets could be resolved and their velocities determined by using a local oscillator with a coherence length longer than the round trip length between the receiver and the target. This process was further generalized by the addition of a second target close to the receiver. This multiple target realization showed the ability of the signal to resolve both targets in range and in velocity.

The final work presented in this thesis took advantage of the inherent nonlinearities in the acousto-optic modulator. The nonlinearities were characterized in terms of the two metrics used throughout the research, namely range resolution and PSLR. It found that by working in a specific nonlinear regime, the range resolution could be increased from about 3.3 m to 2.3 m and the PSLR could be improved from about -14.9 dB to around -23.4 dB.

APPENDIX A -
DERIVATION OF A TWO CHIRP SPARSE FREQUENCY DOPPLER MODEL

A. Baseband Signal

$$s(t) = \frac{1}{\sqrt{2T}} Rect\left[\frac{t}{T}\right]\left[\tilde{A}_1 e^{i\left(2\pi f_0 t + \frac{1}{2}\beta t^2\right)} + \tilde{A}_2 e^{i\left(2\pi (f_0 + df) t + \frac{1}{2}\beta t^2\right)}\right]$$

Where T is the signal period, $\tilde{A}_1$ & $\tilde{A}_2$ are the complex amplitudes, f_0 is the AOM offset, β is the chirp coefficient given by $\beta = 2\pi/T$, and df is the difference frequency between lines.

B. Matched Filter Impulse Response

$$h(t) = Ks^*(t_0 - t)$$

Where K is a scaling constant which is set equal to 1 and t_0 is a reference point which is set equal to 0.

$$h(t) = s^*(-t)$$

$$= \frac{1}{\sqrt{2T}} Rect\left[\frac{-t}{T}\right]\left[\tilde{A}_1^* e^{i\left(2\pi f_0 t - \frac{1}{2}\beta t^2\right)} + \tilde{A}_2^* e^{i\left(2\pi (f_0 + df) t - \frac{1}{2}\beta t^2\right)}\right]$$

C. Return Signal

The return signal to be used is a delayed Doppler shifted version of the baseband signal.

$s_R(t) =$

$$\frac{1}{\sqrt{2T}} Rect\left[\frac{t-t_1}{T}\right]\left[\tilde{A}_3 e^{i\left(2\pi f_0(t-t_1)+\frac{1}{2}\beta(t-t_1)^2\right)} + \tilde{A}_4 e^{i\left(2\pi(f_0+df)(t-t_1)+\frac{1}{2}\beta(t-t_1)^2\right)}\right] e^{i2\pi\nu(t-t_1)}$$

D. Matched Filter Output

The matched filter output is given by the convolution of the return signal with the impulse response.

$$(s_R * h)(t) = \int_{-\infty}^{\infty} s_R(\tau)h(t-\tau)d\tau = \int_{-\infty}^{\infty} s_R(t-\tau)h(\tau)d\tau$$

$=$

$$\int_{-\infty}^{\infty} \frac{1}{\sqrt{2T}} Rect\left[\frac{t-\tau-t_1}{T}\right]\left[\tilde{A}_3 e^{i\left(2\pi f_0(t-\tau-t_1)+\frac{1}{2}\beta(t-\tau-t_1)^2\right)} + \right.$$

$$\left.\tilde{A}_4 e^{i\left(2\pi(f_0+df)(t-\tau-t_1)+\frac{1}{2}\beta(t-\tau-t_1)^2\right)}\right] e^{i2\pi\nu(t-\tau-t_1)} \frac{1}{\sqrt{2T}} Rect\left[\frac{-\tau}{T}\right]\left[\tilde{A}_1^* e^{i\left(2\pi f_0\tau-\frac{1}{2}\beta\tau^2\right)} + \right.$$

$$\left.\tilde{A}_2^* e^{i\left(2\pi(f_0+df)\tau-\frac{1}{2}\beta\tau^2\right)}\right] d\tau$$

$=$

$$\frac{1}{2T}\int_{-T/2}^{T/2} Rect\left[\frac{t-\tau-t_1}{T}\right]\left[\tilde{A}_3 e^{i\left(2\pi f_0(t-\tau-t_1)+\frac{1}{2}\beta(t-\tau-t_1)^2\right)} + \right.$$

$$\left.\tilde{A}_4 e^{i\left(2\pi(f_0+df)(t-\tau-t_1)+\frac{1}{2}\beta(t-\tau-t_1)^2\right)}\right]\left[\tilde{A}_1^* e^{i\left(2\pi f_0\tau-\frac{1}{2}\beta\tau^2\right)} + \right.$$

$$\left.\tilde{A}_2^* e^{i\left(2\pi(f_0+df)\tau-\frac{1}{2}\beta\tau^2\right)}\right] e^{i2\pi\nu(t-\tau-t_1)} d\tau$$

$=$

$$\frac{1}{2T}\int_{-T/2}^{T/2} Rect\left[\frac{t-\tau-t_1}{T}\right]\left[\tilde{A}_1^*\tilde{A}_3 e^{i\left(2\pi f_0(t-\tau-t_1)+\frac{1}{2}\beta(t-\tau-t_1)^2+2\pi f_0\tau-\frac{1}{2}\beta\tau^2\right)} + \right.$$

$$\tilde{A}_2^*\tilde{A}_3 e^{i\left(2\pi f_0(t-\tau-t_1)+\frac{1}{2}\beta(t-\tau-t_1)^2+2\pi(f_0+df)\tau-\frac{1}{2}\beta\tau^2\right)} +$$

$$\tilde{A}_1^*\tilde{A}_4 e^{i\left(2\pi(f_0+df)(t-\tau-t_1)+\frac{1}{2}\beta(t-\tau-t_1)^2+2\pi f_0\tau-\frac{1}{2}\beta\tau^2\right)} +$$

$$\left.\tilde{A}_2^*\tilde{A}_4 e^{i\left(2\pi(f_0+df)(t-\tau-t_1)+\frac{1}{2}\beta(t-\tau-t_1)^2+2\pi(f_0+df)\tau-\frac{1}{2}\beta\tau^2\right)}\right] e^{i2\pi\nu(t-\tau-t_1)} d\tau$$

Substitution: $\eta = t - t_1$.

$=$

$$\frac{1}{2T}\int_{-T/2}^{T/2} Rect\left[\frac{-\tau+\eta}{T}\right]\left[\tilde{A}_1^*\tilde{A}_3 e^{i\left(2\pi f_0(-\tau+\eta)+\frac{1}{2}\beta(-\tau+\eta)^2+2\pi f_0\tau-\frac{1}{2}\beta\tau^2\right)}+\right.$$

$$\tilde{A}_2^*\tilde{A}_3 e^{i\left(2\pi f_0(-\tau+\eta)+\frac{1}{2}\beta(-\tau+\eta)^2+2\pi(f_0+df)\tau-\frac{1}{2}\beta\tau^2\right)}+$$

$$\tilde{A}_1^*\tilde{A}_4 e^{i\left(2\pi(f_0+df)(-\tau+\eta)+\frac{1}{2}\beta(-\tau+\eta)^2+2\pi f_0\tau-\frac{1}{2}\beta\tau^2\right)}+$$

$$\left.\tilde{A}_2^*\tilde{A}_4 e^{i\left(2\pi(f_0+df)(-\tau+\eta)+\frac{1}{2}\beta(-\tau+\eta)^2+2\pi(f_0+df)\tau-\frac{1}{2}\beta\tau^2\right)}\right] e^{i2\pi\nu(-\tau+\eta)}d\tau$$

$$=\frac{1}{2T}\int_{-T/2}^{T/2} Rect\left[\frac{-\tau+\eta}{T}\right]\left[\tilde{A}_1^*\tilde{A}_3 e^{i\left(2\pi f_0\eta+\frac{1}{2}\beta\left(\eta^2-2\eta\tau\right)\right)}+\tilde{A}_2^*\tilde{A}_3 e^{i\left(2\pi f_0\eta+2\pi df\tau+\frac{1}{2}\beta\left(\eta^2-2\eta\tau\right)\right)}+\right.$$

$$\left.\tilde{A}_1^*\tilde{A}_4 e^{i\left(2\pi(f_0+df)\eta-2\pi df\tau+\frac{1}{2}\beta\left(\eta^2-2\eta\tau\right)\right)}+\tilde{A}_2^*\tilde{A}_4 e^{i\left(2\pi(f_0+df)\eta+\frac{1}{2}\beta\left(\eta^2-2\eta\tau\right)\right)}\right] e^{i2\pi\nu(-\tau+\eta)}d\tau$$

Substitution: $\tilde{\gamma} = e^{i\left(2\pi f_0\eta+\frac{1}{2}\beta\eta^2+2\pi\nu\eta\right)}$

$$=\frac{\tilde{\gamma}}{2T}\int_{-T/2}^{T/2} Rect\left[\frac{-\tau+\eta}{T}\right]\left[\tilde{A}_1^*\tilde{A}_3 e^{-i\beta\eta\tau}+\tilde{A}_2^*\tilde{A}_3 e^{i(2\pi df-\beta\eta)\tau}+\tilde{A}_1^*\tilde{A}_4 e^{i2\pi df\eta}\,e^{i(-2\pi df-\beta\eta)\tau}+\right.$$

$$\left.\tilde{A}_2^*\tilde{A}_4 e^{i2\pi df\eta}\,e^{-i\beta\eta\tau}\right]e^{-i2\pi\nu\tau}\,d\tau$$

E. Assumptions

$0 < t_1 < T$ A real return signal can only have a positive value

An equal change in path length of each laser line results in:

$\tilde{A}_3 = \tilde{B}\tilde{A}_1$ & $\tilde{A}_4 = \tilde{B}\tilde{A}_2$, where $\tilde{B}$ is a phase change

$|\tilde{A}_1| = |\tilde{A}_2| = 1$

$\angle\tilde{A}_1 = \phi_1$ & $\angle\tilde{A}_2 = \phi_2$

$\phi_1 - \phi_2 = \Delta\phi$

F. Simplification

$$= \frac{\tilde{\gamma}}{2T}\int_{-T/2}^{T/2} Rect\left[\frac{-\tau+\eta}{T}\right]\left[\tilde{B}\tilde{A}_1\tilde{A}_1^* e^{-i\beta\eta\tau} + \tilde{B}\tilde{A}_1\tilde{A}_2^* e^{i(2\pi df-\beta\eta)\tau} + \tilde{B}\tilde{A}_1^*\tilde{A}_2 e^{i2\pi df\eta}\, e^{i(-2\pi df-\beta\eta)\tau} + \tilde{B}\tilde{A}_2\tilde{A}_2^* e^{i2\pi df\eta}\, e^{-i\beta\eta\tau}\right] e^{-i2\pi\nu\tau}\, d\tau$$

$$= \frac{\tilde{B}\tilde{\gamma}}{2T}\int_{-T/2}^{T/2} Rect\left[\frac{-\tau+\eta}{T}\right]\left[e^{-i\beta\eta\tau} + \tilde{A}_1\tilde{A}_2^* e^{i(2\pi df-\beta\eta)\tau} + \tilde{A}_1^*\tilde{A}_2 e^{i2\pi df\eta}\, e^{i(-2\pi df-\beta\eta)\tau} + e^{i2\pi df\eta}\, e^{-i\beta\eta\tau}\right] e^{-i2\pi\nu\tau}\, d\tau$$

$$= \frac{\tilde{B}\tilde{\gamma}}{2T}\int_{-T/2}^{T/2} Rect\left[\frac{-\tau+\eta}{T}\right]\left[\left(1 + e^{i2\pi df\eta}\right) e^{-i\beta\eta\tau} + \tilde{A}_1\tilde{A}_2^* e^{i(2\pi df-\beta\eta)\tau} + \tilde{A}_1^*\tilde{A}_2 e^{i2\pi df\eta}\, e^{i(-2\pi df-\beta\eta)\tau}\right] e^{-i2\pi\nu\tau}\, d\tau$$

Three cases now exist: $t = t_1, t < t_1, \& \ t_1 < t$

Case: $t = t_1$

$$\eta = t - t_1 = 0$$

$$\tilde{\gamma} = e^{i\left(2\pi f_0 \eta + \frac{1}{2}\beta \eta^2 + 2\pi \nu \eta\right)} = 1$$

$$(s_R * h)(t) = \frac{\tilde{B}}{2T} \int_{-T/2}^{T/2} Rect\left[\frac{-\tau}{T}\right] \left[2 + \tilde{A}_1 \tilde{A}_2^* e^{i2\pi df\tau} + \tilde{A}_1^* \tilde{A}_2 e^{-i2\pi df\tau}\right] e^{-i2\pi\nu\tau}\, d\tau$$

$$= \frac{\tilde{B}}{2T} \int_{-T/2}^{T/2} 2e^{-i2\pi\nu\tau} + \tilde{A}_1 \tilde{A}_2^* e^{i(2\pi df - 2\pi\nu)\tau} + \tilde{A}_1^* \tilde{A}_2 e^{-i(2\pi df + 2\pi\nu)\tau} d\tau$$

Integral 1

$$\frac{\tilde{B}}{T} \int_{-T/2}^{T/2} e^{-i2\pi\nu\tau}\, d\tau$$

$$= \frac{\tilde{B}}{T} \frac{1}{-i2\pi\nu} \left[e^{-i\pi\nu T} - e^{i\pi\nu T}\right]$$

$$= \frac{\tilde{B}}{T} \frac{1}{\pi\nu} \sin(\pi\nu T)$$

$$= \tilde{B}\, \mathrm{sinc}(\pi\nu T)$$

Integral 2

$$\frac{\tilde{B}}{2T} \int_{-T/2}^{T/2} \tilde{A}_1 \tilde{A}_2^* e^{i(2\pi df - 2\pi\nu)\tau} d\tau$$

$$= \frac{\tilde{B}\tilde{A}_1\tilde{A}_2^*}{2T} \frac{1}{i(2\pi df - 2\pi\nu)} \left[e^{i(\pi df - \pi\nu)T} - e^{-i(\pi df - \pi\nu)T}\right]$$

$$= \frac{\tilde{B}\tilde{A}_1\tilde{A}_2^*}{T} \frac{1}{(2\pi df - 2\pi\nu)} \sin\big((\pi df - \pi\nu)T\big)$$

$$= \frac{\tilde{B}\tilde{A}_1\tilde{A}_2^*}{2} \mathrm{sinc}\big((\pi df - \pi\nu)T\big)$$

Integral 3

$$\frac{\tilde{B}}{2T} \int_{-T/2}^{T/2} \tilde{A}_1^* \tilde{A}_2 e^{-i(2\pi df + 2\pi\nu)\tau} d\tau$$

$$= \frac{\tilde{B}\tilde{A}_1^*\tilde{A}_2}{2T} \frac{1}{-i(2\pi df + 2\pi\nu)} \left[e^{-i(\pi df + \pi\nu)T} - e^{i(\pi df + \pi\nu)T}\right]$$

$$= \frac{\tilde{B}\tilde{A}_1^*\tilde{A}_2}{T} \frac{1}{(2\pi df + 2\pi\nu)} \sin\big((\pi df + \pi\nu)T\big)$$

$$= \frac{\tilde{B}\tilde{A}_1^*\tilde{A}_2}{2}\,\mathrm{sinc}\big((\pi df + \pi\nu)T\big)$$

Combine

$$(s_R * h)(t) = \tilde{B}\,\mathrm{sinc}(\pi\nu T) + \frac{\tilde{B}\tilde{A}_1\tilde{A}_2^*}{2}\,\mathrm{sinc}\big((\pi df - \pi\nu)T\big) + \frac{\tilde{B}\tilde{A}_1^*\tilde{A}_2}{2}\,\mathrm{sinc}\big((\pi df + \pi\nu)T\big)$$

$$= \tilde{B}\left[\mathrm{sinc}(\pi\nu T) + \frac{e^{i\Delta\phi}}{2}\,\mathrm{sinc}\big((\pi df - \pi\nu)T\big) + \frac{e^{-i\Delta\phi}}{2}\,\mathrm{sinc}\big((\pi df + \pi\nu)T\big)\right]$$

$$\boxed{(s_R * h)(t) = \tilde{B}\left[\mathrm{sinc}(\pi\nu T) + \frac{e^{i\Delta\phi}}{2}\,\mathrm{sinc}\big((\pi df - \pi\nu)T\big) + \frac{e^{-i\Delta\phi}}{2}\,\mathrm{sinc}\big((\pi df + \pi\nu)T\big)\right]}$$

Case: $t < t_1$

$$(s_R * h)(t) = \frac{\tilde{B}\tilde{\gamma}}{2T}\int_{-T/2}^{T/2} Rect\left[\frac{-\tau+\eta}{T}\right]\left[\left(1 + e^{i2\pi df\eta}\right)e^{-i\beta\eta\tau} + \tilde{A}_1\tilde{A}_2^* e^{i(2\pi df-\beta\eta)\tau} + \right.$$

$$\left.\tilde{A}_1^*\tilde{A}_2 e^{i2\pi df\eta}\, e^{i(-2\pi df-\beta\eta)\tau}\right]e^{-i2\pi\nu\tau}\, d\tau$$

$$=$$

$$\frac{\tilde{B}\tilde{\gamma}}{2T}\int_{-T/2}^{T/2+\eta}\left(1 + e^{i2\pi df\eta}\right)e^{-i(\beta\eta+2\pi\nu)\tau} + \tilde{A}_1\tilde{A}_2^* e^{i(2\pi df-\beta\eta-2\pi\nu)\tau} +$$

$$\tilde{A}_1^*\tilde{A}_2 e^{i2\pi df\eta}\, e^{-i(2\pi df+\beta\eta+2\pi\nu)\tau} d\tau$$

Integral 1

$$\frac{\tilde{B}\tilde{\gamma}}{2T}\int_{-T/2}^{T/2+\eta}\left(1 + e^{i2\pi df\eta}\right)e^{-i(\beta\eta+2\pi\nu)\tau} d\tau$$

$$= \left(1 + e^{i2\pi df\eta}\right)\frac{\tilde{B}\tilde{\gamma}}{2T}\frac{1}{-i(\beta\eta+2\pi\nu)}\left[e^{-i(\beta\eta+2\pi\nu)(T/2+\eta)} - e^{i(\beta\eta+2\pi\nu)T/2}\right]$$

$$= \left(1 + e^{i2\pi df\eta}\right)\frac{\tilde{B}\tilde{\gamma}}{2T}\frac{1}{-i(\beta\eta+2\pi\nu)}\left[e^{-i\left(\frac{1}{2}\beta\eta+\pi\nu\right)T} e^{-i(\beta\eta+2\pi\nu)\eta} - e^{i(\beta\eta+2\pi\nu)T/2}\right]$$

$$= \left(1 + e^{i2\pi df\eta}\right)\frac{\tilde{B}\tilde{\gamma}}{2T}\frac{e^{-i\left(\frac{1}{2}\beta\eta+\pi\nu\right)\eta}}{-i(\beta\eta+2\pi\nu)}\left[e^{-i\left(\frac{1}{2}\beta\eta+\pi\nu\right)T} e^{-i\left(\frac{1}{2}\beta\eta+\pi\nu\right)\eta} - e^{i\left(\frac{1}{2}\beta\eta+\pi\nu\right)T} e^{i\left(\frac{1}{2}\beta\eta+\pi\nu\right)\eta}\right]$$

$$= \left(1 + e^{i2\pi df\eta}\right)\frac{\tilde{B}\tilde{\gamma}}{2T}\frac{e^{-i\left(\frac{1}{2}\beta\eta+\pi\nu\right)\eta}}{-i(\beta\eta+2\pi\nu)}\left[e^{-i\left(\frac{1}{2}\beta\eta+\pi\nu\right)(T+\eta)} - e^{i\left(\frac{1}{2}\beta\eta+\pi\nu\right)(T+\eta)}\right]$$

$$= \left(1 + e^{i2\pi df\eta}\right)\frac{\tilde{B}\tilde{\gamma}}{2T}\frac{e^{-i\left(\frac{1}{2}\beta\eta+\pi\nu\right)\eta}}{-i(\beta\eta+2\pi\nu)}\left[e^{-i\left(\frac{1}{2}\beta\eta+\pi\nu\right)(T+\eta)} - e^{i\left(\frac{1}{2}\beta\eta+\pi\nu\right)(T+\eta)}\right]\frac{\left(1+\frac{\eta}{T}\right)}{\left(1+\frac{\eta}{T}\right)}$$

$$= \left(1 + \frac{\eta}{T}\right)\left(1 + e^{i2\pi df\eta}\right)\frac{\tilde{B}\tilde{\gamma}}{2(T+\eta)}\frac{e^{-i\left(\frac{1}{2}\beta\eta+\pi\nu\right)\eta}}{-i(\beta\eta+2\pi\nu)}\left[e^{-i\left(\frac{1}{2}\beta\eta+\pi\nu\right)(T+\eta)} - e^{i\left(\frac{1}{2}\beta\eta+\pi\nu\right)(T+\eta)}\right]$$

$$= \left(1 + \frac{\eta}{T}\right)\left(1 + e^{i2\pi df\eta}\right)\frac{\tilde{B}\tilde{\gamma}}{(T+\eta)}\frac{e^{-i\left(\frac{1}{2}\beta\eta+\pi\nu\right)\eta}}{(\beta\eta+2\pi\nu)}\sin\left[\left(\frac{1}{2}\beta\eta + \pi\nu\right)(T+\eta)\right]$$

$$= \left(1 + \frac{\eta}{T}\right)\left(1 + e^{i2\pi df\eta}\right)\frac{\tilde{B}\tilde{\gamma}}{2}e^{-i\left(\frac{1}{2}\beta\eta+\pi\nu\right)\eta}\ \mathrm{sinc}\left[\left(\frac{1}{2}\beta\eta + \pi\nu\right)(T+\eta)\right]$$

$$= \left(1 + \frac{\eta}{T}\right)\left(1 + e^{i2\pi df\eta}\right)\frac{\tilde{B}}{2}e^{i(2\pi f_0+\pi\nu)\eta}\ \mathrm{sinc}\left[\left(\frac{1}{2}\beta\eta + \pi\nu\right)(T+\eta)\right]$$

$$= \left(1+\frac{\eta}{T}\right) e^{i\pi df\eta} \left(e^{-i\pi df\eta} + e^{i\pi df\eta}\right) \frac{\tilde{B}}{2} e^{i(2\pi f_0+\pi\nu)\eta} \operatorname{sinc}\left[\left(\frac{1}{2}\beta\eta+\pi\nu\right)(T+\eta)\right]$$

$$= \tilde{B} e^{i(2\pi f_0+\pi df+\pi\nu)\eta} \left(1+\frac{\eta}{T}\right) \cos[\pi df\eta] \operatorname{sinc}\left[\left(\frac{1}{2}\beta\eta+\pi\nu\right)(T+\eta)\right]$$

Integral 2

$$= \frac{\tilde{B}\tilde{\gamma}}{2T} \int_{-T/2}^{T/2+\eta} \tilde{A}_1 \tilde{A}_2^* e^{i(2\pi df-\beta\eta-2\pi\nu)\tau} d\tau$$

$$= \frac{\tilde{A}_1\tilde{A}_2^*\tilde{B}\tilde{\gamma}}{2T} \frac{1}{i(2\pi df-\beta\eta-2\pi\nu)} \left[e^{i(\pi df-\beta\eta-2\pi\nu)(T/2+\eta)} - e^{-i(2\pi df-\beta\eta-2\pi\nu)T/2}\right]$$

$$= \frac{\tilde{A}_1\tilde{A}_2^*\tilde{B}\tilde{\gamma}}{2T} \frac{1}{i(2\pi df-\beta\eta-2\pi\nu)} \left[e^{i\left(\pi df-\frac{1}{2}\beta\eta-\pi\nu\right)T} e^{i(2\pi df-\beta\eta-2\pi\nu)\eta} - e^{-i(2\pi df-\beta\eta-2\pi\nu)T/2}\right]$$

$$=$$

$$\frac{\tilde{A}_1\tilde{A}_2^*\tilde{B}\tilde{\gamma}}{2T} \frac{e^{i\left(\pi df-\frac{1}{2}\beta\eta-\pi\nu\right)\eta}}{i(2\pi df-\beta\eta-2\pi\nu)} \left[e^{i\left(\pi df-\frac{1}{2}\beta\eta-\pi\nu\right)T} e^{i\left(\pi df-\frac{1}{2}\beta\eta-\pi\nu\right)\eta} -\right.$$

$$\left. e^{-i\left(\pi df-\frac{1}{2}\beta\eta-\pi\nu\right)T} e^{-i\left(\pi df-\frac{1}{2}\beta\eta-\pi\nu\right)\eta}\right]$$

$$= \frac{\tilde{A}_1\tilde{A}_2^*\tilde{B}\tilde{\gamma}}{2T} \frac{e^{i\left(\pi df-\frac{1}{2}\beta\eta-\pi\nu\right)\eta}}{i(2\pi df-\beta\eta-2\pi\nu)} \left[e^{i\left(\pi df-\frac{1}{2}\beta\eta-\pi\nu\right)(T+\eta)} - e^{-i\left(\pi df-\frac{1}{2}\beta\eta-\pi\nu\right)(T+\eta)}\right] \frac{\left(1+\frac{\eta}{T}\right)}{\left(1+\frac{\eta}{T}\right)}$$

$$= \left(1+\frac{\eta}{T}\right) \frac{\tilde{A}_1\tilde{A}_2^*\tilde{B}\tilde{\gamma}}{2(T+\eta)} \frac{e^{i\left(\pi df-\frac{1}{2}\beta\eta-\pi\nu\right)\eta}}{i(2\pi df-\beta\eta-2\pi\nu)} \left[e^{i\left(\pi df-\frac{1}{2}\beta\eta-\pi\nu\right)(T+\eta)} - e^{-i\left(\pi df-\frac{1}{2}\beta\eta-\pi\nu\right)(T+\eta)}\right]$$

$$= \left(1+\frac{\eta}{T}\right) \frac{\tilde{A}_1\tilde{A}_2^*\tilde{B}\tilde{\gamma}}{(T+\eta)} \frac{e^{i\left(\pi df-\frac{1}{2}\beta\eta-\pi\nu\right)\eta}}{(2\pi df-\beta\eta-2\pi\nu)} \sin\left[\left(\pi df-\frac{1}{2}\beta\eta-\pi\nu\right)(T+\eta)\right]$$

$$= \left(1+\frac{\eta}{T}\right) \frac{\tilde{A}_1\tilde{A}_2^*\tilde{B}}{2} e^{i(2\pi f_0+\pi df+\pi\nu)\eta} \operatorname{sinc}\left[\left(\pi df-\frac{1}{2}\beta\eta-\pi\nu\right)(T+\eta)\right]$$

$$= \tilde{B}\tilde{A}_1\tilde{A}_2^* e^{i(2\pi f_0+\pi df+\pi\nu)\eta} \frac{1}{2}\left(1+\frac{\eta}{T}\right) \operatorname{sinc}\left[\left(\pi df-\frac{1}{2}\beta\eta-\pi\nu\right)(T+\eta)\right]$$

Integral 3

$$\frac{\tilde{B}\tilde{\gamma}}{2T} \int_{-T/2}^{T/2+\eta} \tilde{A}_1^* \tilde{A}_2 e^{i2\pi df\eta} e^{-i(2\pi df+\beta\eta+2\pi\nu)\tau} d\tau$$

$$= \frac{\tilde{B}\tilde{A}_1^*\tilde{A}_2\tilde{\gamma}}{2T} e^{i2\pi df\eta} \frac{1}{-i(2\pi df+\beta\eta+2\pi\nu)} \left[e^{-i(2\pi df+\beta\eta+2\pi\nu)(T/2+\eta)} - e^{i(2\pi df+\beta\eta+2\pi\nu)T/2}\right]$$

$$=$$

$$\frac{\tilde{B}\tilde{A}_1^*\tilde{A}_2\tilde{\gamma}}{2T}e^{i2\pi df\eta}\ \frac{1}{-i(2\pi df+\beta\eta+2\pi\nu)}\Big[e^{-i\left(\pi df+\frac{1}{2}\beta\eta+\pi\nu\right)T}e^{-i(2\pi df+\beta\eta+2\pi\nu)\eta}-$$

$$e^{i(2\pi df+\beta\eta+2\pi\nu)T/2}\Big]$$

$$=$$

$$\frac{\tilde{B}\tilde{A}_1^*\tilde{A}_2\tilde{\gamma}}{2T}e^{i2\pi df\eta}\ \frac{e^{-i\left(\pi df+\frac{1}{2}\beta\eta+\pi\nu\right)\eta}}{-i(2\pi df+\beta\eta+2\pi\nu)}\Big[e^{-i\left(\pi df+\frac{1}{2}\beta\eta+\pi\nu\right)T}e^{-i\left(\pi df+\frac{1}{2}\beta\eta+\pi\nu\right)\eta}-$$

$$e^{i\left(\pi df+\frac{1}{2}\beta\eta+\pi\nu\right)T}e^{i\left(\pi df+\frac{1}{2}\beta\eta+\pi\nu\right)\eta}\Big]$$

$$=\frac{\tilde{B}\tilde{A}_1^*\tilde{A}_2\tilde{\gamma}}{2T}e^{i2\pi df\eta}\ \frac{e^{-i\left(\pi df+\frac{1}{2}\beta\eta+\pi\nu\right)\eta}}{-i(2\pi df+\beta\eta+2\pi\nu)}\Big[e^{-i\left(\pi df+\frac{1}{2}\beta\eta+\pi\nu\right)(T+\eta)}-e^{-i\left(\pi df+\frac{1}{2}\beta\eta+\pi\nu\right)(T+\eta)}\Big]$$

$$=\frac{\tilde{B}\tilde{A}_1^*\tilde{A}_2\tilde{\gamma}}{2T}e^{i2\pi df\eta}\ \frac{e^{-i\left(\pi df+\frac{1}{2}\beta\eta+\pi\nu\right)\eta}}{-i(2\pi df+\beta\eta+2\pi\nu)}\Big[e^{-i\left(\pi df+\frac{1}{2}\beta\eta+\pi\nu\right)(T+\eta)}-e^{-i\left(\pi df+\frac{1}{2}\beta\eta+\pi\nu\right)(T+\eta)}\Big]\frac{\left(1+\frac{\eta}{T}\right)}{\left(1+\frac{\eta}{T}\right)}$$

$$=$$

$$\left(1+\frac{\eta}{T}\right)\frac{\tilde{B}\tilde{A}_1^*\tilde{A}_2\tilde{\gamma}}{2(T+\eta)}e^{i2\pi df\eta}\ \frac{e^{-i\left(\pi df+\frac{1}{2}\beta\eta+\pi\nu\right)\eta}}{-i(2\pi df+\beta\eta+2\pi\nu)}\Big[e^{-i\left(\pi df+\frac{1}{2}\beta\eta+\pi\nu\right)(T+\eta)}-e^{-i\left(\pi df+\frac{1}{2}\beta\eta+\pi\nu\right)(T+\eta)}\Big]$$

$$=\left(1+\frac{\eta}{T}\right)\frac{\tilde{B}\tilde{A}_1^*\tilde{A}_2\tilde{\gamma}}{(T+\eta)}e^{i2\pi df\eta}\ \frac{e^{-i\left(\pi df+\frac{1}{2}\beta\eta+\pi\nu\right)\eta}}{(2\pi df+\beta\eta+2\pi\nu)}\sin\left[\left(\pi df+\frac{1}{2}\beta\eta+\pi\nu\right)(T+\eta)\right]$$

$$=\left(1+\frac{\eta}{T}\right)\frac{\tilde{B}\tilde{A}_1^*\tilde{A}_2\tilde{\gamma}}{2}e^{-i\left(-\pi df+\frac{1}{2}\beta\eta+\pi\nu\right)\eta}\ \mathrm{sinc}\left[\left(\pi df+\frac{1}{2}\beta\eta+\pi\nu\right)(T+\eta)\right]$$

$$=\tilde{B}\tilde{A}_1^*\tilde{A}_2e^{i(2\pi f_0+\pi df+\pi\nu)\eta}\,\frac{1}{2}\left(1+\frac{\eta}{T}\right)\mathrm{sinc}\left[\left(\pi df+\frac{1}{2}\beta\eta+\pi\nu\right)(T+\eta)\right]$$

Combine

$$(s_R*h)(t)=\tilde{B}e^{i(2\pi f_0+\pi df+\pi\nu)\eta}\ \left(1+\frac{\eta}{T}\right)\cos[\pi df\eta]\,\mathrm{sinc}\left[\left(\frac{1}{2}\beta\eta+\pi\nu\right)(T+\eta)\right]+$$

$$\tilde{B}\tilde{A}_1\tilde{A}_2^*e^{i(2\pi f_0+\pi df+\pi\nu)\eta}\,\frac{1}{2}\left(1+\frac{\eta}{T}\right)\mathrm{sinc}\left[\left(\pi df-\frac{1}{2}\beta\eta-\pi\nu\right)(T+\eta)\right]+$$

$$\tilde{B}\tilde{A}_1^*\tilde{A}_2e^{i(2\pi f_0+\pi df+\pi\nu)\eta}\,\frac{1}{2}\left(1+\frac{\eta}{T}\right)\mathrm{sinc}\left[\left(\pi df+\frac{1}{2}\beta\eta+\pi\nu\right)(T+\eta)\right]$$

$$= \tilde{B} e^{i(2\pi f_0 + \pi df + \pi\nu)\eta} \left(1 + \frac{\eta}{T}\right) \left\{ \begin{matrix} \cos[\pi df\eta] \operatorname{sinc}\left[\left(\frac{1}{2}\beta\eta + \pi\nu\right)(T+\eta)\right] + \\ \frac{e^{i\Delta\phi}}{2} \operatorname{sinc}\left[\left(\pi df - \frac{1}{2}\beta\eta - \pi\nu\right)(T+\eta)\right] + \\ \frac{e^{-i\Delta\phi}}{2} \operatorname{sinc}\left[\left(\pi df + \frac{1}{2}\beta\eta + \pi\nu\right)(T+\eta)\right] \end{matrix} \right\}$$

$$\boxed{(s_R * h)(t) = \tilde{B} e^{i(2\pi f_0 + \pi df + \pi\nu)\eta} \left(1 + \frac{\eta}{T}\right) \left\{ \begin{matrix} \cos[\pi df\eta] \operatorname{sinc}\left[\left(\frac{1}{2}\beta\eta + \pi\nu\right)(T+\eta)\right] + \\ \frac{e^{i\Delta\phi}}{2} \operatorname{sinc}\left[\left(\pi df - \frac{1}{2}\beta\eta - \pi\nu\right)(T+\eta)\right] + \\ \frac{e^{-i\Delta\phi}}{2} \operatorname{sinc}\left[\left(\pi df + \frac{1}{2}\beta\eta + \pi\nu\right)(T+\eta)\right] \end{matrix} \right\}}$$

Case: $t_1 < t$

$$(s_R * h)(t) = \frac{\tilde{B}\widetilde{\gamma}}{2T}\int_{-T/2}^{T/2} Rect\left[\frac{-\tau+\eta}{T}\right]\left[\left(1+e^{i2\pi df\eta}\right)e^{-i\beta\eta\tau} + \tilde{A}_1\tilde{A}_2^* e^{i(2\pi df-\beta\eta)\tau} + \right.$$

$$\left.\tilde{A}_1^*\tilde{A}_2 e^{i2\pi df\eta}\, e^{i(-2\pi df-\beta\eta)\tau}\right]e^{-i2\pi\nu\tau}\, d\tau$$

$$=$$

$$\frac{\tilde{B}\widetilde{\gamma}}{2T}\int_{-T/2+\eta}^{T/2}\left(1+e^{i2\pi df\eta}\right)e^{-i(\beta\eta+2\pi\nu)\tau} + \tilde{A}_1\tilde{A}_2^* e^{i(2\pi df-\beta\eta-2\pi\nu)\tau} +$$

$$\tilde{A}_1^*\tilde{A}_2 e^{i2\pi df\eta}\, e^{-i(2\pi df+\beta\eta+2\pi\nu)\tau} d\tau$$

Integral 1

$$\frac{\tilde{B}\widetilde{\gamma}}{2T}\int_{-T/2+\eta}^{T/2}\left(1+e^{i2\pi df\eta}\right)e^{-i(\beta\eta+2\pi\nu)\tau} d\tau$$

$$= \left(1+e^{i2\pi df\eta}\right)\frac{\tilde{B}\widetilde{\gamma}}{2T}\frac{1}{-i(\beta\eta+2\pi\nu)}\left[e^{-i(\beta\eta+2\pi\nu)T/2} - e^{i(\beta\eta+2\pi\nu)(T/2-\eta)}\right]$$

$$= \left(1+e^{i2\pi df\eta}\right)\frac{\tilde{B}\widetilde{\gamma}}{2T}\frac{1}{-i(\beta\eta+2\pi\nu)}\left[e^{-i(\beta\eta+2\pi\nu)T/2} - e^{i\left(\frac{1}{2}\beta\eta+\pi\nu\right)T} e^{-i(\beta\eta+2\pi\nu)\eta}\right]$$

$$= \left(1+e^{i2\pi df\eta}\right)\frac{\tilde{B}\widetilde{\gamma}}{2T}\frac{e^{-i\left(\frac{1}{2}\beta\eta+\pi\nu\right)\eta}}{-i(\beta\eta+2\pi\nu)}\left[e^{-i\left(\frac{1}{2}\beta\eta+\pi\nu\right)T} e^{i\left(\frac{1}{2}\beta\eta+\pi\nu\right)\eta} - e^{i\left(\frac{1}{2}\beta\eta+\pi\nu\right)T} e^{-i\left(\frac{1}{2}\beta\eta+\pi\nu\right)\eta}\right]$$

$$= \left(1+e^{i2\pi df\eta}\right)\frac{\tilde{B}\widetilde{\gamma}}{2T}\frac{e^{-i\left(\frac{1}{2}\beta\eta+\pi\nu\right)\eta}}{-i(\beta\eta+2\pi\nu)}\left[e^{-i\left(\frac{1}{2}\beta\eta+\pi\nu\right)(T-\eta)} - e^{i\left(\frac{1}{2}\beta\eta+\pi\nu\right)(T-\eta)}\right]$$

$$= \left(1+e^{i2\pi df\eta}\right)\frac{\tilde{B}\widetilde{\gamma}}{2T}\frac{e^{-i\left(\frac{1}{2}\beta\eta+\pi\nu\right)\eta}}{-i(\beta\eta+2\pi\nu)}\left[e^{-i\left(\frac{1}{2}\beta\eta+\pi\nu\right)(T-\eta)} - e^{i\left(\frac{1}{2}\beta\eta+\pi\nu\right)(T-\eta)}\right]\frac{\left(1-\frac{\eta}{T}\right)}{\left(1-\frac{\eta}{T}\right)}$$

$$= \left(1-\frac{\eta}{T}\right)\left(1+e^{i2\pi df\eta}\right)\frac{\tilde{B}\widetilde{\gamma}}{2(T-\eta)}\frac{e^{-i\left(\frac{1}{2}\beta\eta+\pi\nu\right)\eta}}{-i(\beta\eta+2\pi\nu)}\left[e^{-i\left(\frac{1}{2}\beta\eta+\pi\nu\right)(T-\eta)} - e^{i\left(\frac{1}{2}\beta\eta+\pi\nu\right)(T-\eta)}\right]$$

$$= \left(1-\frac{\eta}{T}\right)\left(1+e^{i2\pi df\eta}\right)\frac{\tilde{B}\widetilde{\gamma}}{(T-\eta)}\frac{e^{-i\left(\frac{1}{2}\beta\eta+\pi\nu\right)\eta}}{(\beta\eta+2\pi\nu)}\sin\left[\left(\frac{1}{2}\beta\eta+\pi\nu\right)(T-\eta)\right]$$

$$= \left(1-\frac{\eta}{T}\right)\left(1+e^{i2\pi df\eta}\right)\frac{\tilde{B}}{2}e^{i(2\pi f_0\eta+\pi\nu\eta)}\operatorname{sinc}\left[\left(\frac{1}{2}\beta\eta+\pi\nu\right)(T-\eta)\right]$$

$$= \left(1-\frac{\eta}{T}\right)e^{i\pi df\eta}\left(e^{-i\pi df\eta} + e^{i2\pi df\eta}\right)\frac{\tilde{B}}{2}e^{i(2\pi f_0+\pi\nu)\eta}\operatorname{sinc}\left[\left(\frac{1}{2}\beta\eta+\pi\nu\right)(T-\eta)\right]$$

$$= \tilde{B}e^{i(2\pi f_0+\pi df+\pi\nu)\eta}\left(1-\frac{\eta}{T}\right)\cos[\pi df\eta]\operatorname{sinc}\left[\left(\frac{1}{2}\beta\eta+\pi\nu\right)(T-\eta)\right]$$

Integral 2

$$\frac{\tilde{B}\tilde{\gamma}}{2T}\int_{-T/2+\eta}^{T/2}\tilde{A}_1\tilde{A}_2^* e^{i(2\pi df-\beta\eta-2\pi\nu)\tau}d\tau$$

$$=\frac{\tilde{B}\tilde{A}_1\tilde{A}_2^*\tilde{\gamma}}{2T}\frac{1}{i(2\pi df-\beta\eta-2\pi\nu)}\left[e^{i(2\pi df-\beta\eta-2\pi\nu)T/2}-e^{-i(2\pi df-\beta\eta-2\pi\nu)(T/2-\eta)}\right]$$

$$=\frac{\tilde{B}\tilde{A}_1\tilde{A}_2^*\tilde{\gamma}}{2T}\frac{1}{i(2\pi df-\beta\eta-2\pi\nu)}\left[e^{i(2\pi df-\beta\eta-2\pi\nu)T/2}-e^{-i\left(\pi df-\frac{1}{2}\beta\eta-\pi\nu\right)T}e^{i(2\pi df-\beta\eta-2\pi\nu)\eta}\right]$$

$$=$$

$$\frac{\tilde{B}\tilde{A}_1\tilde{A}_2^*\tilde{\gamma}}{2T}\frac{e^{i\left(\pi df-\frac{1}{2}\beta\eta-\pi\nu\right)\eta}}{i(2\pi df-\beta\eta-2\pi\nu)}\left[e^{i\left(\pi df-\frac{1}{2}\beta\eta-\pi\nu\right)T}e^{-i\left(\pi df-\frac{1}{2}\beta\eta-\pi\nu\right)\eta}-\right.$$

$$\left.e^{-i\left(\pi df-\frac{1}{2}\beta\eta-\pi\nu\right)T}e^{i\left(\pi df-\frac{1}{2}\beta\eta-\pi\nu\right)\eta}\right]$$

$$=\frac{\tilde{B}\tilde{A}_1\tilde{A}_2^*\tilde{\gamma}}{2T}\frac{e^{i\left(\pi df-\frac{1}{2}\beta\eta-\pi\nu\right)\eta}}{i(2\pi df-\beta\eta-2\pi\nu)}\left[e^{i\left(\pi df-\frac{1}{2}\beta\eta-\pi\nu\right)(T-\eta)}-e^{-i\left(\pi df-\frac{1}{2}\beta\eta-\pi\nu\right)(T-\eta)}\right]$$

$$=\frac{\tilde{B}\tilde{A}_1\tilde{A}_2^*\tilde{\gamma}}{2T}\frac{e^{i\left(\pi df-\frac{1}{2}\beta\eta-\pi\nu\right)\eta}}{i(2\pi df-\beta\eta-2\pi\nu)}\left[e^{i\left(\pi df-\frac{1}{2}\beta\eta-\pi\nu\right)(T-\eta)}-e^{-i\left(\pi df-\frac{1}{2}\beta\eta-\pi\nu\right)(T-\eta)}\right]\frac{\left(1-\frac{\eta}{T}\right)}{\left(1-\frac{\eta}{T}\right)}$$

$$=\left(1-\frac{\eta}{T}\right)\frac{\tilde{B}\tilde{A}_1\tilde{A}_2^*\tilde{\gamma}}{2(T-\eta)}\frac{e^{i\left(\pi df-\frac{1}{2}\beta\eta-\pi\nu\right)\eta}}{i(2\pi df-\beta\eta-2\pi\nu)}\left[e^{i\left(\pi df-\frac{1}{2}\beta\eta-\pi\nu\right)(T-\eta)}-e^{-i\left(\pi df-\frac{1}{2}\beta\eta-\pi\nu\right)(T-\eta)}\right]$$

$$=\left(1-\frac{\eta}{T}\right)\frac{\tilde{B}\tilde{A}_1\tilde{A}_2^*\tilde{\gamma}}{(T-\eta)}\frac{e^{i\left(\pi df-\frac{1}{2}\beta\eta-\pi\nu\right)\eta}}{(2\pi df-\beta\eta-2\pi\nu)}\sin\left[\left(\pi df-\frac{1}{2}\beta\eta-\pi\nu\right)(T-\eta)\right]$$

$$=\left(1-\frac{\eta}{T}\right)\frac{\tilde{B}\tilde{A}_1\tilde{A}_2^*\tilde{\gamma}}{2}e^{i\left(\pi df-\frac{1}{2}\beta\eta-\pi\nu\right)\eta}\ \mathrm{sinc}\left[\left(\pi df-\frac{1}{2}\beta\eta-\pi\nu\right)(T-\eta)\right]$$

$$=\left(1-\frac{\eta}{T}\right)\frac{\tilde{B}\tilde{A}_1\tilde{A}_2^*}{2}e^{i(2\pi f_0\eta+\pi df+\pi\nu\eta)}\ \mathrm{sinc}\left[\left(\pi df-\frac{1}{2}\beta\eta-\pi\nu\right)(T-\eta)\right]$$

$$=\tilde{B}\tilde{A}_1\tilde{A}_2^*e^{i(2\pi f_0\eta+\pi df+\pi\nu\eta)}\frac{1}{2}\left(1-\frac{\eta}{T}\right)\mathrm{sinc}\left[\left(\pi df-\frac{1}{2}\beta\eta-\pi\nu\right)(T-\eta)\right]$$

Integral 3

$$\frac{\tilde{B}\tilde{\gamma}}{2T}\int_{-T/2+\eta}^{T/2}\tilde{A}_1^*\tilde{A}_2 e^{i2\pi df\eta}\,e^{-i(2\pi df+\beta\eta+2\pi\nu)\tau}d\tau$$

$$=\frac{\tilde{B}\tilde{A}_1^*\tilde{A}_2\tilde{\gamma}}{2T}e^{i2\pi df\eta}\ \frac{1}{-i(2\pi df+\beta\eta+2\pi\nu)}\left[e^{-i(2\pi df+\beta\eta+2\pi\nu)T/2}-e^{i(2\pi df+\beta\eta+2\pi\nu)(T/2-\eta)}\right]$$

$$=$$

$$\frac{\tilde{B}\tilde{A}_1^*\tilde{A}_2\tilde{\gamma}}{2T}e^{i2\pi df\eta}\ \frac{1}{-i(2\pi df+\beta\eta+2\pi\nu)}\left[e^{-i(2\pi df+\beta\eta+2\pi\nu)T/2}-\right.$$

$$\left.e^{i(2\pi df+\beta\eta+2\pi\nu)T/2}e^{-i(2\pi df+\beta\eta+2\pi\nu)\eta}\right]$$

$$=$$

$$\frac{\tilde{B}\tilde{A}_1^*\tilde{A}_2\tilde{\gamma}}{2T}e^{i2\pi df\eta}\ \frac{e^{-i\left(\pi df+\frac{1}{2}\beta\eta+\pi\nu\right)\eta}}{-i(2\pi df+\beta\eta+2\pi\nu)}\left[e^{-i\left(\pi df+\frac{1}{2}\beta\eta+\pi\nu\right)T}e^{i\left(\pi df+\frac{1}{2}\beta\eta+\pi\nu\right)\eta}-\right.$$

$$\left.e^{i\left(\pi df+\frac{1}{2}\beta\eta+\pi\nu\right)T}e^{-i\left(\pi df+\frac{1}{2}\beta\eta+\pi\nu\right)\eta}\right]$$

$$=\frac{\tilde{B}\tilde{A}_1^*\tilde{A}_2\tilde{\gamma}}{2T}e^{i2\pi df\eta}\ \frac{e^{-i\left(\pi df+\frac{1}{2}\beta\eta+\pi\nu\right)\eta}}{-i(2\pi df+\beta\eta+2\pi\nu)}\left[e^{-i\left(\pi df+\frac{1}{2}\beta\eta+\pi\nu\right)(T-\eta)}-e^{i\left(\pi df+\frac{1}{2}\beta\eta+\pi\nu\right)(T-\eta)}\right]$$

$$=\frac{\tilde{B}\tilde{A}_1^*\tilde{A}_2\tilde{\gamma}}{2T}e^{i2\pi df\eta}\ \frac{e^{-i\left(\pi df+\frac{1}{2}\beta\eta+\pi\nu\right)\eta}}{-i(2\pi df+\beta\eta+2\pi\nu)}\left[e^{-i\left(\pi df+\frac{1}{2}\beta\eta+\pi\nu\right)(T-\eta)}-e^{i\left(\pi df+\frac{1}{2}\beta\eta+\pi\nu\right)(T-\eta)}\right]\frac{\left(1-\frac{\eta}{T}\right)}{\left(1-\frac{\eta}{T}\right)}$$

$$=\left(1-\frac{\eta}{T}\right)\frac{\tilde{B}\tilde{A}_1^*\tilde{A}_2\tilde{\gamma}}{2(T-\eta)}e^{i2\pi df\eta}\ \frac{e^{-i\left(\pi df+\frac{1}{2}\beta\eta+\pi\nu\right)\eta}}{-i(2\pi df+\beta\eta+2\pi\nu)}\left[e^{-i\left(\pi df+\frac{1}{2}\beta\eta+\pi\nu\right)(T-\eta)}-e^{i\left(\pi df+\frac{1}{2}\beta\eta+\pi\nu\right)(T-\eta)}\right]$$

$$=\left(1-\frac{\eta}{T}\right)\frac{\tilde{B}\tilde{A}_1^*\tilde{A}_2\tilde{\gamma}}{(T-\eta)}e^{i2\pi df\eta}\ \frac{e^{-i\left(\pi df+\frac{1}{2}\beta\eta+\pi\nu\right)\eta}}{(2\pi df+\beta\eta+2\pi\nu)}\sin\left[\left(\pi df+\frac{1}{2}\beta\eta+\pi\nu\right)(T-\eta)\right]$$

$$=\left(1-\frac{\eta}{T}\right)\frac{\tilde{B}\tilde{A}_1^*\tilde{A}_2\tilde{\gamma}}{2}e^{i2\pi df\eta}\ e^{-i\left(\pi df+\frac{1}{2}\beta\eta+\pi\nu\right)\eta}\ \mathrm{sinc}\left[\left(\pi df+\frac{1}{2}\beta\eta+\pi\nu\right)(T-\eta)\right]$$

$$=\left(1-\frac{\eta}{T}\right)\frac{\tilde{B}\tilde{A}_1^*\tilde{A}_2}{2}e^{i(2\pi f_0+\pi df+\pi\nu)\eta}\ \mathrm{sinc}\left[\left(\pi df+\frac{1}{2}\beta\eta+\pi\nu\right)(T-\eta)\right]$$

$$=\tilde{B}\tilde{A}_1^*\tilde{A}_2e^{i(2\pi f_0+\pi df+\pi\nu)\eta}\,\frac{1}{2}\left(1-\frac{\eta}{T}\right)\mathrm{sinc}\left[\left(\pi df+\frac{1}{2}\beta\eta+\pi\nu\right)(T-\eta)\right]$$

Combine

$$(s_R * h)(t) = \tilde{B}e^{i(2\pi f_0+\pi df+\pi\nu)\eta}\left(1-\frac{\eta}{T}\right)\cos[\pi df\eta]\,\mathrm{sinc}\left[\left(\frac{1}{2}\beta\eta+\pi\nu\right)(T-\eta)\right]+$$

$$\tilde{B}\tilde{A}_1\tilde{A}_2^* e^{i(2\pi f_0\eta+\pi df+\pi\nu\eta)}\frac{1}{2}\left(1-\frac{\eta}{T}\right)\mathrm{sinc}\left[\left(\pi df-\frac{1}{2}\beta\eta-\pi\nu\right)(T-\eta)\right]+$$

$$\tilde{B}\tilde{A}_1^*\tilde{A}_2 e^{i(2\pi f_0+\pi df+\pi\nu)\eta}\frac{1}{2}\left(1-\frac{\eta}{T}\right)\mathrm{sinc}\left[\left(\pi df+\frac{1}{2}\beta\eta+\pi\nu\right)(T-\eta)\right]$$

$$=$$

$$\tilde{B}e^{i(2\pi f_0+\pi df+\pi\nu)\eta}\left(1-\frac{\eta}{T}\right)\left\{\cos[\pi df\eta]\,\mathrm{sinc}\left[\left(\frac{1}{2}\beta\eta+\pi\nu\right)(T-\eta)\right]+\right.$$

$$\left.\tilde{A}_1\tilde{A}_2^*\frac{1}{2}\mathrm{sinc}\left[\left(\pi df-\frac{1}{2}\beta\eta-\pi\nu\right)(T-\eta)\right]+\tilde{A}_1^*\tilde{A}_2\frac{1}{2}\mathrm{sinc}\left[\left(\pi df+\frac{1}{2}\beta\eta+\pi\nu\right)(T-\eta)\right]\right\}$$

$$=$$

$$\tilde{B}e^{i(2\pi f_0+\pi df+\pi\nu)\eta}\left(1-\frac{\eta}{T}\right)\left\{\cos[\pi df\eta]\,\mathrm{sinc}\left[\left(\frac{1}{2}\beta\eta+\pi\nu\right)(T-\eta)\right]+\frac{\tilde{A}_1\tilde{A}_2^*}{2}\mathrm{sinc}\left[\left(\pi df-\right.\right.\right.$$

$$\left.\left.\left.\frac{1}{2}\beta\eta-\pi\nu\right)(T-\eta)\right]+\frac{\tilde{A}_1^*\tilde{A}_2}{2}\mathrm{sinc}\left[\left(\pi df+\frac{1}{2}\beta\eta+\pi\nu\right)(T-\eta)\right]\right\}$$

$$\boxed{(s_R * h)(t) = \tilde{B}e^{i(2\pi f_0+\pi df+\pi\nu)\eta}\left(1-\frac{\eta}{T}\right)\left\{\begin{array}{c}\cos[\pi df\eta]\,\mathrm{sinc}\left[\left(\frac{1}{2}\beta\eta+\pi\nu\right)(T-\eta)\right]+\\ \frac{e^{i\Delta\phi}}{2}\mathrm{sinc}\left[\left(\pi df-\frac{1}{2}\beta\eta-\pi\nu\right)(T-\eta)\right]+\\ \frac{e^{-i\Delta\phi}}{2}\mathrm{sinc}\left[\left(\pi df+\frac{1}{2}\beta\eta+\pi\nu\right)(T-\eta)\right]\end{array}\right\}}$$

$$\boxed{(s_R * h)(t) = \tilde{B}\left[\operatorname{sinc}(\pi\nu T) + \frac{e^{i\Delta\phi}}{2}\operatorname{sinc}\big((\pi df - \pi\nu)T\big) + \frac{e^{-i\Delta\phi}}{2}\operatorname{sinc}\big((\pi df + \pi\nu)T\big)\right]}$$

$t = t_1$

$$\boxed{(s_R * h)(t) = \tilde{B}e^{i(2\pi f_0 + \pi df + \pi\nu)\eta}\left(1 + \frac{\eta}{T}\right)\left\{\begin{matrix} \cos[\pi df\eta]\operatorname{sinc}\left[\left(\frac{1}{2}\beta\eta + \pi\nu\right)(T + \eta)\right] + \\ \frac{e^{i\Delta\phi}}{2}\operatorname{sinc}\left[\left(\pi df - \frac{1}{2}\beta\eta - \pi\nu\right)(T + \eta)\right] + \\ \frac{e^{-i\Delta\phi}}{2}\operatorname{sinc}\left[\left(\pi df + \frac{1}{2}\beta\eta + \pi\nu\right)(T + \eta)\right] \end{matrix}\right\}}$$

$t < t_1$

$$\boxed{(s_R * h)(t) = \tilde{B}e^{i(2\pi f_0 + \pi df + \pi\nu)\eta}\left(1 - \frac{\eta}{T}\right)\left\{\begin{matrix} \cos[\pi df\eta]\operatorname{sinc}\left[\left(\frac{1}{2}\beta\eta + \pi\nu\right)(T - \eta)\right] + \\ \frac{e^{i\Delta\phi}}{2}\operatorname{sinc}\left[\left(\pi df - \frac{1}{2}\beta\eta - \pi\nu\right)(T - \eta)\right] + \\ \frac{e^{-i\Delta\phi}}{2}\operatorname{sinc}\left[\left(\pi df + \frac{1}{2}\beta\eta + \pi\nu\right)(T - \eta)\right] \end{matrix}\right\}}$$

$t_1 < t$

G. Conclusion

At the limit of $t = t_1$, for either the case of $t < \mathrm{t}_1$ or $t_1 < t$, the function reduces to the case of $t_1 = \tau$. The functions $t < \mathrm{t}_1$ and $t_1 < t$ case differ only by a sign in two portions of the function. Therefore the final function given the assumptions stated at the beginning can be given as:

$$\boxed{(s_R * h)(t) = \tilde{B}e^{i(2\pi f_0 + \pi df + \pi\nu)\eta}\left(1 - \frac{|\eta|}{T}\right)\left\{\begin{matrix} \cos[\pi df\eta]\operatorname{sinc}\left[\left(\frac{1}{2}\beta\eta + \pi\nu\right)(T - |\eta|)\right] + \\ \frac{e^{i\Delta\phi}}{2}\operatorname{sinc}\left[\left(\pi df - \frac{1}{2}\beta\eta - \pi\nu\right)(T - |\eta|)\right] + \\ \frac{e^{-i\Delta\phi}}{2}\operatorname{sinc}\left[\left(\pi df + \frac{1}{2}\beta\eta + \pi\nu\right)(T - |\eta|)\right] \end{matrix}\right\}}$$

For: $|t - t_1| \leq T$

Remember: $\eta = t - t_1$.

As long as the relative phase difference between the two lines, the difference frequency between the two lines, the frequency offset of the AOM, the velocity of the target remain constant. By looking exactly one period later a phase difference can be deduced and the velocity backed out.

APPENDIX B -
Matlab Code

```
%%%%%%%%%%%%%%%%%%%%%%%%%%%%%%%%%%%%%%%%%%%%%%%%%%%%%%%%%%%%%%%%%%%
%                                                           7/14/09
%
%Eric S. Bailey
%University of Dayton - Ladar and Optical Communications Institute
%
%This M-file contains the matlab code for useful functions used in
%this thesis
%%%%%%%%%%%%%%%%%%%%%%%%%%%%%%%%%%%%%%%%%%%%%%%%%%%%%%%%%%%%%%%%%%%

%% Plots the frequency spectrum of a multiple chrip SF-LFM signal.

%Clear variables, command window, & close open figures
clear; clc; close;

%%%%%%%%%%%%%%%%%%%%%%%%%%%%%%%%%%%%%%%%%%%%%%%%%%%%%%%%%%%%%%%%%%%
%                          USER VARIABLES                         %
%%%%%%%%%%%%%%%%%%%%%%%%%%%%%%%%%%%%%%%%%%%%%%%%%%%%%%%%%%%%%%%%%%%
%Chirp bandwidth, Hz
B = 37*10^6;

%Signal period, s
T = 4*10^-6;

%Difference frequency, Hz
df = 60*10^6;

%AOM frequency shift, Hz
aoshift = 750*10^6;

%Number of chirps
chirps = 2;

%Number of datapoints
datapoints = 16000;
%%%%%%%%%%%%%%%%%%%%%%%%%%%%%%%%%%%%%%%%%%%%%%%%%%%%%%%%%%%%%%%%%%%

%%%%%%%%%%%%%%%%%%%%%%%%%%%%%%%%%%%%%%%%%%%%%%%%%%%%%%%%%%%%%%%%%%%
%                 CALCULATED PARAMETERS/CONSTANTS                 %
%%%%%%%%%%%%%%%%%%%%%%%%%%%%%%%%%%%%%%%%%%%%%%%%%%%%%%%%%%%%%%%%%%%
```

```
%Chirp Coeffecient, 1/s^2
beta = 2*pi*B/T;

%Angular difference frequency, rad/s
dw = 2*pi*df;

%AOM Angular frequency shift, rad
aowshift = 2*pi*aoshift;

%Time domain spacing, s
dt = T/datapoints;

%Frequency domain spacing, Hz
deltaf = 1/(datapoints*dt);

%Max frequency, Hz
maxfreq = 1/dt;
%%%%%%%%%%%%%%%%%%%%%%%%%%%%%%%%%%%%%%%%%%%%%%%%%%%%%%%%%%%%%%%%%%%

%%%%%%%%%%%%%%%%%%%%%%%%%%%%%%%%%%%%%%%%%%%%%%%%%%%%%%%%%%%%%%%%%%%
%                          START OF CODE                          %
%%%%%%%%%%%%%%%%%%%%%%%%%%%%%%%%%%%%%%%%%%%%%%%%%%%%%%%%%%%%%%%%%%%
%Populate time array
t = 0:dt:T;

%Populate frequency array
frequency = -maxfreq/2:deltaf:maxfreq/2;

%Initialize data array
data = zeros(1,datapoints+1);

%Sum each chirp
for i = 0:chirps-1;
    data = data + exp(j*((aowshift + i*dw)*t + .5*beta*t.^2));
end

%FFT data
fftdata = fftshift(fft(data));

%Absolute value FFT
fftdata = abs(fftdata);

%Normalize FFT
fftdata = fftdata/max(fftdata);

%Plot FFT
figure
plot(frequency,fftdata)
axis([0 max(frequency) 0 1])
xlabel('Frequency (Hz)')
title('Frequency Spectrum of Signal')
%%%%%%%%%%%%%%%%%%%%%%%%%%%%%%%%%%%%%%%%%%%%%%%%%%%%%%%%%%%%%%%%%%%

%% Plots the autocorrelation of a multiple chirp SF-LFM Signal.
```

```
%Clear variables & command window
clear; clc;

%%%%%%%%%%%%%%%%%%%%%%%%%%%%%%%%%%%%%%%%%%%%%%%%%%%%%%%%%%%%%%%%%%%
%                          USER VARIABLES                         %
%%%%%%%%%%%%%%%%%%%%%%%%%%%%%%%%%%%%%%%%%%%%%%%%%%%%%%%%%%%%%%%%%%%
%Chirp bandwidth, Hz
B = 37*10^6;

%Signal period, s
T = 4*10^-6;

%Difference frequency, Hz
df = 60*10^6;

%AOM frequency shift, Hz
aoshift = 750*10^6;

%Number of chirps
chirps = 2;

%Number of datapoints
datapoints = 16000;
%%%%%%%%%%%%%%%%%%%%%%%%%%%%%%%%%%%%%%%%%%%%%%%%%%%%%%%%%%%%%%%%%%%

%%%%%%%%%%%%%%%%%%%%%%%%%%%%%%%%%%%%%%%%%%%%%%%%%%%%%%%%%%%%%%%%%%%
%                 CALCULATED PARAMETERS/CONSTANTS                 %
%%%%%%%%%%%%%%%%%%%%%%%%%%%%%%%%%%%%%%%%%%%%%%%%%%%%%%%%%%%%%%%%%%%
%Chirp Coeffecient, 1/s^2
beta = 2*pi*B/T;

%Angular difference frequency, rad/s
dw = 2*pi*df;

%AOM Angular frequency shift, rad
aowshift = 2*pi*aoshift;

%Time domain spacing, s
dt = T/datapoints;
%%%%%%%%%%%%%%%%%%%%%%%%%%%%%%%%%%%%%%%%%%%%%%%%%%%%%%%%%%%%%%%%%%%

%%%%%%%%%%%%%%%%%%%%%%%%%%%%%%%%%%%%%%%%%%%%%%%%%%%%%%%%%%%%%%%%%%%
%                          START OF CODE                          %
%%%%%%%%%%%%%%%%%%%%%%%%%%%%%%%%%%%%%%%%%%%%%%%%%%%%%%%%%%%%%%%%%%%
%Populate time array
t = 0:dt:T;

%Initialize data array
data = zeros(1,datapoints+1);

%Sum each chirp
for i = 0:chirps-1;
    data = data + exp(j*((aowshift + i*dw)*t + .5*beta*t.^2));
```

```
end

%Autocorrelation of signal
[acorr,lag] = xcorr(data,2*length(data));

%Time displacment array
tau = dt.*lag;

%Abs auto-correlation
acorr = abs(acorr);

%Normalize autocorrelation
acorr = acorr/max(acorr);

%Autocorrelation in dB
acorr = 20*log10(acorr);

%Plot autocorrelation
figure
plot(tau/T,acorr)
axis([-1 1 -60 0])
xlabel('\tau/T')
ylabel('dB')
%%%%%%%%%%%%%%%%%%%%%%%%%%%%%%%%%%%%%%%%%%%%%%%%%%%%%%%%%%%%%%%%%%%

%% Calculates dR & PSLR of a multiple chirp SF-LFM Signal.

%Clear variables & command window
clear; clc;

%%%%%%%%%%%%%%%%%%%%%%%%%%%%%%%%%%%%%%%%%%%%%%%%%%%%%%%%%%%%%%%%%%%
%                          USER VARIABLES                         %
%%%%%%%%%%%%%%%%%%%%%%%%%%%%%%%%%%%%%%%%%%%%%%%%%%%%%%%%%%%%%%%%%%%
%Chirp bandwidth, Hz
B = 37*10^6;

%Signal period, s
T = 4*10^-6;

%Difference frequency, Hz
df = 60*10^6;

%AOM frequency shift, Hz
aoshift = 750*10^6;

%Number of chirps
chirps = 2;

%Number of datapoints
datapoints = 16000;
%%%%%%%%%%%%%%%%%%%%%%%%%%%%%%%%%%%%%%%%%%%%%%%%%%%%%%%%%%%%%%%%%%%

%%%%%%%%%%%%%%%%%%%%%%%%%%%%%%%%%%%%%%%%%%%%%%%%%%%%%%%%%%%%%%%%%%%
%                  CALCULATED PARAMETERS/CONSTANTS                %
```

```
%%%%%%%%%%%%%%%%%%%%%%%%%%%%%%%%%%%%%%%%%%%%%%%%%%%%%%%%%%%%%%%%%%%%%%%%%%%%%%%%%%%%%%%%%%%%%%%%%%%%%%%%%%%%%%%%%%%%%%%%%%%%%%%%%%%%%%%%%%%%%%%%%%%%%%%
%Chirp Coeffecient, 1/s^2
beta = 2*pi*B/T;

%Angular difference frequency, rad/s
dw = 2*pi*df;

%AOM Angular frequency shift, rad
aowshift = 2*pi*aoshift;

%Time domain spacing, s
dt = T/datapoints;

%Speed of light, m/s
c = 299792458;
%%%%%%%%%%%%%%%%%%%%%%%%%%%%%%%%%%%%%%%%%%%%%%%%%%%%%%%%%%%%%%%%%%%%%%%%%%%%%%%%%%%%%%%%%%%%%%%%%%%%%%%%%%%%%%%%%%%%%%%%%%%%%%%%%%%%%%%%%%%%%%%%%%%%%%%

%%%%%%%%%%%%%%%%%%%%%%%%%%%%%%%%%%%%%%%%%%%%%%%%%%%%%%%%%%%%%%%%%%%%%%%%%%%%%%%%%%%%%%%%%%%%%%%%%%%%%%%%%%%%%%%%%%%%%%%%%%%%%%%%%%%%%%%%%%%%%%%%%%%%%%%%
%                          START OF CODE                           %
%%%%%%%%%%%%%%%%%%%%%%%%%%%%%%%%%%%%%%%%%%%%%%%%%%%%%%%%%%%%%%%%%%%%%%%%%%%%%%%%%%%%%%%%%%%%%%%%%%%%%%%%%%%%%%%%%%%%%%%%%%%%%%%%%%%%%%%%%%%%%%%%%%%%%%%
%Populate time array
t = 0:dt:T;

%Initialize data array
data = zeros(1,datapoints+1);

%Sum each chirp
for i = 0:chirps-1;
    data = data + exp(j*((aowshift + i*dw)*t + .5*beta*t.^2));
end

%Autocorrelation of signal
[acorr,lag] = xcorr(data,2*length(data));

%Time displacment vector
tau = dt.*lag;

%Abs auto-correlation
acorr = abs(acorr);

%Normalized autocorrelation
acorr = acorr/max(acorr);

%dB
acorr = 20*log10(acorr);

%Midpoint in autocorrelation
midpoint = 2*length(data)+1;

%Derivative loop
for i = midpoint:(length(acorr)-1);
    d(i) = acorr(i+1)-acorr(i);
end
```

```
%Finds first minima
i = midpoint;
while d(i) <= 0;
    i = i+1;
end

%Find the -3 dB point
[row,col] = find(acorr(midpoint:i-1) > acorr(midpoint)-3);

%Location of -3 dB point
arraylocation = max(col)+midpoint;

%FWHM
fwhm = 2*tau(arraylocation);

%Range Resolution
range = (fwhm*c)/2;

%Peak (dB)
center_lobe = max(acorr);

%Side lobe (dB)
side_lobe = max(acorr(i-1:length(acorr)));

%PSLR
pslr = side_lobe - center_lobe;

range
pslr
%%%%%%%%%%%%%%%%%%%%%%%%%%%%%%%%%%%%%%%%%%%%%%%%%%%%%%%%%%%%%%%%%%%
```

REFERENCES

[1] North, D. O. *Analysis of Factors Which Determine Signal-to-Noise Discrimination in Radar*. Report PTR-6c. RCA Laboratories. Princeton, NJ.

[2] Van Vleck, J. H., and D. Middleton. "A Theoretical Comparison of Visual, Aural, and Meter Reception of Pulsed Signals in the Presence of Noise." *Journal of Applied Physics* 17 (1946): 940-71.

[3] Woodward, P. M. *Probability and Information Theory with Applications to Radar*. Oxford: Pergamon, 1953.

[4] Cook, C. E. *Modification of Pulse-compression Waveforms*. Proc. of Proceedings National Electronics Conference. Vol. 14. 1958. 1058-067.

[5] Chin, J. E., and C. E. Cook. "The Mathematics of Pulse Compression-A Problem in Systems Analysis." *Sperry Engineering Review* 12 (1959): 11-16.

[6] Fowle, E. N. *The Design of Radar Signals*. Rep. no. SR-98. Bedford, Massachusetts: MITRE Corporation, 1963.

[7] Bernfeld, M., C. E. Cook, J. Paolillo, and C. A. Palmieri. "Matched Filtering, Pulse Compression, and Waveform Design, Parts I-IV." *Microwave Journal* No. 10 57-64, No.11 81-90, No. 12 70-76 (1964). No. 1 73-81 (1965).

[8] Hughes, A. J., E. R. Pike, and J. Oshaughn. "FM-CW RADAR Range Measurement at 10-MU Wavelength." *IEEE JOURNAL OF QUANTUM ELECTRONICS* QE 8.12 (1972): 909.

[9] Hulme, K. F., B. S. Collins, G. D. Constant, and J. T. Pinson. "A CO2-Laser Rangefinder Using Heterodyne-Detection and Chirp Pulse-Compression." *Optical and Quantum Electronics* 13.1 (1981): 35-45.

[10] Forrester, P. A., and K. F. Hulme. "Review: Laser Rangefinders." *Optical and Quantum Electronics* 13 (1981): 259-93.

[11] Collins, B. S., K. F. Hulme, and N. A. Loude. "An Acoustooptic Modulator For A CO2-Laser Rangefinder Using Heterodyne-Detection." *Optical and Quantum Electronics* 12.5: 419-26.

[12] Adany, P., C. Allen, and R. Q. Hui. "Chirped Lidar Using Simplified Homodyne Detection." *Journal of Lightwave Technology* 27.16 (2009): 3351-357.

[13] Tsuji, K., K. Shimizu, T. Horiguchi, and Y. Koyamada. "Spatial-resolution Improvement in Long-range Coherent Optical Frequency Domain Reflectometry by Frequency-sweep Linearisation." *Electronics Letters* 33.5: 408-10.

[14] Chimenti, Robert V. *Sparse frequency linearly frequency modulated laser radar signal generation, detection, and processing*. Thesis. University of Dayton, 2009.

[15] Chimenti, Robert V., Matthew P. Dierking, Peter E. Powers, and Joseph W. Haus. "Sparse frequency LFM ladar signals." *Optics Express* 17.10 (2009).

[16] Holman, Kevin W., David G. Kocher, and Sumanth Kaushik. *Time-Multiplexed Optical Waveform Generation for High-Resolution Imaging*. Proc. of CLEO/QELS. 2008.

[17] Homan, Kevin W., David G. Kocher, and Sumanth Kaushik. "Waveform Synthesis." *Optical Waveform Generation for Coherent High-Resolution Imaging*. Proc. of Coherent Optical Technologies and Applications, Boston, Massachusetts. 2008.

[18] Roos, Peter A., W. Randall Babbitt, Zachary Cole, Brant Kaylor, Trenton Berg, Kristian D. Merkel, and Randy R. Reibel. "Coherent LIDAR II." *High-Resolution Range and Dopler LADAR Using Broadband Coherent Optical Processing*. Proc. of Coherent Optical Technologies and Applications, Whistler, Canada. 2006.

[19] Cole, Z., P. A. Roos, T. Berg, B. Kaylor, K. D. Merkel, W. R. Babbittt, and R. R. Reibel. "Unambiguous Range-Doppler LADAR Processing Using 2 Giga-Sample-Per-Second Noise Waveforms." *Journal of Luminescence* 127.1 (2007): 146-51.

[20] Dierking, Matthew P. *Multi-Mode Coherent LADAR Imaging Via Diverse Periodic Pseudo Noise Waveforms and Code Division Multiple Access Aperatures*. Diss. University of Dayton, 2009.

[21] Zheng, Jesse. "Analysis of Optical Frequency-Modulated Continuous-Wave InterferenceJesse." *Applied Optics* 43.21 (2004): 4189-198.

[22] Duarte, Cristina C., B. Pablo Dorta Naranjo, Alberto A. Lopez, and Alvaro Blanco Del Campo. "Security Technology." *High Resolution CWLFM Radar for Vessel Detection and Idenfication for Maritime Border Security*. Proc. of International Carnahan Conference. 2005.

[23] Khoury, Jed, Charles L. Woods, Joseph Lorenzo, and John Kierstead. *Resolution Limits for Time-of-Flight Imaging Laser Radar*. Proc. of Optical Pattern Recognition XVI. Vol. 5816. 2005. 270-76.

[24] Brian Krause, Philip Gatt, Carl Embry, and Joe Buck. *High-Resolution 3D Coherent Laser Radar Imaging*. Proc. of Laser Radar Technology and Applications XI. Vol. 6214. 2006.

[25] Johnson, S., T. Nichols, P. Gatt, and T. J. Klausutis. *Range Precision of Direct Detection Laser Radar Systems*. Proc. of Laser Radar Technology and Applications IX. Vol. 5421. 2004. 72-86.

[26] Gatt, P., S. W. Henderson, J. A. Thomson, and D. L. Thomson. *Micro-Doppler Lidar Signals and Noise Mechanisms: Theory and Experiment*. Proc. of Laser Radar Technology and Applications V. 2000. 422-35.

[27] Levanon, Nadav, and Eli Mozeson. *Radar Signals*. New York: Wiley-IEEE, 2004.

[28] Cook, Charles E., and Marvin Bernfeld. *Radar signals an introduction to theory and application*. Boston: Artech House, 1993.

[29] Boulet, Benoit. *Fundamentals of signals and systems*. Hingham, Mass: Da Vinci Engineering, 2005.

[30] Haykin, Simon S. *Signals and systems*. New York: Wiley, 1998. Print.
31 Hsu, Hwei P. *Schaum's outline of theory and problems of signals and systems*. New York, NY: McGraw-Hill, 1995.

[32] Weisstein, Eric W. *CRC concise encyclopedia of mathematics*. Boca Raton, Fla: CRC, 1999.

[33] Miller, Nicholas J., Matthew P. Dierking, and Bradley D. Duncan. "Optical sparse aperture imaging."*Applied Optics* 46.23 (2007): 5933-943. *Optics Infobase*. Optical Society of America. Web. <http://www.opticsinfobase.org/ao/abstract.cfm?URI=ao-46-23-5933>.

[34] Lucke, R. L. *Fundamentals of Wide-Field Sparse-Aperture Imaging*. Proc. of IEEE Aerospace Conference. Big Sky, Montana, 2001. Print.
[35] Chimenti, Robert V., Matthew P. Dierking, Peter E. Powers, and Joseph W. Haus. *Multiple chirp sparse frequency LFM ladar signals*. Proc. of SPIE Defense, Security & Sensing, Orlando, FL.

[36] Chimenti, Robert V., Matthew P. Dierking, Peter E. Powers, Joseph W. Haus, and Eric S. Bailey. *A Review of Sparse Frequency Linearly Frequency Modulated (SF-LFM)*

Laser Radar Signal Modeling with Preliminary Experimental Results. Proc. of 15th Coherent Laser Radar Conference, Toulouse, France.

[37] Chimenti, Robert V., Matthew P. Dierking, Peter E. Powers, Joseph W. Haus, and Eric S. Bailey. "Experimental verification of sparse frequency linearly frequency modulated ladar signals modeling." *Optics Express*. (To be published)

[38] Brimrose Corporation of America. *Technical Manual: Model No. VFF-800-100-V-A-F1.*

[39] ThorLabs. *Technical manual: Item No. SIR5-FC.*

[40] Agilent. *U1065A Specifications Document.*

[41] Eilbeck, Chris. "John Scott Russell and the Doppler effect." *Mathematics, Computer Science and Actuarial Courses at Heriot-Watt University, Edinburgh*. 2 Mar. 2000. Web. <http://www.ma.hw.ac.uk/~chris/doppler.html>.

[42] NP Photonics. *The Rock Manual.*

[43] Hecht, Eugene. *Optics*. Reading, Mass: Addison-Wesley, 2002.

[44] Pedrotti, Frank L., Leno M. Pedrotti, and Leno S. Pedrotti. *Introduction to optics*. Englewood Cliffs: Prentice-Hall, 1993.